

Design and Development of a Point of Care device using Nano-transducers for Monitoring and Analysis of Thyroid Hormones

A Thesis submitted to the

UPES

For the Award of

Doctor of Philosophy

in

Pharmaceutical Sciences

by

Deepanmol Singh

July 2024

Supervisor

Dr. Ashish Mathur

External Supervisor

Dr. Neeraj Mahindroo



**Department of Pharmaceutical Sciences
School of Health Sciences and Technology (SOHST)**

UPES

Dehradun - 248007: Uttarakhand

Design and Development of a Point of Care device using Nano-transducers for Monitoring and Analysis of Thyroid Hormones

A Thesis submitted to the

UPES

For the Award of

Doctor of Philosophy

in

Pharmaceutical Sciences

by

Deepanmol Singh

(SAP ID: 500080036)

July 2024

Supervisor

Dr. Ashish Mathur

Professor

Centre for Interdisciplinary Research and Innovation

UPES

External Supervisor

Dr. Neeraj Mahindroo

Professor

School of Health Sciences and Technology

Dr. Vishwanath Karad MIT World Peace University



Department of Pharmaceutical Sciences

School of Health Sciences and Technology (SOHST)

UPES

Dehradun - 248007: Uttarakhand

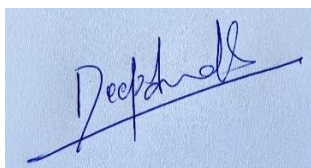
DECLARATION

I hereby declare that the submission, being presented in the abstract entitled “Design and Development of Point of Care device using Nano-transducers for Monitoring and Analysis of Thyroid Hormones” in partial fulfillment of the award of the degree of Doctor of Philosophy submitted to Department of Pharmaceutical Sciences, School of Health Sciences and Technology, UPES, Knowledge Acres, Dehradun, Uttarakhand, India is a verified and authentic record of my own research conducted out under the supervision of:

Dr. Ashish Mathur, Professor, Centre of Interdisciplinary Research, and Innovation, UPES, Dehradun, India.

Dr. Neeraj Mahindroo, Professor, School of Health Sciences and Technology, Dr. Vishwanath Karad MIT World Peace University, Pune, India

I declare that this work has not been submitted anywhere else for any part-time or full-time award for a diploma or degree program to the best of my knowledge. Additionally, this work doesn't contain any previously published results or material by any person except where the due acknowledgment and references have been mentioned in the text.

A blue rectangular box containing a handwritten signature in blue ink. The signature appears to be 'Deepanmol Singh' written in a cursive style.

Deepanmol Singh

PhD Scholar

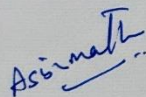
School of Health Sciences and Technology (SOHST), UPES

Dehradun-248007, Uttarakhand

Date: 25 July 2024

CERTIFICATE

I certify that **Deepanmol Singh** has prepared his thesis titled “**Design and Development of a Pointof Care device using nano-transducers for monitoring and analysis of Thyroid Hormones**”, for the award of PhD degree from UPES, under my guidance. He has carried out his research work at the School of Health Sciences and Technology, UPES.



Dr. Ashish Mathur

Professor

Centre for Interdisciplinary Research and Innovation

UPES

Dehradun – 248007, Uttarakhand, India



Dr. Vishwanath Karad
**MIT WORLD PEACE
UNIVERSITY** | PUNE
TECHNOLOGY. KNOWLEDGE. SOCIAL RESPONSIBILITY. HUMANITY.

CERTIFICATE

July 24, 2024

I certify that **Deepanmol Singh** has prepared his thesis titled “**Design and Development of a Point of Care device using nano-transducers for monitoring and analysis of Thyroid Hormones**”, for the award of PhD degree from UPES, under my guidance. He has carried out his research work at the School of Health Sciences and Technology, UPES.

(Dr. Neeraj Mahindroo)
Professor & Dean
School of Health Sciences and Technology,
Dr Vishwanath Karad MIT-World Peace University,
124 Paud Road, Kothrud, Pune 411038 India
Email: neeraj.mahindroo@mitwpu.edu.in; Neeraj.Mahindroo@yahoo.com
Ph: + 91 981 601 7554

ABSTRACT

Thyroxine (T₄) and Liothyronine (T₃), which are released by the thyroid gland, are essential for controlling the body's metabolic activities. Any disturbance in the levels of these thyroid hormones can lead to disturbance in normal growth and development of human body. Hypothyroidism and hyperthyroidism are two major thyroid disorders, which require timely diagnosis and treatment to avoid any life-threatening condition. Presently, available diagnostic techniques are time-consuming and require costly instruments. An early, accurate, and efficient diagnosis of thyroid disorders and regular monitoring of thyroid functioning can reduce the chances of serious complications. In the present work, molecular imprinted polymer and antibody-based biosensing methods were developed for thyroxine and liothyronine.

This doctoral research aims to advance the field of biosensing of thyroid hormones (thyroxine and liothyronine) through the development of different strategies such as Molecularly Imprinted Polymer (MIP) and Antibody-based approaches. The ultimate goal is to create an advanced sensing system capable of estimating thyroid hormone(s) in biological/pharmaceutical matrices.

In the **first phase** of this study, MIP was chemically synthesized for the sensitive and selective estimation of thyroxine in the range of 5pg/mL - 50 pg/mL. The MIP was meticulously optimized to exhibit superior molecular recognition behaviour for accurate estimation of thyroxine (T₄). The characterization studies such as Atomic Force Microscopy (AFM), Fourier Transform Infrared Spectroscopy (FT-IR) and contact angle studies were performed to characterize the synthesized MIPs. Further, these synthesized MIPs were coated onto the Indium Tin Oxide (ITO) glass electrode surface to be used as a working electrode in electrochemical studies. Sensor performance studies such as effect of scan rate, effect of binding of thyroxine to MIP cavities, linearity and interference testing were also performed.

Using cyclic voltammetry, a calibration plot in the concentration range of 5pg/mL - 50pg/mL was developed against peak anodic current (I_{pa}). The normal concentration of free thyroxine in the blood of a normal human is in the range of 9pg/mL - 18 pg/mL. The response of thyroxine was studied by spiking 50pg/mL in saliva. The percentage of spiked thyroxine on electrochemical analysis was found to be between 96% - 115.2%. The developed method showed high sensitivity and selectivity which enables it to be used as an alternative for estimation of thyroxine in biological fluids.

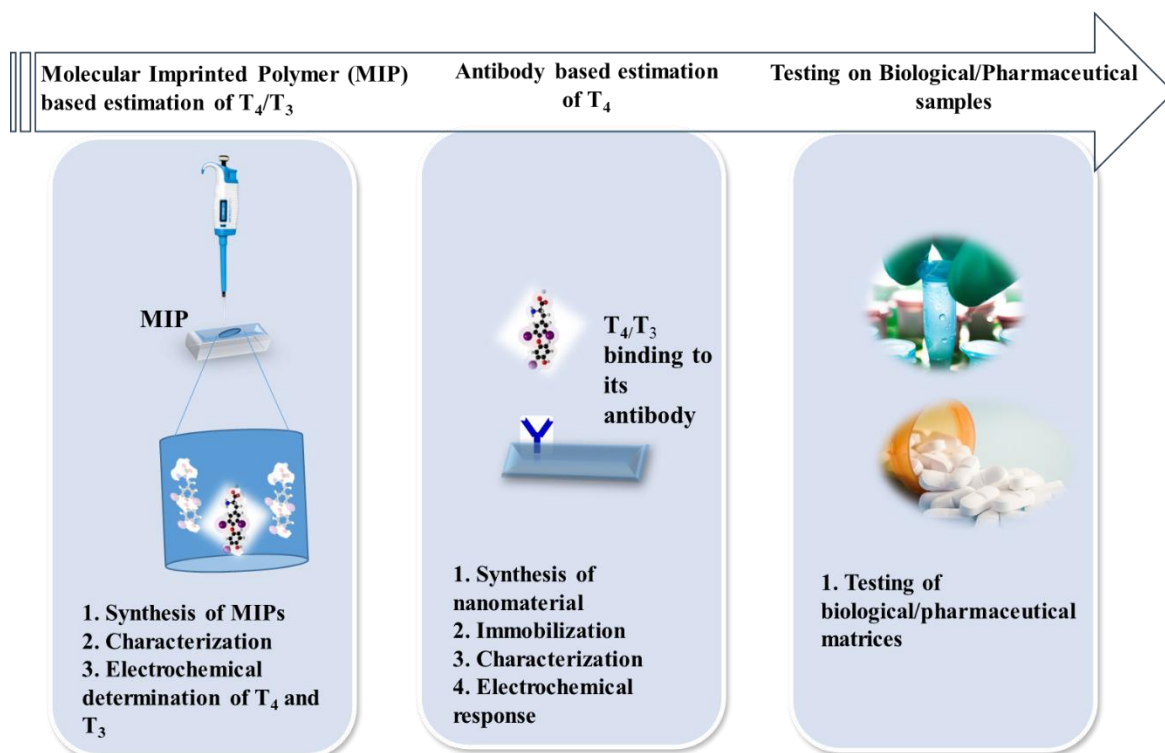
The **second phase** of this research focused on electrochemical synthesis and deposition of a thin conducting film of molecularly imprinted polymer onto the ITO electrode for biosensing of liothyronine (T_3). Pyrrole was used as a monomer for the synthesis of thin polymer film. The characterization studies were performed with AFM, FT-IR and cyclic voltammetry to confirm the electrochemical synthesis of the MIP. Sensor performance studies such as effect of scan rate, effect of binding of thyroxine to MIP cavities, linearity, interference testing, effect of pH and effect of time were also performed. The method showed linearity between 50-300pg/mL concentration and was found to be highly selective to liothyronine even in the presence of potential interfering biomolecules. The developed MIP-based electrochemical method showed success in estimating T_3 in commercially available liothyronine sodium tablets (5 μ g). The results obtained were comparable with high performance liquid chromatography (HPLC). This method can be used as an alternative for development of point-of-care biosensor for quality control of liothyronine tablets.

The **third phase** of this study aims to perform antibody-based estimation of thyroxine. Gold-graphene quantum dots (Au-GQD) were prepared as nanomaterial to immobilize antibodies for selective biosensing of thyroxine. The characterization of Au-GQD was done using scanning electron microscope (SEM), FT-IR and cyclic voltammetry. The electrochemical response was analyzed using cyclic voltammetry. To test the electrochemical performance several parameters were

studied such as current-concentration response, effect of antibody concentration, effect of scan rate, effect of pH and effect of interfering substances. The developed sensor showed linearity in the range of 5pg/mL - 50pg/mL. The developed method showed high sensitivity which enables it to be used for estimation of thyroxine in biological matrices.

The biosensor developed for thyroxine can be further miniaturized to be used as a point-of-care device for estimating T₄ in biological matrices. The novel MIP based liothyronine biosensors can be further developed into a point-of-care device for spot determination of quality of T₃ tablets.

GRAPHICAL ABSTRACT



ACKNOWLEDGMENTS

I feel immense pleasure in expressing my sincere and profound gratitude to my thesis supervisor Prof. Ashish Mathur and External-supervisor Prof. Neeraj Mahindroo whose guidance helped me in carrying out my research work. I would also like to express my gratitude to Dr. Souradeep Roy for his valuable suggestions and instrumental training. I am thankful to Ms. Akanksha, Mr. Divakar, Mr. Mitva, Ms. Sonam, Ms. Reema, Ms. Garima (and other members of sensor fabrication lab) for providing necessary support during this study.

I would like to thank the Vice Chancellor, Dean R & D, Dean SOHST and Cluster Heads of UPES for providing me with the required infrastructure and best resources to complete my research work. Special thanks to Mcleods Pharma for providing me the pure API (thyroxine).

Next, I extend my gratitude to my parents for their unconditional support throughout my PhD journey. Without their motivation and consistent belief in me, it would not have been possible to complete this research within the prescribed time. I am extremely thankful to my wife Dr. Tejdeep Kaur whose holistic support, motivation, and sacrifice helped me throughout the PhD journey. I express my utmost gratitude to my parents Daljit Kaur and Parvinder Singh and to my sister Navroop Kaur.

The blessings of my mentors, teachers and colleagues of SoHST have been crucial for me in achieving the goal of this study.

Deepanmol Singh

PhD Scholar

CONTENTS

ABSTRACT.....	iv
GRAPHICAL ABSTRACT.....	vii
ACKNOWLEDGMENTS	viii
LIST OF FIGURES	xii
LIST OF TABLES.....	xvii
LIST OF ABBREVIATIONS.....	xix
LIST OF SYMBOLS.....	xxi
Chapter 1.....	1
Aim of PhD Project.....	4
Objectives of PhD Project.....	4
Chapter 2.....	7
2.1. Introduction.....	8
2.1.1. Thyroxine (T ₄).....	9
2.1.2. Liothyronine.....	10
2.2. Diagnostic Techniques for Thyroid Hormones (T ₃ /T ₄).....	12
2.2.1. Biorecognition Elements.....	14
2.3. Matrices for the study of Thyroid Hormones (T ₄ /T ₃)	19
2.4. Biosensors for the estimation of thyroxine and liothyronine	20
Chapter 3.....	24
3.1. Introduction.....	27
3.2. Experimental.....	30
3.2.1. Materials	30
3.2.2. Instruments.....	31
3.2.3. Methodology	31

3.3. Results and Discussion	38
3.3.1. Preliminary studies.....	38
3.3.2. Synthesis of MIP and NIP.....	40
3.3.3. Optimization of Template Removal.....	41
3.3.5. Characterization studies	48
3.4. Conclusion	54
Chapter 4.....	55
4.1. Introduction.....	58
4.2. Experimental.....	59
4.2.1 Materials	59
4.2.2. Instruments and Electrodes	60
4.2.3. Methodology	60
4.3. Results and Discussion	62
4.3.1. Response on different stages of fabrication	62
4.3.2. Scan rate study	65
4.3.3. Linearity and Interference Studies	66
4.4 Estimation of Thyroxine in Saliva: Spiking study	70
4.5. Conclusion	74
Chapter 5.....	75
5.1. Introduction.....	78
5.2. Experimental.....	80
5.2.1. Materials	80
5.2.2. Electrodes and Instruments	80
5.2.3. Methodology	81
5.3. Results and Discussion	85
5.3.1. Synthesis and Characterization	87

5.3.2 Sensor Performance: Scan rate, linearity, interference, and stability.....	91
5.3.3. Estimation of liothyronine in Liothyronine Tablet	96
5.4. Conclusion	99
Chapter 6.....	100
6.1. Introduction.....	103
6.1. Experimental.....	105
6.1.1. Materials	105
6.2.2. Electrodes and Instruments	106
6.2.3. Methodology	106
6.3. Results and Discussions.....	109
6.3.2. Sensor Performance: Electrochemical studies	112
6.4. Conclusion	122
Chapter 7.....	123
7.1. Conclusions.....	124
7.2. Future Outlook	125
References.....	127
List of Publications	145
Annexure I: Ethical Approval.....	147

LIST OF FIGURES

Figure 2.1. Description of the physiological mechanism for the release of thyroid hormones.....	8
Figure 2.2. Structure of thyroxine and liothyronine.....	10
Figure 2.3. Conversion of thyroxine to Liothyronine.....	11
Figure 2.4. Different elements of a conventional biosensor.....	14
Figure 2.5. Steps in the preparation of molecularly imprinted polymer via electro-polymerization.....	18
Figure 2.6. Conductive and non-conductive forms of polyaniline synthesized by oxidative polymerization of aniline monomer.....	19
Figure 3.1. Structures of Functional monomers.....	28
Figure 3.2. Flow chart showing all the steps involved in synthesis of MIPs.....	29
Figure 3.3. Representation of chemical structures-based formation of molecular imprinted polymers.....	34
Figure 3.4. The graphical representation of the process of removal of thyroxine from the polyaniline matrix, collection of supernatant and analysis using HPLC.....	37
Figure 3.5. UV spectra of thyroxine taken from 260nm to 400nm shows a lambda max of 326nm.....	39
Figure 3.6. FT-IR spectra of thyroxine.....	39
Figure 3.7. HPLC chromatogram of thyroxine (mAU vs mins).....	39
Figure 3.8. The dried solid polyaniline after the oxidative polymerization of aniline.....	40
Figure 3.9 (a) Chromatogram of pure thyroxine (b) Chromatogram after extraction from NIP (c) Chromatogram after extracted from polyaniline with T ₄ (d) Chromatogram after three consecutive extractions from polyaniline.....	41

Figure 3.10 The effect of time and temperature (at 75mM NaOH concentration) on the removal efficiency of thyroxine from polyaniline. The contour plot shows that the removal is maximum when temperature is between 40-50°C, and time is 15 mins.....	44
Figure 3.11 The effect of time and temperature (at 100mM NaOH concentration) on the removal efficiency of thyroxine from polyaniline. The contour plot shows very small changes in the removal with different temperature and time conditions.....	44
Figure 3.12 The effect of time and temperature (at 125mM NaOH concentration) on the removal efficiency of thyroxine from polyaniline. The contour plot shows negligible change in the removal with different temperature and time conditions.....	45
Figure 3.13 The effect of time and NaOH concentration (at 30°C) on the removal efficiency of thyroxine from polyaniline. The contour plot shows maximum removal at low concentration (75mM) and less time (15 mins).....	46
Figure 3.14 The effect of time and NaOH concentration (at 40°C) on the removal efficiency of thyroxine from polyaniline. The contour plot shows maximum removal at low concentration (75mM), but time has almost negligible effect.....	46
Figure 3.15 The effect of time and NaOH concentration (at 50°C) on the removal efficiency of thyroxine from polyaniline. The contour plot shows maximum removal at low concentration (75mM) and less time (15 mins).....	47
Figure 3.16 HPLC chromatogram for calculation of imprinting factor for MIP.....	48
Figure 3.17 (A) shows the scan range of 4000-400 cm ⁻¹ MIP, NIP and thyroxine rebound MIP (MIP+T ₄) and (B) shows zoomed FT-IR scan of range 1100cm ⁻¹ -400 cm ⁻¹ for MIP, NIP and thyroxine rebound MIP (MIP+T ₄).....	50
Figure 3.18. AFM images of MIP and NIP at 10µm x 10µm resolution.....	51
Figure 3.19 (A) Contact angle for NIP with water (I) and ethylene glycol (II) and (B) Contact angle for MIP with water (I) and ethylene glycol (II).....	52
Figure 4.1. ITO coated glass electrodes of dimensions 10 mm x 7 x 1.1mm.....	60

Figure 4.2 (A) Stages of fabrication of biosensor. (B) Current and voltage profile for NIP, MIP, MIP +T ₄ and ITO. (C) Nyquist plot for Bare ITO, NIP, MIP and T ₄ rebound MIP. The dotted lines show the simulated plots obtained using Zview software. Randle’s circuit is shown in the islet.....	63
Figure 4.3. Study of scan rate vs current response from 10 mV/s to 180 mV/s.....	65
Figure 4.4. Change of peak anodic current (I _{pa}) with v ^{1/2}	66
Figure 4.5. (A) CV profile for different concentration of thyroxine solutions and (B) calibration plot between peak anodic current (I) and concentration.....	67
Figure 4.6. Effect of potential interferants on the response of molecularly imprinted PANI sensor towards the detection of T ₄	69
Figure 4.7 Comparison of determination of thyroxine using Chemiluminescence (CLIA) analyzer and MIP based biosensor.....	71
Figure 4.8. (A) Effect of concentration and current response (B) Calibration plot between peak anodic current (I) and concentration.....	72
Figure 5.1 Schematic representation of molecular imprinting process of poly-pyrrole with liothyronine (T ₃) and subsequent sensing with cyclic voltammetry.....	83
Figure 5.2. UV scan of liothyronine solution taken between 260nm to 400nm. The maximum absorbance is observed at 297nm.....	86
Figure 5.3. FT-IR spectra of liothyronine.....	86
Figure 5.4. HPLC chromatogram of liothyronine.....	87
Figure 5.5. (A) ITO electrode with and without coating of polypyrrole B. SEM image of polypyrrole coated on ITO glass (3 cycles). The thickness of polypyrrole layer is around 1000nm.....	88
Figure 5.6. FT-IR spectra for MIP, NIP and MIP + Liothyronine.....	89
Figure 5.7 (A). AFM image of NIP surface (A) and MIP surface (B).....	89
Figure 5.8. CV scan for NIP, MIP, MIP + Liothyronine, and bare ITO.....	90

Figure 5.9. (A) Study of scan rate vs current response from 10 mV/s to 90 mV/s. (B) Linearity between peak anodic and cathodic current with square root of scan rate.....	91
Figure 5.10. CV scans for different concentration of T ₃ solutions from 50pg/mL to 300pg/mL.....	92
Figure 5.11. Calibration plot shows linearity in the range 50-300pg/mL concentration for liothyronine using developed biosensor.....	93
Figure 5.12. Bar graph showing the effect of potential interferants on the response of MIP-Ppy based sensor towards the detection of T ₃	94
Figure 5.13. Bar graph showing the effect of pH on the biosensor response.....	95
Figure 5.14. Bar graph showing the effect of time on the biosensor response.....	95
Figure 5.15. Liothyronine tablets (Linorma) manufacture by Abbott	96
Figure 5.16. A. The plot shows a change in CV response with different concentrations. B. Calibration plot between current and concentration of liothyronine in the range of 50-300pg/mL.....	96
Figure 5.17 Chromatogram of pure liothyronine (above). Chromatogram of solution prepared using liothyronine tablet (below).....	97
Figure 5.18 Calibration plot between current and concentration of liothyronine in the range 1-5µg/mL.....	98
Figure 6.1. Electrode fabrication steps for the development of electrochemical biosensor of thyroxine.....	107
Figure 6.2. Portable electrochemical analyzer with surface modified working electrode for analysis of thyroxine.....	109
Figure 6.3. UV spectra of Au-GQD in the wavelength range of 200-780nm against absorbance (au).....	110
Figure 6.4. A. SEM image of Au-GQD. B. Particle size pattern for Au-GQD.....	111

Figure 6.5. FT-IR spectra of Au-GQD in the range of 4000 cm^{-1} - 400 cm^{-1} against percentage transmittance.....	112
Figure 6.6. FT-IR spectra of Au-GQD, Au-GQD immobilized Ab and Au-GQD-Ab with thyroxine.....	113
Figure 6.7. Cyclic voltammetric curves for different stages of biosensor fabrication....	114
Figure 6.8. (A) Effect of antibody concentration on current response (B) Effect of pH on current Response.....	115
Figure 6.9. Variation of Current with change in scan rate from (10mV/s - 130mV/s).....	117
Figure 6.10. Change of peak anodic current (I_{pc}) with $v^{1/2}$ in the range of 20mV/s – 90mV/s.....	118
Figure 6.11. A. The plot shows a change in CV response with different concentrations. B. Calibration plot between current and concentration of thyroxine in the range of 5-50pg/mL.....	119
Figure 6.12. The effect of interference by liothyronine, creatinine, tyrosine, ascorbic acid and water as control.....	120
Figure 7.1 Schematic of parts of portable biosensor for determination of thyroxine.....	125

LIST OF TABLES

Table 2.1 Reference values for thyroid hormones in blood.....	11
Table 2.2. Different types of bioreceptors used in biosensors and their properties.....	15
Table 2.3 Reported levels of free T ₄ in different biological matrices of euthyroid population.....	20
Table 2.4. Summary of studies performed to develop liothyronine biosensors.....	22
Table 3.1. HPLC parameters for identification of thyroxine.....	32
Table 3.2 Different factors and levels selected for optimization study.....	36
Table 3.3. Different conditions for sonication were performed to remove thyroxine from MIP + T ₄ . The maximum peak area in Run 13 gives the best conditions for thyroxine removal.....	42
Table 3.4. Statistical parameters related to analysis of variance (ANOVA).....	43
Table 3.5. Polar, dispersive and total solid surface energy of NIP and MIP calculated using water and ethylene glycol contact angles.....	53
Table 4.1. Simulated values of circuit elements incorporated for modelling the sensor electrolyte interface, for MIP and NIP.....	64
Table 4.2. Different studies for development of thyroxine biosensors	68
Table 5.1. HPLC parameters for testing the purity of liothyronine.....	82
Table 5.2. Comparison of sensitivity other techniques for determination of T ₃	93

Table 5.3. Summary of results obtained for liothyronine tablets using MIP-Ppy biosensor and HPLC method.....	98
Table 6.1. Different reported biosensing techniques for the estimation of thyroxine biosensors.....	121
Table 7.1. Results of different techniques for analysis of thyroid hormones.....	124

LIST OF ABBREVIATIONS

S. No	Abbreviation	Complete Name
1.	Ab	Antibody
2.	AFM	Atomic Force Microscope
3.	ANOVA	Analysis of Variance
4.	CLIA	Chemiluminescence Immunoassay
5.	cm ⁻¹	Centimeter Inverse
6.	Da	Dalton
7.	CV	Cyclic voltammetry
8.	EDC	1-Ethyl-3-(3-dimethylaminopropyl)-carbodiimide
9.	EIS	Electrochemical Impedance Spectroscopy
10.	FT-IR	Fourier Transfer Infrared
11.	I _{pa}	Peak Anodic Current
12.	I _{pc}	Peak Cathodic Current
13.	ITO	Indium Tin Oxide
14.	GQD	Graphene Quantum Dots
15.	HPLC	High Performance Liquid Chromatography
16.	LOD	Limit of Detection
17.	MIP	Molecular Imprinted Polymer

18.	M	Molar
19.	mM	Millimolar
20.	Nm	Nanometer
21.	NIP	Non-imprinted Polymer
22.	NHS	N-hydroxysuccinimide
23.	PANI	Polyaniline
24.	Py	Pyrrole
25.	Ppy	Polypyrrole
26.	ppm	Parts Per Million
27.	pg/mL	Picogram/milliliter
28.	RIA	Radio Immunoassay
29.	r^2	Coefficient of Determination
30.	SEM	Scanning Electron Microscope
31.	Sqrt	Square Root
32.	T ₄	Thyroxine
33.	T ₃	Liothyronine
34.	TSH	Thyroid Stimulating Hormone
35.	UV	Ultraviolet
36.	V	Voltage

LIST OF SYMBOLS

S. No	Symbol	Name
1.	μg	Microgram
2.	μL	Microliter
3.	μA	Microampere
4.	Ng	Nanogram
5.	$^{\circ}\text{C}$	Degree Celsius
6.	Γ	Surface Tension
7.	Λ	Wavelength
8.	Ω	Ohm
9.	%	Percent
10.	N	Scan rate



Chapter 1

Introduction

Thyroid disorders affect the biological and functional aspects of the human body. The two major types of thyroid disorders are hypothyroidism and hyperthyroidism (Leso et al., 2020). Thyroxine is one of the common biomarkers for the diagnosis of thyroid disorders. The levels of thyroxine in the blood of a normal human body are in the range of 9pg/mL -18 pg/mL. In hypothyroidism, the thyroid gland does not produce sufficient thyroid hormone for the body's requirements. People with hypothyroidism may experience heart disease, fatigue, increased body weight, and unhappiness, and eventually, it can result in compromised quality of life. In hyperthyroidism, excess of thyroid hormones is produced in the body. Hyperthyroid patients suffer from, fatigue, palpitations tremor, anxiety, sleep disturbance, weight loss, heat intolerance, polydipsia and sweating (De Leo et al., 2016).

The major reason for hypothyroidism in several underdeveloped parts of the world is the deficiency of iodine in food (Chiovato et al., 2019). Hypothyroidism is one of the most common disorders in almost all parts of the world (D'Aurizio et al., 2023). The prevalence of thyroid disorders is more than 10.95% in India (Unnikrishnan et al., 2013), 4.3% in the United States of America (Chiovato et al., 2019), 2% in the United Kingdom (Werhun et al., 2013), 0.5% in Australia (S. J. Kim et al., 2008), 14% in Korea (H. Kim et al., 2020), and 10.5% in Croatia (Strikić Đula et al., 2022). Moreover, it has been observed that the incidence of thyroid disorders in females is at least 5 times higher than in males (Gietka-Czernel, 2017).

Presently, chemiluminescence immunoassay (CLIA), radioimmunoassay, and chromatographic-mass spectroscopy-based techniques are used to assess the T₄ levels in the blood (Collier et al., 2011). These techniques require skilled professionals, costly consumables, and prolonged testing time. Alternatively, biosensing techniques are emerging as rapid, cost-effective, and highly specific methods of analysis. With increasing advancements in technology several biosensing platforms are developing rapidly. The first thyroxine biosensing

technology was developed in 2004, however since then, thyroxine biosensor development has advanced relatively slowly. From finger-prick based devices to continuous monitoring systems, glucose sensors have come a long way. On the other hand, the market does not have any T₄ biosensors of this kind. (Staal et al., 2018). The present research is envisaged for the development of a biosensing technique for the estimation of thyroid hormones.

Liothyronine (T₃) is the other important thyroid hormone which is an active form of thyroxine and has more potent action than thyroxine. Liothyronine is presently explored as an adjunct drug to be used with thyroxine as a hormonal replacement therapy for the treatment of hypothyroidism (Spencer, 2000). The market retail cost of liothyronine tablets is around Rs 1500 per bottle with 100 tablets containing liothyronine in the range of 5-100µg in one tablet. Liothyronine tablets have been shown to have poor stability which results in product recalls. In addition to the high cost of liothyronine tablet it has shown to have poor stability resulting in product recalls. In December 2023, Sun Pharma (a major pharmaceutical company) recalled 96192 bottles of liothyronine sodium due to poor product quality (The Times of India, 2023). To check the quality of tablets under various manufacturing and storage conditions, rapid and robust testing methods for liothyronine estimation are required.

In this work, biosensing techniques were developed for estimating thyroxine and liothyronine in different biological and pharmaceutical matrices respectively. The thyroxine biosensor was developed using molecular imprinted polymer method and antibody-based method which is sensitive enough to measure thyroxine in saliva and blood. Liothyronine biosensor was developed to estimate levels of liothyronine in commercial tablets.

Aim of PhD Project

Design and Development of a Point of Care device using Nano-transducers for Monitoring and Analysis of Thyroid Hormones

Objectives of PhD Project

- 1a. To fabricate nano-transducer surfaces for selective recognition of thyroid hormones.
- 1b. To synthesize molecularly imprinted polymers (MIPs) for selective recognition of thyroid hormones.
- 2a. To develop and optimise thin films of MIP which are mechanically flexible, conductive, and capable of detecting thyroid hormones.
- 2b. To develop and optimise an antibody-antigen based sensor for detecting thyroid hormones.
- 3a. To integrate the film system with a portable electronic controller.
- 3b. Performance-based evaluation of the optimized sensing system in various sample matrices (blood/urine/sweat/saliva).

Chapter Schemes

Chapter one (present chapter) discusses the background, objectives, and motivation for pursuing this project.

Chapter two presents the literature about the thyroxine, liothyronine and their existing biosensing techniques. It also gives insights about different elements required for the development of a biosensor.

Chapter three presents the chemical synthesis of molecularly imprinted polymer (MIP) using pyrrole as the functional monomer. The optimization study was performed to generate the highest imprinting factor. The product was characterized using Atomic Force Microscope (AFM), Fourier Transform Infrared (FT-IR) spectroscopy, and contact angle analysis. The synthesized and characterized material was stored for further electrochemical studies.

Chapter four discusses the electrochemical analysis (cyclic voltammetry, and electrochemical impedance spectroscopy) of synthesized MIPs coated onto Indium Tin Oxide (ITO) electrode surface for determination of thyroxine. The biosensor was developed to analyse the concentration range of 5pg/mL - 50pg/mL. This range covers the normal levels of thyroxine in biological matrices (blood and saliva). Further, the response of developed biosensor was studied by spiking 50pg/mL of thyroxine in human saliva. The concentration of recovered thyroxine after spiking thyroxine was found by electrochemical analysis was between 96%-115.2%. The developed ultra-sensitive biosensor can be used as an alternative technique for the estimation of thyroxine in blood and saliva.

Chapter five discusses the electrochemical synthesis and deposition of a thin conducting film of molecularly imprinted polymer onto the ITO electrode for the biosensing of liothyronine (T₃). This is the first time that MIP based biosensor was developed for liothyronine. Pyrrole was used as a functional monomer for the synthesis of polypyrrole based MIPs. The characterization studies of synthesized MIPs were performed with AFM, FT-IR, and CV. The biosensor was developed to

analyse the concentration range of 50pg/mL - 300pg/mL. This developed biosensor was used for the determination of liothyronine tablets. It has the potential to be used as an alternate for assay of liothyronine in different pharmaceutical dosage forms.

In *sixth chapter*, detailed insights abouts the study of electrochemical biosensor developed by using antibodies as a recognition element for the detection of thyroxine are given. Gold-graphene quantum dots were used as the nanomaterial for the immobilization of the anti-thyroxine antibody. Characterization for the synthesized nanomaterial was performed with scanning electron microscope (SEM), FT-IR, and UV-Visible spectrophotometer. The electrochemical response was analyzed using cyclic voltammetry. Electrochemical sensor performance was studied by measuring current-concentration response, the effect of antibody concentration, the effect of scan rate, effect of pH. The developed sensor showed linearity in the range of 50pg/mL -300pg/mL. This sensor has the potential to be used for the estimation of thyroxine in biological matrices.

Chapter seventh gives the conclusion and summary of the complete project. It highlights the application of the study and gives the future directions for biosensors-based estimation of thyroid hormones.

Chapter 2

Literature Review: Thyroid Hormones and existing Biosensing Techniques

2.1. Introduction

Thyroid hormones are secreted in the body through the Hypothalamus-Pituitary-Thyroid axis. The hypothalamus in the brain secretes a chemical called thyrotropin-releasing hormone (TRH). The anterior pituitary gland secretes thyroid-stimulating hormone in response to TRH which subsequently stimulates the thyroid gland to secrete two essential hormones thyroxine (T_4) and liothyronine (T_3) (Chiamolera et al., 2009). In humans, around 80% of T_4 and 20% of T_3 is secreted by the thyroid gland (Figure 2.1). With the help of deiodinase enzyme, the peripheral tissues convert around 50% of T_4 to T_3 , which is its active metabolite. Both these hormones show their action by binding to thyroid receptor proteins present in the nucleus of the cell.

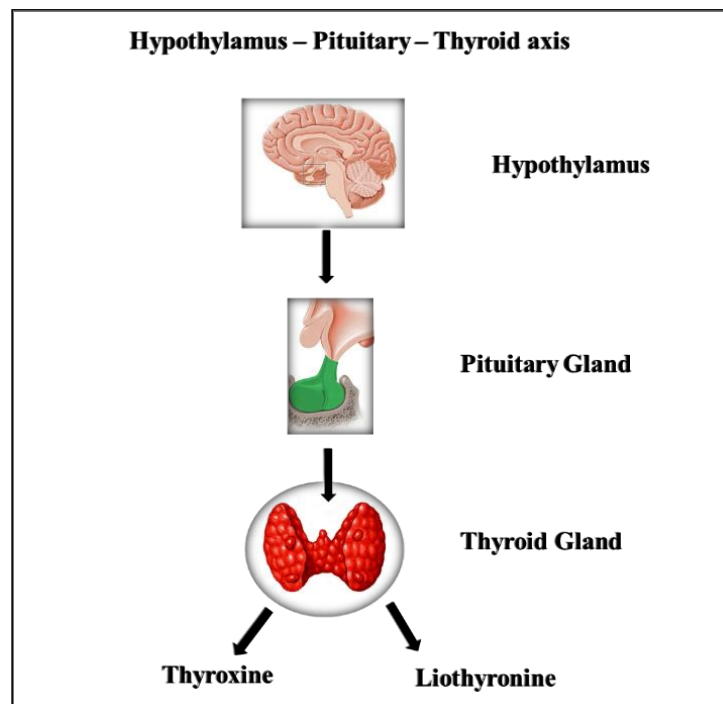


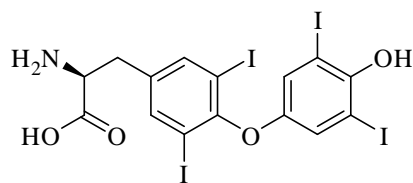
Figure 2.1. Description of the physiological mechanism for the release of thyroid hormones in human body

Thyroid hormones play a major role in metabolism of human body. It directly influence the transcription of DNA to increase the metabolism by increasing the frequency of protein synthesis, gluconeogenesis, the mobilization of glycogen stores, *etc* (Fröhlich et al., 2021; Mullur et al., 2014). The physico-chemical properties of T₄ and T₃ are discussed in the next sections.

2.1.1. Thyroxine (T₄)

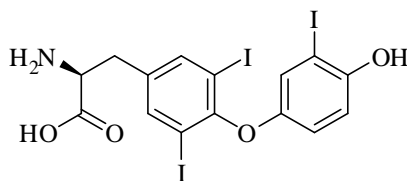
T₄ is the major hormone that influences the metabolism in the human body. T₄ is also prescribed in the form of levothyroxine as hormonal replacement therapy to patients suffering from hypothyroidism. Underdosing on levothyroxine can cause blood pressure abnormalities, metabolic alterations, hyperlipidemia, heart failure, and depression (Danzi et al., 2003; Kostoglou-Athanassiou et al., 2010; Romero-Gómez et al., 2019). Overdosing of levothyroxine, on the other hand, can cause hair loss in people (Yerawar et al., 2019). As a result, it is critical to maintain and monitor the hormone's balanced levels in the body.

Synthetic form of T₄ exists as sodium salt. It melts in the range of 231 - 323°C. It is insoluble in water, ethanol, and most organic solvents but is soluble in acidic or basic ethanol and in dilute alkali hydroxide (Wu, 2022). The pH affects the solubility of T₄, the solubility decreases as pH increases from 1 to 3, it remains constant between 3 and 7, and increases above pH 7 (Kaur et al., 2021). It has three ionizable functional groups, a carboxyl, phenolic hydroxyl, and an amino group with pK_a values of 2.4, 6.9, and 10.1, respectively. T₄ can exist in unionized, cationic, anionic, dianionic, and zwitter ionic forms. It is highly sensitive to sunlight, humidity, and temperature (Collier et al., 2010; Ledeți et al., 2020). The structure of thyroxine is given in figure 2.2. It shows reddish-pink color when reacted with nitrous acid followed by ammonia solution. This reaction was earlier used as an identification test for thyroxine and was named as Kendall-Osterberg color reaction after the scientists Kendall and Osterberg (Kendall, 1926; Anthony et al., 1958).



Thyroxine

(*S*)-2-amino-3-(4-(4-hydroxy-3,5-diiodophenoxy)-3,5-diiodophenyl)propanoic acid



Liothyronine

(*S*)-2-amino-3-(4-(4-hydroxy-3-iodophenoxy)-3,5-diiodophenyl)propanoic acid

Figure 2.2. Structure of thyroxine and liothyronine

Environmental stability is a major concern with both thyroxine and liothyronine. pH is an important factor that can affect the stability of T₄ in solution state. In most electrochemical methods an electrolyte solution such as potassium ferri-ferrocyanide is used to measure the response. Hence, pH of the electrolyte solution becomes a critical parameter. The stability of the *levo* form of T₄ increases at pH 8 while it reduces at a lower pH (Svirskis et al., 2018). Reports also showed that levothyroxine remains stable in 0.9% sodium chloride solutions (Strong et al., 2010).

2.1.2. Liothyronine

Liothyronine (T₃) is another important hormone secreted by the thyroid gland that regulates metabolism of human body. The sodium salt of T₃ is used in combination with thyroxine in the treatment of hypothyroid patients who do not respond to thyroxine alone (Jonklaas et al., 2021). T₃ also improves dermal heat loss and hair growth (Bjerkreim et al., 2021; Safer et al., 2001). Physiologically, around 35% of thyroxine gets converted to liothyronine by undergoing deiodination in the presence of enzyme 5-deiodinase in peripheral tissues (figure 2.3) (Thienpont et al., 2010).

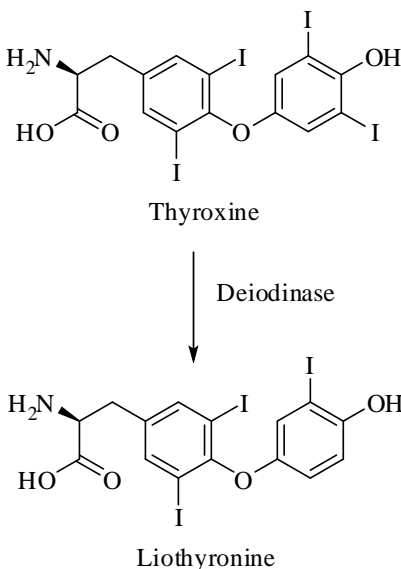


Figure 2.3. Conversion of thyroxine to Liothyronine

It has a molecular weight of 650Da, and melting point of 230°C. It is insoluble in water, and organic solvents but dissolves in dilute alkalis by forming sodium salt.

Thyroid Stimulating Hormone (TSH) is a peptide hormone produced by the anterior pituitary. It has two chains: an alpha chain and a beta chain. Its molecular mass is around 28,000 Da. The chemical composition of TSH is very similar to other glycoprotein hormones produced by the anterior pituitary (Danzi et al., 2003).

Thyroxine (T₄), liothyronine (T₃), and thyroid stimulating hormone (TSH) are major biomarkers of hypothyroidism and hyperthyroidism. The normal levels of these biomarkers are given in Table 2.1 (Colucci et al., 2013). Out of these biomarkers, T₄ is the most estimated for diagnosing the disorder. In the present work, biosensors for thyroxine and liothyronine are developed.

Table 2.1 Reference values for thyroid hormones in blood

Biomarker	Method	Reference Ranges
Total Thyroxine (TT₄)	Roche Cobas	45-12.5 ug/dL
Free Thyroxine	Roche Cobas	9-25 pg/mL
Total Triiodothyronine (T₃)	Roche Cobas	80-180 ng/dL
Free Liothyronine	Roche Cobas	1.6-3.6 pg/mL
Thyrotropin (TSH)	Roche Cobas	0.3 - 4.0 mIU/L

2.2. Diagnostic Techniques for Thyroid Hormones (T₃/T₄)

The detection of thyroid hormones requires very sensitive instruments as their concentration in the human body is in the picogram/milliliter range. The sensitivity and specificity of thyroid testing procedures have had a significant impact on clinical strategies for diagnosing thyroid diseases over the last five decades. In the 1950s, thyroid testing was done for an indirect estimate of free + protein-bound thyroxine (T₄) concentration in the serum. Protein-bound iodine (PBI) and butanol extractable iodine techniques were the most commonly available tests. Since 1970, technological developments in radioimmunoassay (RIA), immunometric assay (IMA), and liquid chromatography-tandem mass spectrometry (LC-MS/MS) have gradually increased the specificity, repeatability, and sensitivity of thyroid tests. Presently, the serum-based chemiluminescence immunoassays (CLIA) technique is commonly used for the measurement of total and free thyroid hormones in blood samples (Colucci et al., 2013).

In CLIA technique, a luminescent molecule is used as a label, *i.e.* the true “indicator” of the analytic reaction. The principle of the technique is that the luminescence (emission) of visible or near visible ($\lambda = 300-800$ nm) radiation occurs when an electron transitions from a higher energy excited state to a lower energy ground state. As a result, the potential energy in the atom is released in the form of light energy. An advantage of luminescence over absorbance is that it is an

absolute measure whereas the latter is relative. However, the method has several disadvantages such as need of luminophore markers, high cost, requirement of sophisticated equipment, skilled operators, limited test panels, and closed analytical systems. Moreover, this technique is used for the determination of thyroid hormones in serum samples only (Cinquanta et al., 2017). It has also been reported that free thyroxine and free liothyronine levels are affected by interfering substances present in the blood due to interaction with the reagents used in the assay. Biotin is one such interfering molecule that can affect the results of thyroid function tests (Favresse et al., 2018). The issue is not only with the diagnostic technique but several factors related to hospitals that can affect the diagnostic results (Wu, 2022). Improper blood collection and storage were found to be the most significant ones (Couto et al., 2017; Ruuskanen et al., 2018; Tanoue et al., 2018). These factors frequently lead to incorrect or delayed diagnosis and treatment, which can have severely detrimental effects. Thus, the creation of next-generation diagnostic tools is necessary for the accurate and timely identification of thyroid disorders. Biosensors are emerging diagnostic platforms that analyse target molecules with high sensitivity and selectively.

International Union of Pure and Applied Chemistry (IUPAC) defines a biosensor as “an independently integrated receptor transducer device, which is capable of providing selective quantitative or semi-quantitative analytical information using a biological recognition element” (Luka et al., 2015). Biosensors have several advantages over traditional analytical approaches, such as real-time detection, cheap cost, simplicity, and compactness. These biosensors have found usefulness in the area of biomedical sciences, environment monitoring, industrial monitoring and point-of-care diagnostics.

Biosensors consist of biological elements, transducers, and signal processors (Figure 2.4). Biological elements dictate the selectivity and specificity that allows the biosensor to respond to a specific target or group of analytes, decreasing the possibility of interference with undesired substances. The biological recognition elements are immobilized on sensor surface using different methods such as

adsorption, covalent binding, entrapment, and membrane confinement (Karunakaran et al., 2022).

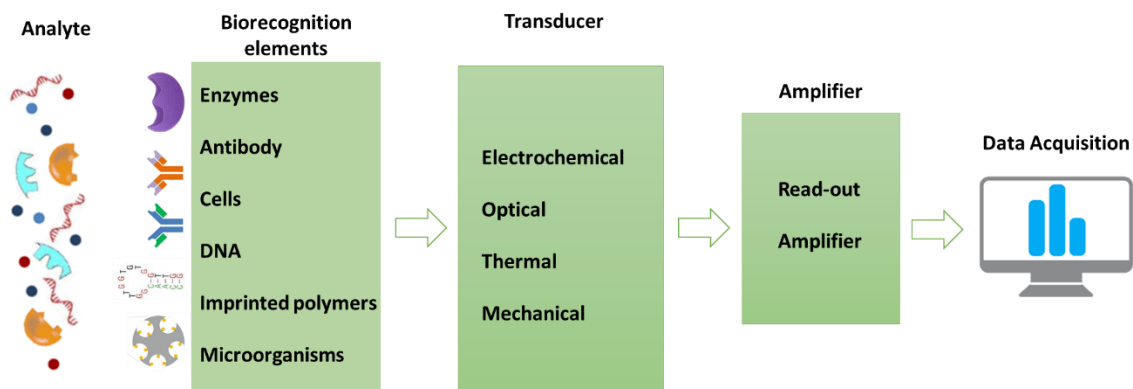


Figure 2.4. Different elements of a conventional biosensor

Different biorecognition elements used are summarized in table 2.2. The most common types of transducers are based on electrochemical, optical, colorimetric, gravimetric, piezoelectric and magnetic detection. The transducer transforms the biomolecule-analyte interaction into a measurable signal.

2.2.1. Biorecognition Elements

The biorecognition element is the most essential part of fabrication of any biosensor. It provides specificity for the estimation of the target molecule. The most used bioreceptors are antibodies, enzymes, aptamers, and molecularly imprinted polymers (table 2.2).

Table 2.2. Different types of bioreceptors used in biosensors and their properties

S. No.	Bio-receptors	Advantages	Drawbacks	References
1	Antibody	High specificity and sensitivity	Poor stability, high cost due to larger size, difficult to immobilize properly on transducer surface	(Arshavsky-Graham et al., 2022; Sharma et al., 2016)
2	Aptamer	Chemical stability, versatile design, high sensitivity	Affinity with target vary with concentration	(McConnell et al., 2020)
3	Enzyme	High sensitivity and specificity, portability, cost-effective	Membrane biofouling, electrode passivation or membrane biodegradation, Not available for all molecules	(Fopase et al., 2020; Rocchitta et al., 2016)
4	Molecular imprinted polymer	High sensitivity and specificity, cost-effective, higher stability, and shelf life	Requirement of <i>in-silico</i> studies for monomer selection, Optimization of template removal	(Crapnell et al., 2020; Rajpal et al., 2022)

2.2.1.1. Antibodies

Since antibodies (Abs) have such high antigen specificity, they have become the most widely employed bioreceptors. The electrochemical/optical response changes because of Ab's interactions with the target analyte; this change may be quantified and is correlated with the target concentration. The immobilization of Ab is a critical factor as the antigen binding site should be accessible for the recognizing antigen. Both covalent and non-covalent immobilization are frequently employed methods for antibody entrapment. The basis of non-covalent interaction is the electrostatic forces that exist between Ab and the sensor surface. Covalent immobilization is made by the interaction between certain reactive groups on the sensor surface (or nanomaterials coated on the sensor surface) and on Ab.

The amine group on the lysine amino acid of Ab is typically used for covalent interaction with a carboxylic group found on nanomaterials. Alternatively, a very reactive succinimide ester of a carboxylic group is created by combining N-hydroxysuccinimide (NHS) and 1-ethyl-3-(3-dimethylaminopropyl)-carbodiimide (EDC). The orientation of Ab can be controlled considerably more effectively via thiol group coupling. -SH groups are added to Ab for thiol coupling and the sensor surface for thiol disulfide exchange (Feysa et al., 2013; Sharma et al., 2016).

2.2.1.2. Aptamers

Aptamers are single-stranded DNA or RNA sequences produced through systematic evolution of ligands by exponential enrichment. These have the ability to fold into secondary and tertiary sequence geometries and are capable of identifying a wide range of target analytes, such as metal ions, microbes, cancer cells, and tiny compounds (Keefe et al., 2010; Ning et al., 2020).

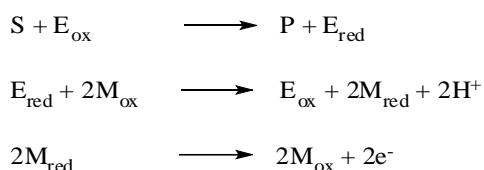
The aptamers are selected by following a series of steps, (a) a library of oligonucleotides is created by combinatorial chemistry, (b) the target molecule is incubated with the library of molecules for several minutes, (c) aptamer-target complexes are collected and washed, (d) target is replaced with analogs and incubation is done and the nucleic acid sequences which are bound to analogs are removed, and (e) sequences which bind the target are amplified using PCR (polymerase chain reaction). This cycle is repeated to obtain an aptamer with high specificity (Ning et al., 2020). The aptamers act similar to that of Abs as interaction of an analyte with the aptamer causes a change in response which is correlated with the concentration of analyte.

2.2.1.3. Enzymes

Principle of enzyme-based biosensors is based on their capability to transform the substrate into an electroactive material. The response produced by the transducer is correlated to the electroactive material. Dehydrogenases and oxidases are two common categories of enzymes used for biosensing. Some of the examples include

glucose oxidase for sensing β -D- glucose, glutamate oxidase for sensing L- glutamate, and ethanol dehydrogenase for sensing ethanol.

Enzyme based biosensors have undergone evolution from the first generation of sensors to third generation of sensors. In first generation of biosensors the products or analytes permeate to the transducer surface and cause a reaction. In second-generation biosensors mediator (ferro-ferricyanide, methylene blue, etc.) is employed to operate as electron carriers and increase the current response. The reaction involved in 2nd generation of enzyme-based sensor are:



S is substrate, E is enzyme M is the redox mediator

In third-generation biosensors, direct transfer of electrons occur between enzyme and electrode surface, and the process relies on bio-electrocatalysis. Three elements of third-generation biosensor are: the enzyme (bio-recognition element), the redox probe (for signal propagation), and the sensor electrode. Third-generation biosensors are still at the stage of development and are relatively uncommon (Ning et al., 2020).

2.2.1.4. Molecularly Imprinted Polymers

MIPs have gained a lot of attention for biosensing application in the past two decades. The major reason better longer shelf life and chemical stability as receptors.

A functional monomer, such as pyrrole, aniline, dopamine, etc., is chosen for the synthesis of molecularly imprinted polymer. It is then combined with the analyte be evaluated before polymerization. After that, the mixture is polymerized using an electrochemical, photolytic, or chemical process (figure 2.5). The analyte gets entrapped inside the conjugated monomer units. In the next step, the analyte is removed from the polymer matrix usually by sonication with suitable solvents.

After removal of the analyte, cavities are formed which have the shape of the removed analyte (Mustafa et al., 2022; Rajpal et al., 2022). This process is known as the imprinting of a molecule on a polymer matrix. The cavities which are formed by the process of imprinting are specific for the analyte for rebinding (Mustafa et al., 2022).

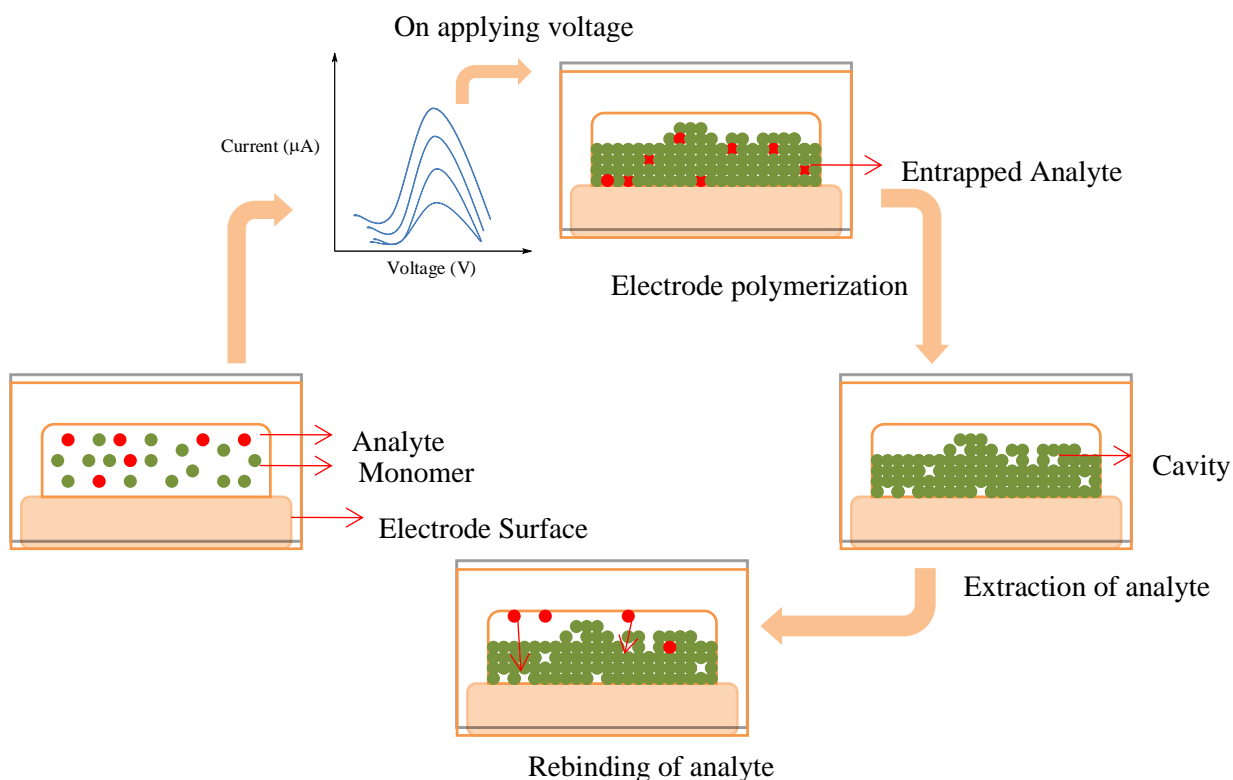


Figure 2.5. Steps in the preparation of molecularly imprinted polymer via electrode polymerization

The polymers formed from monomers such as pyrrole, aniline, *etc.* have π bond conjugation system due to which these polymers are conductive (Yussuf et al., 2018). These are complexes that can transfer the charges. They exist in two forms: reduced and oxidized form (as shown in Figure 2.6). Emeraldine base is the reduced form and is non-conductive which gets converted to salt form on the addition of a dopant (here HCl). In the presence of HCl, defects (holes) are formed in the polymer network which enables electrons to move through the polymer network and hence, increases the conductivity of the polymers (Tang et al., 2011).

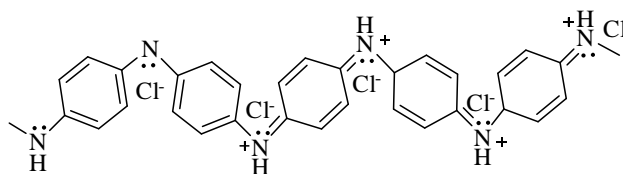


Figure 2.6. Conductive and non-conductive forms of polyaniline synthesized by oxidative polymerization of aniline monomer

2.3. Matrices for the study of Thyroid Hormones (T₄/T₃)

Thyroxine and liothyronine are present in blood, saliva, sweat, tears, urine, hairs etc (Elson et al., 1983; Orden et al., 1987). Thyroxine is a more commonly used biomarker for diagnosing thyroid disorder and hence, its levels are more commonly estimated. Blood is the most used matrix for the analysis of thyroxine. Blood is centrifuged and serum for final analysis. Around 2-4 mL of blood is required for the complete thyroid profile (estimation of T₄, T₃, and TSH). Moreover, sampling time and food intake also affect the final results (Mahadevan et al., 2017). With the advances in more sensitive techniques, the focus is slowly shifting from blood to other biological fluids that were earlier inaccessible. Saliva, urine, and sweat are some of the other matrices that resolve problems or impediments of traditional matrices as they are non-invasive, allow detection of long-term exposure, are relatively cleaner matrices, and have lesser levels of contamination (Lendoiro, 2022). The levels of thyroxine in some of the different biological matrices are described in table 2.3.

Table 2.3 Reported levels of free T₄ in different biological matrices of euthyroid population

<i>S. No.</i>	<i>Biological Matrix</i>	<i>Measurement Technique</i>	<i>Thyroxine levels as per reports</i>	<i>Reference</i>
1	Serum	Radioimmunoassay	45pg/mL - 125pg/mL (total T ₄)	(Thienpont et al., 2010)
2	Saliva	Radioimmunoassay	Up to 350pg/mL (total T ₄)	(Elson et al., 1983)
3	Saliva	-	Around 130pg/mL (free T ₄)	(Naresh et al., 2018)
4	Saliva	LC-MS/MS	Male: 78pg/mL ± 28.5pg/mL (free T ₄) Females: 56.4pg/mL ± 27.4pg/mL (free T ₄)	(Higashi et al., 2011)
5	Serum	Radioimmunoassay	Pregnant women: 0.96pg/mL (free T ₄)	(Khadem et al., 2012)
6	Breast milk	Radioimmunoassay	7pg/mL - 13pg/mL (free T ₄)	(van Wassenaer et al., 2002)
7.	Serum	Radioimmunoassay	6pg/mL - 13pg/mL (free T ₄)	(Wu, 2022)

Apart from biological specimens, thyroxine and liothyronine are also present in the form of pharmaceutical tablets used as hormonal replacement therapy for hypothyroid patients. In pharmaceutical tablets, thyroxine is usually present in the form of levothyroxine sodium and liothyronine is present in the form of liothyronine sodium. The levels of thyroxine and liothyronine in the tablets are in the range of 5µg –100µg (Gottwald-Hostalek et al., 2022).

2.4. Biosensors for the estimation of thyroxine and liothyronine

Researchers have explored the biosensing techniques for the estimation of thyroxine and liothyronine. When compared to other biological molecules such as glucose, cortisol, and dopamine the biosensing studies performed for thyroxine and liothyronine are significantly less (Kinnamon et al., 2017; Liu et al., 2021). One of the major reason for this could be very low concentration of these hormones.

David et al. developed an electrochemical biosensor based on differential pulse voltammetry (DPV) for the estimation of thyroxine. The team used carbon nanotubes and gold nanoparticles which were coated on screen-printed electrodes for the selective estimation of thyroxine. The limit of detection (LOD) for this method was 30nM (David et al., 2022). Another technique developed by Smajdor et al. used renewable mercury film silver-based electrodes to study the voltametric response for thyroxine. Differential pulse stripping voltammetry was used for the determination. The methods showed a LOD of 18nM. This method was used to determine the levels of thyroxine in the pharmaceutical tablets (for 3 different brands; Euthyrox, Letrox, Eltroxin) and the recovery was found to be in the range of 98-106% (Smajdor et al., 2016). Hu et al. studied the effect of surfactant cetyltrimethylammonium ammonium bromide on the electrochemical response at the carbon paste electrode. The response was significantly increased as it increases the interaction of thyroxine at the hydrophobic electrode surface. The limit of detection for the developed method was further improved to 6.5nM (Hu et al., 2004). More recently, Park et al. developed a biosensing technique using DNA aptamers. They used a rhodium nanoplate heterolayer for the amplification of response and immobilizing the aptamers. The response was studied using cyclic voltammetry and electrochemical impedance spectroscopy. The limit of detection was found to be 11.4pM (Park et al., 2020).

In 2022, Mradula et al. developed a biosensor by immobilizing thyroxine-specific monoclonal antibody (Ab) onto copper metal-oxide framework (Cu-MOF) and polyaniline (PANI) composite which was coated on screen-printed carbon electrode (SPCE). The detection limit obtained with cyclic voltammetry was found to be as low as 0.33 pM. The method showed more than 90% recovery on spiking in blood serum (Mradula et al., 2021).

Liothyronine biosensors have not been explored much when compared with thyroxine biosensors. There exists huge scope for the studies on liothyronine biosensors especially with respect to the use of different bioreceptors. Although, immunological bioreceptors such as antibodies and enzymes have been used but

more robust bioreceptors such as molecular imprinted polymers and aptamers have not yet been studied. Some of the studies on liothyronine biosensors are mentioned in table 2.4.

Table 2.4. Summary of studies performed to develop liothyronine biosensors

Electrode	Materials	Method	Sensitivity Range	References
Gold Electrode	Gold nanoparticles coated with anti-T ₃ antibodies	Impedance Spectroscopy	10 - 10 ⁵ pg/mL r ² = 0.946 LOD~10pg/mL	(Nguyen et al., 2020)
Carbon paste electrode	Enzyme modified carbon paste	Amperometry	340 - 17x10 ³ pg/mL r ² = 0.997 LOD: 270pg/mL	(Aboul-Enein et al., 2002)
Glassy carbon electrode	Fe ₃ O ₄ @graphene nanocompositecoated with anti-PDIA3	Differential pulse voltammetry	10 - 200 μM r ² =0.997 LOD: 27nM	(Baluta et al., 2023)
Microcolumn coated with T ₃	Anti-Triiodothyronine monoclonal antibody	Flow fluorimeter	0.1 - 30ng/mL	(Wani et al., 2016)

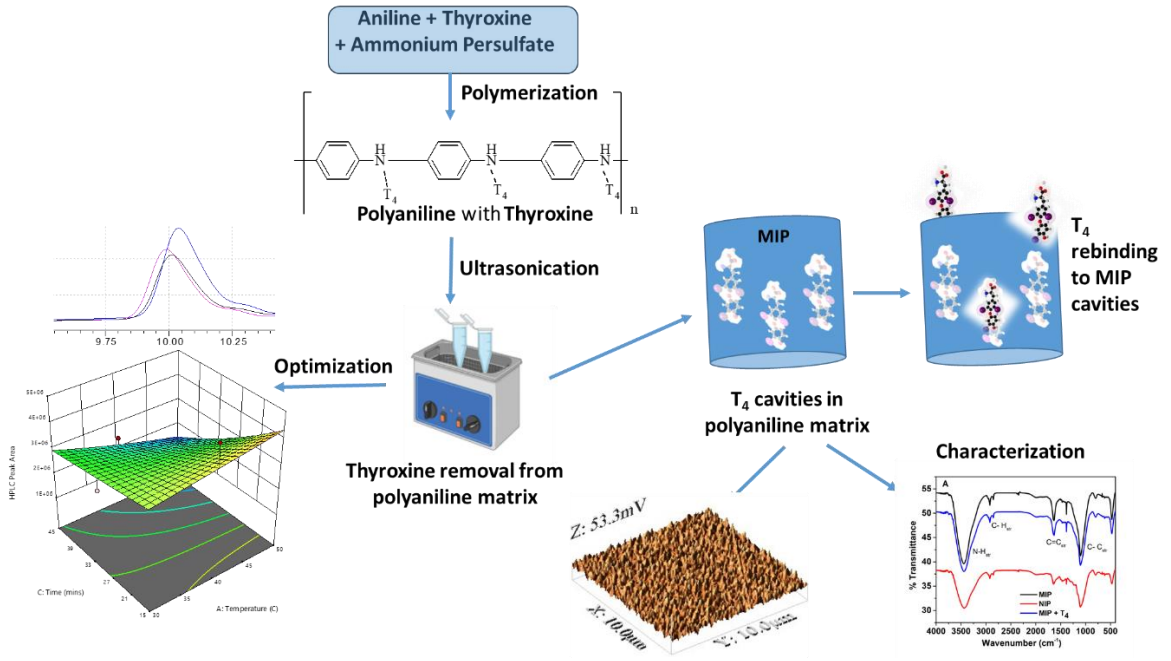
2.5. Conclusion

This chapter presents important aspects related to thyroid disorder, common biomarkers for thyroid disorder and physicochemical properties of these biomarkers. It also includes the basic principles of biosensors including its working, design, elements, applications *etc.* In the last section of this chapter, the previous studies for the development of biosensors of thyroxine and liothyronine are discussed. In the next chapter, the methodology for the synthesis of molecular imprinted polymers as biorecognition element is discussed.

Chapter 3

Synthesis, Characterization,
and Optimization of
Molecular Imprinted
Polymer for Biosensing of
Thyroxine

Graphical Abstract



Abstract

In the present work, molecularly imprinted polymer was synthesized using oxidative polymerization of aniline mixed with thyroxine in presence of ammonium persulfate. After the product was formed, thyroxine was removed from the polymer matrix to generate imprinted cavities. The removal conditions were optimized using response surface methodology. In the optimization process, Box Behnken design was applied as a response surface methodology using Design Expert software. Sodium hydroxide (NaOH) concentration, temperature and sonication time were studied at 3 different levels. The response of thyroxine removed from the polymer matrix after sonication was studied using high performance liquid chromatography (HPLC). The most suitable conditions for the removal of thyroxine were 75mM NaOH concentration, 40⁰C temperature and 15 mins of sonication time. The imprinting factor for the synthesized MIPs was found to be 1.98. The characterization of synthesized molecular imprinted polymer was done with fourier transform infrared spectroscopy (FT-IR), atomic force microscope (AFM) and contact angle studies. The synthesized molecular imprinted polymer was stored at room temperature for further use as a biorecognition element in electrochemical studies.

3.1. Introduction

Molecularly imprinted polymers (MIP) are synthetic polymers with complimentary cavities designed to selectively bind specific target molecules. The mechanism of interaction is like 'lock and key model'. They are used as synthetic antibodies with the advantage of better shelf life and environmental stability (Mostafa et al., 2021). More than 1000 papers are published on MIPs every year. Apart from their application in sensing, they have shown usefulness in several other areas such as binding assays, HPLC columns, solid phase extraction and as catalysts (Beckskereki et al., 2021).

MIP is synthesized in three different steps, (a) formation of template monomer complex (b) polymerization of monomer (c) extraction of template molecule (Shafqat et al., 2023). Different types of molecularly imprinted polymers are synthesized using different monomers as the starting materials. Most commonly used monomers for the synthesis of conducting polymers are pyrrole, aniline, acetylene, thiophene, carbazole, 3,4-ethylenedioxythiophene, phenylene and fluorene (Lakard, 2020). The structures of functional monomers are given in figure 3.1. The presence of conjugated π bond network helps these organic monomers to form a conductive polymers (Rasmussen, 2020). Out of all these monomers, pyrrole and aniline are most used for molecularly imprinted polymer synthesis. The advantage of using pyrrole and aniline as functional monomer includes their high-water solubility, ease of polymerization and formation of robust conductive polymer. Although, polyaniline is the first commercial conductive polymer but pyrrole has been shown to have higher pH stability as compared to polyaniline (Luong et al., 2020).

The template is added in the monomer solution and the solution is allowed to stand for some time so that monomer and template forms a bond. The type of bond formed between monomer and the analyte molecule can be covalent, non-covalent or semi-covalent. Non-covalent bonding is relatively easier to get broken during the removal process as compared to covalent bonding (Qi et al., 2010). The

polymerization can be induced either with the help of an initiator such as ammonium persulfate or it can be done electrochemically (Berkes et al., 2015; Nasajpour-Esfahani et al., 2023). After polymerization step, the added template is removed from the polymer to generate the cavities. The removal of analyte can be performed by ultrasonication, soxhlet extraction, microwave assisted extraction, supercritical fluid extraction *etc* (Lorenzo et al., 2011). After the MIP is synthesized it is separated, dried and stored till further use.

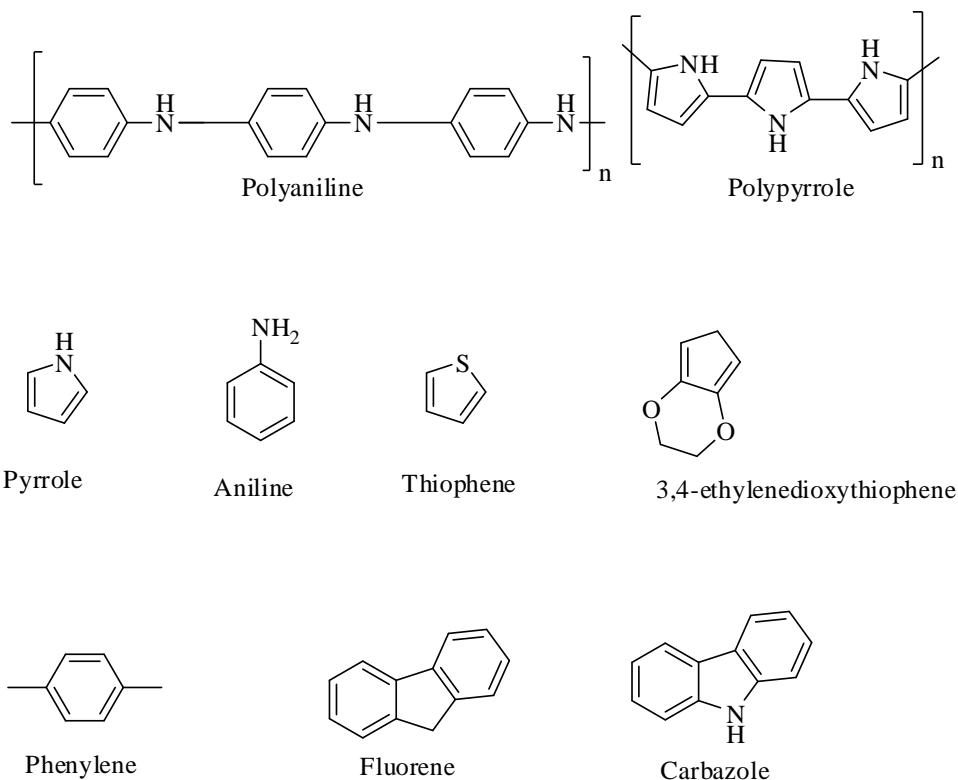


Figure 3.1. Structures of functional monomers

In general, the synthesis and characterization of MIPs can be summarized as the following flow chart (figure 3.2).

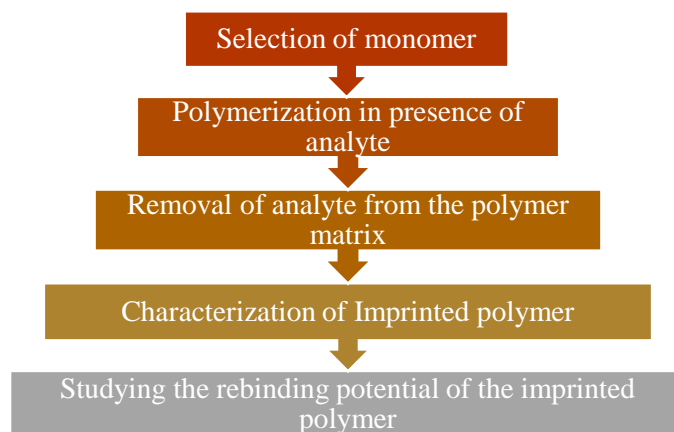


Figure 3.2. Flow chart showing all the steps involved in synthesis of MIPs

Optimization studies are performed for different stages of MIP synthesis. Mostly optimization aims to find the best parameters for ensuring (a) stable template-monomer adduct is formed, (b) template removal is complete and (c) proper rebinding of analyte occurs with the imprinted polymer. Out of the above three stages the most critical one is the removal of template after polymerization. The factors that affect the removal of template include solution pH, temperature, nature of solvent and removal time. Different types of solvents are used for the removal of analyte from the polymer matrix (Garg et al., 2024). Acids such as acetic acid, hydrochloric acid or sulfuric acid are used for removal of template for different molecules in the process of imprinting. The choice of acid depends on different conditions as it can affect other processes as well including polymer stability, interaction between polymer and monomer etc.

Several studies have used acids for template removal during the process of synthesis of MIPs. Troponin imprinted polyaniline was synthesized where 0.5M acetic acid was used for removing troponin from the polyaniline matrix (Phonklam et al., 2020). 5% acetic acid was used by Uygun et al. for the removal of cortisol from the polymer matrix during the development of its electrochemical biosensor (Uygun et al., 2020).

Solvents based template removal has also been tried by many researchers. Generally, acetone, methanol and ethanol have been used for this condition. These

solvents are relatively easier to use and safer as compared to acids. Byun et al. used toluene and ethanol for removal of aspirin from the polymer matrix (Byun et al., 2010). Zhu et al. used acetic acid and methanol mixture (1:9 v/v) to remove kaempferol from the polymer to generate MIPs (Zhu et al., 2011). Methanol causes increase in the solubility of template molecules which results in the shrinkage of polymer. This forces the dissociation of the polymer-template complex; hence, template cavities are generated. Dilute alkalis have also been used for template removal. Valentino and group used sodium hydroxide for the removal of dimethoate from the polypyrrole matrix (Valentino et al., 2023).

Another technique which has been followed for template removal is the use of salts and surfactants. Sodium chloride and sodium dodecyl sulfate (SDS) have been used for the template removal process. Salts change the microenvironment around the template and the polymer that affects their interaction. Rehmati et al. used dilute sodium chloride (0.1M) to remove virus from polydopamine matrix (Rahmati et al., 2022). Surfactants are commonly used for removal of protein templates. In presence of surfactant, proteins undergo denaturation which eventually results in their elution from the polymer matrix (Garg et al., 2024). Cui et al. used 0.34M SDS for the removal of cancer biomarker (CD44) for the synthesis of alginate based MIPs (Cui et al., 2022).

3.2. Experimental

3.2.1. Materials

Thyroxine sodium (MW: 888.92 Da, > 97% using HPLC) was procured from Macleods Pharmaceuticals Limited, India. Aniline (MW: 93.13 Da, \geq 99%), hydrochloric acid (35%) and dimethyl sulfoxide were procured from Rankem (India). Ammonium persulfate (MW: 228.18 Da \geq 99%) was procured from Loba Chemie Pvt. Sodium hydroxide and sodium chloride were procured from Rankem (India). High Performance Liquid Chromatography (HPLC) grade methanol was procured from Rankem (India) and ultrapure water (resistivity \sim 18.2 Ω cm at 298 K) was used from the in-house water purification system (Milli-Q system Millipore

Bedfords, MA, USA). Potassium dihydrogen phosphate (KH_2PO_4 ; MW: 136.08 Da $\geq 99\%$) and di-sodium hydrogen phosphate (Na_2HPO_4 ; MW 141.9 Da, $\geq 99\%$) were procured both from Rankem (India). All chemicals used in the study were of analytical grade.

3.2.2. Instruments

High Performance Liquid Chromatography (HPLC; Shimadzu Prominence-i LC-2030C 3D Plus, Japan) with photo diode array detector was used for identification, characterization and rebinding studies controlled by Lab Solution software. HPLC has a deuterium lamp as a light source with spectral resolution of 1.4nm, wavelength accuracy $< \pm 1\text{nm}$. The surface morphological changes were studied using Atomic Force Microscope (AFM; Nanosurf AG, Switzerland). Tapping mode was used for AFM analysis connected with silicon carbide (SiC) tip. Characterization and template removal studies were performed using Fourier Transfer Infrared (FT-IR; Perkin Elmer) and Drop shape analyser (DSA25 Kruss, Germany). The FT-IT system has a LiTaO_3 MIR detector which covers a range of 8300cm^{-1} to 350cm^{-1} with best resolution of 0.4cm^{-1} . Ultra-Violet spectrophotometer (UV-1900 UV-Vis, Shimadzu, Japan) was used for characterization of analyte. The photometric accuracy is ± 0.0015 Abs at 0.5 Abs and ± 0.002 Abs at 1 Abs and wavelength accuracy of ± 0.3 nm for entire range of 190nm to 1100nm. Centrifugation was done with CPR 24 plus, Remi, India. Analytical weighing balance (Shimadzu AT series, Japan) was used for the accurate measurement of materials for preparation of solutions used in the study. The weighing range is 220g to 0.1g, least count of 0.1mg and an error of 1mg.

3.2.3. Methodology

3.2.3.1. Preliminary studies

Solubility studies of thyroxine were performed using water, dimethyl sulfoxide (DMSO), dilute sodium hydroxide and dilute hydrochloric acid. The identification test of thyroxine was performed using UV-spectrometer as per certificate of analysis given by the manufacturer. FT-IR and HPLC was also performed to check

the purity of thyroxine as per Indian Pharmacopoeia 2018. The characteristic peaks obtained in UV scan and FT-IR spectra were matched with the reported data in the literature.

For UV-scan, 50 ppm of thyroxine solution was prepared in 0.1N sodium hydroxide solution as mentioned in the certificate of analysis. The solution was scanned in the range of 260-400nm.

For FT-IR analysis, 2 mg of thyroxine was mixed uniformly with KBr, and a pellet was formed. This pellet was analyzed with FT-IR in the range of 4000cm^{-1} - 400cm^{-1} . Number of scans were 16 and resolution was 4 cm^{-1} .

For HPLC analysis, 20ppm solution was prepared in dilute sodium hydroxide using ultrapure milliQ water. A gradient reverse phase (C-18) method was used for the analysis of thyroxine with a run time of 20 mins. HPLC parameters for analyzing thyroxine are given in table 3.1 (Collier et al., 2011).

Table 3.1. HPLC parameters for testing the purity of thyroxine

Conditions	Parameters
Column	Reverse phase C-18 column, 4.6 mm x 250 mm and 5 μm particle size
Mobile phase	Methanol - Solvent A Phosphate buffer (1mM, pH 3) - Solvent B
Gradient	45 - 20% solvent A in 7 mins 20% Solvent A for 7 - 12 mins 20 - 45% Solvent A for 12 - 16 mins 45% Solvent A for 16 - 20 mins
Injection volume	20 μL
Flow rate	1 mL/min
Wavelength	228 nm

3.2.3.2. Synthesis of MIP and NIP

There are different ways to polymerize aniline into polyaniline such as chemical, electrochemical, photochemical *etc* (Barros et al., 2003; Ramkumar et al., 2016). Here, the chemical route for synthesizing polyaniline was performed by oxidative polymerization reaction.

Oxidative polymerization of aniline was performed using ammonium sulfate in acidic medium was performed as per the following procedure:

Solution 1: Ammonium persulfate (1.8g) in 50mL of 0.1N HCl was added.

Solution 2: 0.25mL of aniline and thyroxine (5mg) was added in 0.1N HCl (150mL) and solution was mixed thoroughly for 30 mins.

The template: monomer ratio was selected as 1: 50. This ratio was intentionally kept low because the levels of thyroxine to be determined are in pg/mL. Low ratio helps to generate cavities with desired selectivity for the target molecule as there are minimum chances for aggregation of target molecule. Solution 1 was added to solution 2 slowly with constant stirring using a magnetic bead at 300rpm. The final mixture was stirred till the formation of a blue coloured product (Pratama et al., 2020). The product was separated by filtration using whatman filter paper (grade 1). The final product was further air dried at room temperature (Abu-Thabit, 2016). It was then powdered and weighed using analytical balance (Pratama et al., 2020).

The procedure was repeated without adding thyroxine in solution 1 for synthesizing non-imprinted polymer (NIP). The synthesis of NIP (product II) helps to calculate the imprinting efficiency and to study non-specific interactions. Finally, two separate products were obtained, product I contains thyroxine molecule embedded in polyaniline matrix and product II without thyroxine molecule.

Product I was further processed to remove the thyroxine molecule and generate the thyroxine specific cavities (figure 3.3). 20mg of the product was weighed in an eppendorf tube and 1.5 mL of 0.1N of sodium hydroxide solution was added in it. The mixture was ultrasonicated for 30 mins to remove thyroxine (Hamada et al.,

2015). This step is the most critical and least researched step in molecular imprinting as it is important to maintain optimal conditions so as to avoid any damage to the generated cavities (Pirzada et al., 2021). Dilute sodium hydroxide was used as a solvent to study the removal because of higher solubility of thyroxine in it.

After sonication, the mixture was then centrifuged at 10000rpm for 10 mins at 20°C and supernatant was collected. The same procedure was performed for product II (NIP). The collected supernatants were then analyzed using HPLC. The HPLC parameters used are mentioned in table 3.1.

As the template removal process is considered as the most critical step for synthesis of MIPs, hence, different parameters affecting this process were optimized.

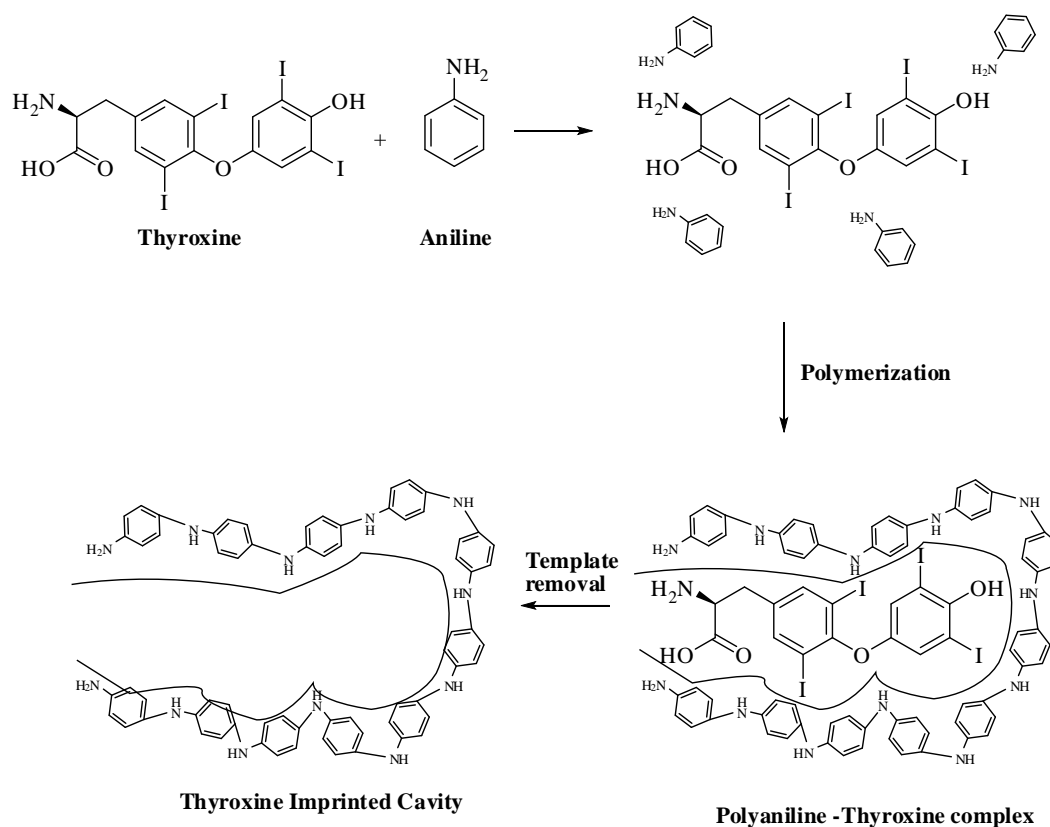


Figure 3.3. Representation of chemical structures-based formation of molecular imprinted polymers

3.2.3.3. Optimization of thyroxine removal using Design of experiments (DoE)

Several factors such as solvent, pH, temperature, extraction technique, extraction time *etc.*, have been reported to affect the removal of template from the polymer matrix (Ariani et al., 2024). Here, optimization of thyroxine removal was done by varying temperature, concentration of NaOH and sonication time. Temperature was selected as one of the critical parameters as it affects the bonding between thyroxine and polymer. The temperature range (30⁰C-50⁰C) was selected according to the stability of the thyroxine (Luong et al., 2020). Solvent was selected according to the solubility of thyroxine. Sonication time was selected as the third parameter to ensure proper removal of thyroxine.

The selected parameters were studied simultaneously using Design of Experiments (DoE) approach. DoE is used to study relationship between input variables and the response. Using DoE, multiple factors affecting a response can be studied simultaneously.

General steps for planning and conducting DOE are:

- a. Define the objectives – list of problem(s) to be studied.
- b. Response variable definition – measurable outcome based on defined objectives.
- c. Determine factors and levels – selection of factors that can affect the response variable. It is usually done using reported literature.
- d. Determine experimental design type – *e. g.* a screening design is needed for identification of critical factors; optimization design is used for optimization of conditions for best response.
- e. Perform experiment using design matrix (Durakovic, 2017).

There are different types of optimization designs such as Central Composite Design (CCD), Box Behnken Design (BBD), Factorial Design *etc* (Thorsteinsdóttir et al., 2021). In this study, the design was prepared and analyzed using Design expert 13 software (Stat ease, Minneapolis, USA). The details of study are given as:

- a. Objectives – To study maximum removal of thyroxine from the polymer after sonication.
- b. Response variable definition – HPLC peak area of thyroxine
- c. Factors and levels – Temperature, concentration of solvent (dilute sodium hydroxide solution) and sonication time (table 3.2)

Table 3.2 Different factors and levels selected for optimization study

Factors	Lower level	Intermediate level	Upper level
Temperature	30 ⁰ C	40 ⁰ C	50 ⁰ C
Concentration of NaOH	75mM	100mM	125mM
Time of sonication	15mins	30mins	45mins

- d. Experimental design type – Optimization design – Box Behnken
- e. Experiment was performed using design matrix summarized in table 3.3

Several trials were performed for template removal according to table 3.3. 20 mg of the material and 1.5 mL of NaOH solution was used for each trial. After sonication, each solution was centrifuged, and the supernatant collected was analyzed using HPLC. The response *i.e.* HPLC peak area of thyroxine was correlated with the removal efficiency of the trials (figure 3.4)

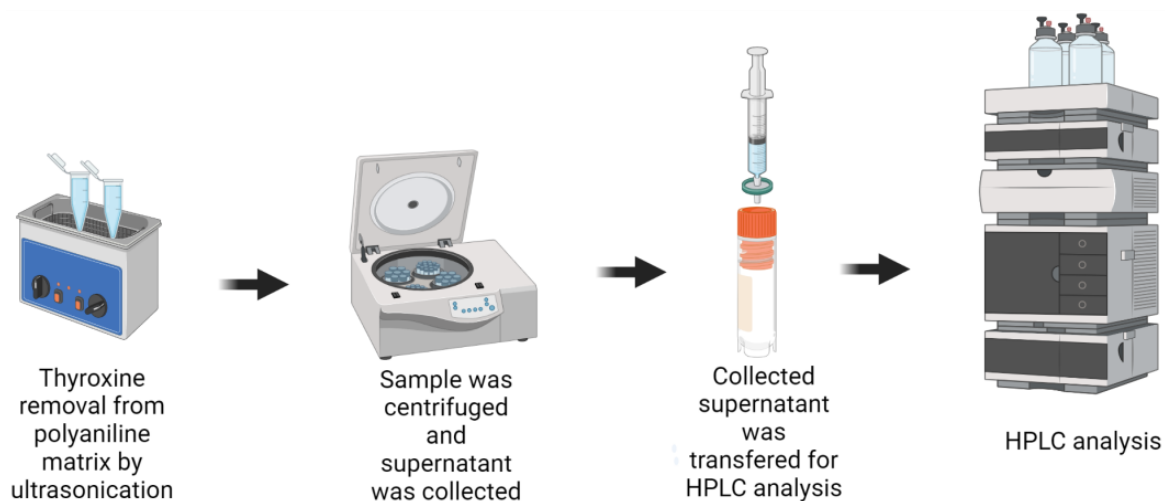


Figure 3.4. The graphical representation of the process of removal of thyroxine from the polyaniline matrix, collection of supernatant and analysis using HPLC

3.2.3.4. Rebinding studies and Imprinting factor

In rebinding study, thyroxine (50 μ g/ml) was incubated with 20mg of MIP and 20mg NIP separately for a duration of 3 hours under constant shaking. Then, these two mixtures were centrifuged at 10,000 rpm for ten mins at a temperature of 10⁰C. After centrifugation, the supernatant collected was analyzed with HPLC. The same HPLC parameters were used as mentioned in the preceding section. The HPLC peaks area of thyroxine was used to determine the concentration of free thyroxine extracted in the supernatant (Roland et al., 2023).

3.2.3.5. Characterization Studies

Characterization of structural features of NIP and MIP surfaces was done using Fourier Transform Infrared spectroscopy (FT-IR), Atomic Force Microscopy (AFM) and contact angle measurements. Contact angle data was also used for the calculation of the surface energy of NIP and MIP coated electrodes.

FT-IR analysis was performed for three different samples (NIP, MIP and T₄-MIP). Approximately 2mg of sample was mixed uniformly with potassium bromide (KBr) and a thin pellet was made using hydraulic press. The sample was then analyzed in 400-4400cm⁻¹ range with 16 scans and resolution of 4cm⁻¹. AFM scan was taken

on 10 x 10 μm surface for both for MIP and NIP coated electrodes. Drop shape analyzer was used for contact angle analysis. The electrodes coated with NIP and MIP (by drop cast method) were used to study the contact angle using water (polar solvent) and ethylene glycol (non-polar solvent). The study was repeated three times. Surface energies for NIP and MIP were also calculated.

3.3. Results and Discussion

3.3.1. Preliminary studies

The experimental results showed that thyroxine was freely soluble in 0.1N sodium hydroxide solution (Kendall, 1926). Its solubility in water, dimethyl sulfoxide (DMSO).

UV spectral scan helped to determine the lambda max of a thyroxine. The UV scan of thyroxine (in dilute alkali solution) showed a lambda max of 326nm (figure 3.5). The observed value matches the reported value mentioned in the certificate of analysis (CoA). The reported lambda max of thyroxine is 326nm in dilute alkaline solution (Gregorini et al., 2013). Literature shows that thyroxine in alkaline solution shows two lambda max values one around 227nm and other around 327nm. The absorbance at 227nm is significantly higher as compared to that at 327nm. The value at 327nm is used for the identification test and 227nm is used for the quantification. The reason for observing peak at 327nm for identification is to distinguish thyroxine from its derivatives (triiodothyronine, diiodothyronine) as they also show lambda max around 227nm (Takikawaa, 1955).

The FT-IR spectra (figure 3.6) showed characteristic stretching frequency peaks of thyroxine including C-I around 680cm^{-1} , C=O around 1650cm^{-1} , O-H around 3500cm^{-1} , C-C around 1100cm^{-1} etc (Rossi et al., 2018). The HPLC chromatograph shows a single peak of pure thyroxine solution at 10.2 mins (figure 3.7).

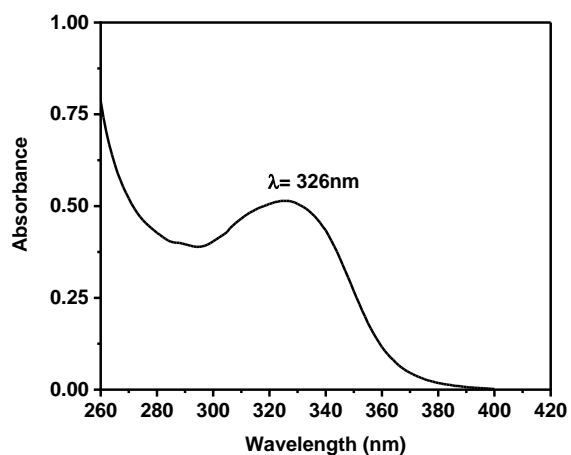


Figure 3.5. UV spectra of thyroxine taken from 260nm to 400nm shows a lambda max of 326nm

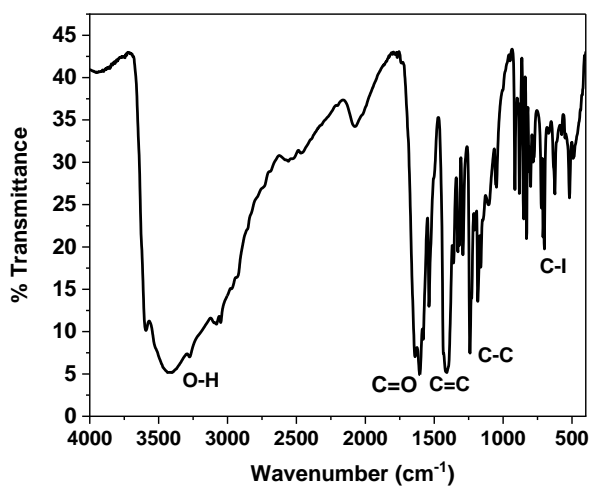


Figure 3.6. FT-IR spectra of thyroxine

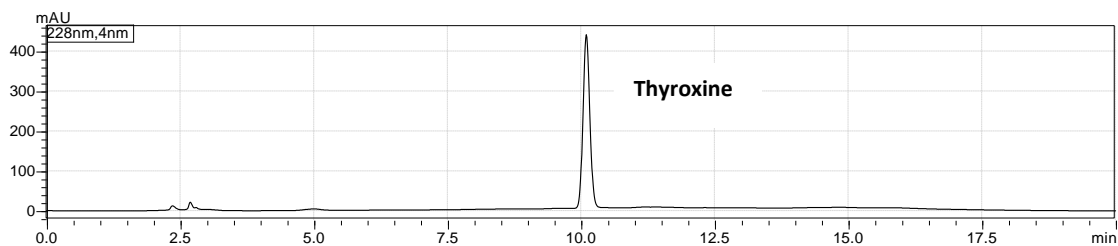


Figure 3.7. HPLC chromatogram of thyroxine (mAU vs mins)

3.3.2. Synthesis of MIP and NIP

Product I and product II were formed after 20 mins in their respective reaction beakers. Both the products were greenish-blue solid suspended in the reaction mixture. The reported literature confirms the greenish blue color of polyaniline in acidic conditions (Abu-Thabit, 2016). After filtration and drying, the weight of the final product formed was approximately 600mg (figure 3.8a).



Figure 3.8. The dried solid polyaniline after the oxidative polymerization of aniline

HPLC chromatogram (figure 3.9a) of 20ppm of thyroxine standard solution showed a peak at retention time of 10.2 mins (Collier et al., 2011). The supernatant collected after sonicating product I (MIP+T₄) at 30°C for 15 mins with 75mM NaOH solution also showed a peak around retention time of 10.2 mins. This indicates the extraction of thyroxine from polymer matrix (figure 3.9b). To further support this assertion, NIP (product II) was also sonicated using same conditions and the supernatant showed no peak around 10.2 mins (figure 3.9c). Supernatant of product I collected without sonication showed a very small peak around 10.2 min in HPLC chromatogram (figure 3.9d). This peak could be due to some of the weakly adsorbed thyroxine on the polyaniline surface. Hence, it is important to note that sonication process was important to remove thyroxine as without sonication very small amounts of thyroxine was removed (Hudson et al., 2019).

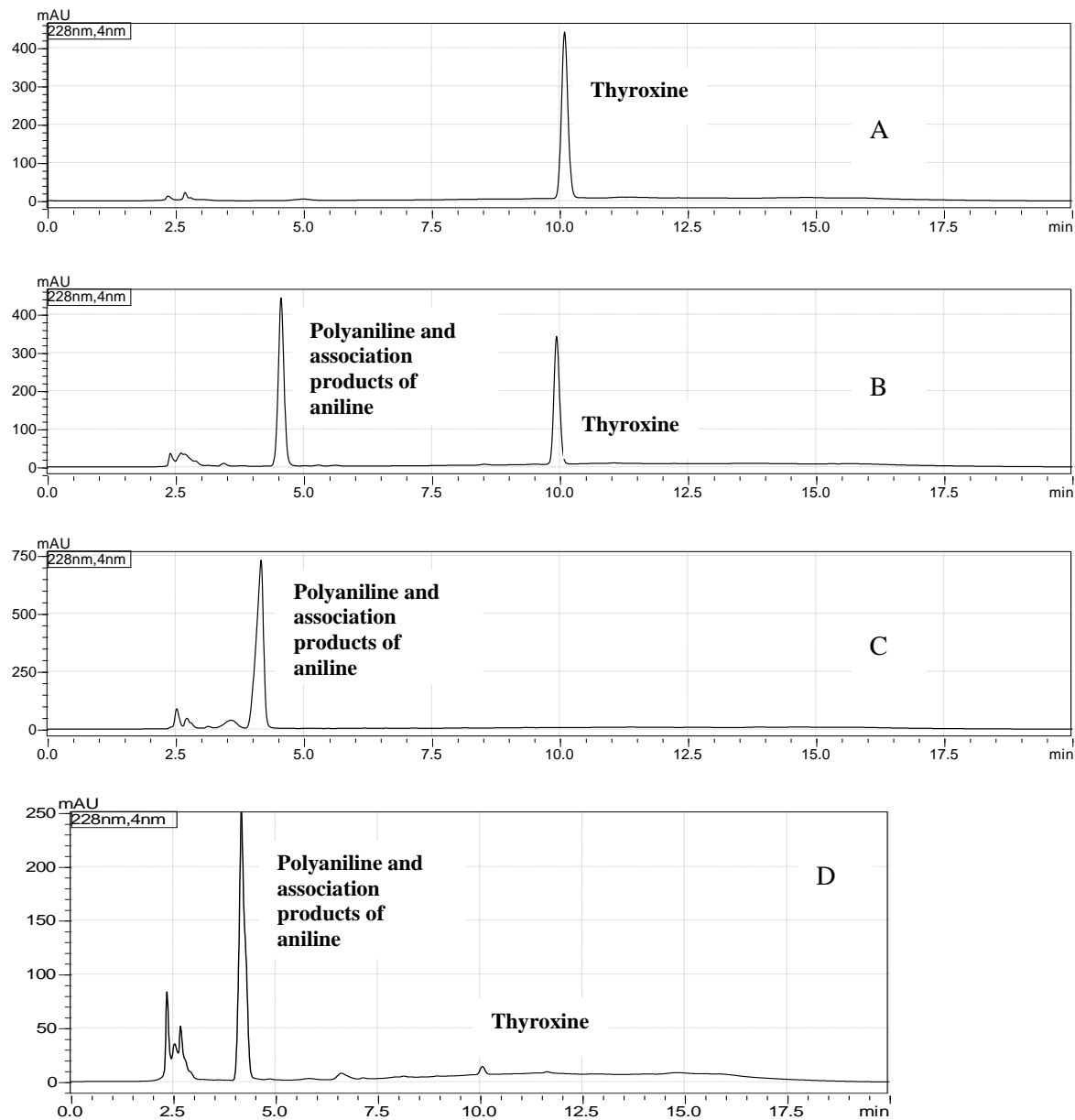


Figure 3.9 (a) Chromatogram of pure thyroxine (b) Chromatogram after extracted from polyaniline with T₄ (c) Chromatogram after extraction from NIP (d) Chromatogram after three consecutive extractions from polyaniline

3.3.3. Optimization of Template Removal

The supernatant collected for all 14 trials showed different peak areas in HPLC chromatogram (table 3.3). The peak area is proportional to the concentration of thyroxine removed from the (MIP+T₄) matrix. The higher the peak area better is

the removal of thyroxine. The responses obtained were analyzed using Design expert software.

Table 3.3. Different conditions for sonication were performed to remove thyroxine from MIP + T4. The maximum peak area in Run 13 gives the best conditions for thyroxine removal

Run	Conc. of NaOH (mM)	Temperature (°C)	Time (mins)	Peak area in HPLC
1	125	30	30	2694652
2	100	30	45	2606173
3	75	40	45	2389787
4	100	30	15	1910671
5	75	30	30	2792259
6	100	40	30	2240712
7	100	50	15	2994670
8	100	40	30	2240712
9	125	40	15	1404862
10	75	50	30	2043485
11	100	50	45	1628344
12	125	50	30	1371182
13	75	40	15	4881631
14	125	40	45	1279771

Using design expert software, a model equation was generated. Equation 3.1 relates HPLC peak area with the selected critical parameters.

$$\text{Sqrt (HPLC Peak Area)} = 2794.2 + 25.6 \times \text{Temperature} - 20.8 \times \text{NaOH Concentration} - 2.7 \times \text{Time} - 1.14 \times \text{Temperature} \times \text{Time} + 0.41 \times \text{NaOH Concentration} \times \text{Time}$$

Equation 3.1

F-value for the above model was found to be 4.35 and it implies that the model is significant and there is only a 2.28% chance that an F-value this large could occur due to noise. Adequate Precision ratio was found to be 7.073 which indicates an

adequate signal. Overall statistics shows that this model can be used to navigate the design space (Singh et al., 2023). The statistical parameters are shown in table 3.4.

Table 3.4. Statistical parameters related to analysis of variance (ANOVA)

Source	Sum of Squares	Df	F-Value	P Value
Model	7.5 x 10 ⁵	5	4.3	0.032
Temperature	61621.9	1	1.7	0.2
NaOH concentration	2.7 x 10 ⁵	1	10.7	0.01
Time	1.1 x 10 ⁵	1	2.1	0.1
Temperature x Time	1.2 x 10 ⁵	1	2.4	0.1
NaOH concentration x Time	92887	1	2.6	0.1

Using Design expert software, different plots were generated which showed the simultaneous effect of factors and the extent of thyroxine removal (measured in terms of HPLC peak response). The 3D contour plots representing the effect of concentration of sodium hydroxide, temperature, and sonication time.

The figures 3.10 - 3.12 shows the effect of time and temperature when concentration of sodium hydroxide is constant. The HPLC peak area (corresponds to removal of thyroxine) was found to be maximum when concentration of sodium hydroxide is 75mM. The response significantly reduces above this concentration without much effect of other two factors. Hence, it can be concluded that concentration of sodium hydroxide is the most critical parameter amongst all three selected parameters.

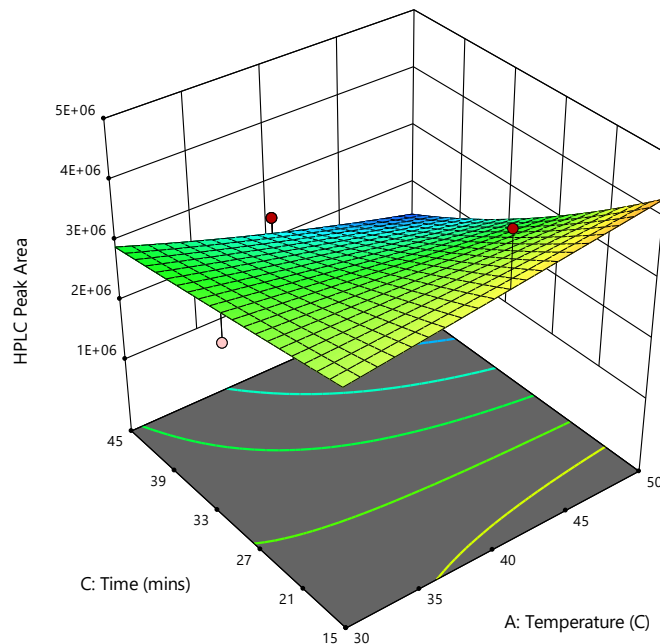


Figure 3.10 The effect of time and temperature (at 75mM NaOH concentration) on the removal efficiency of thyroxine from polyaniline. The contour plot shows that the removal is maximum when temperature is between 40-50°C, and time is 15 mins

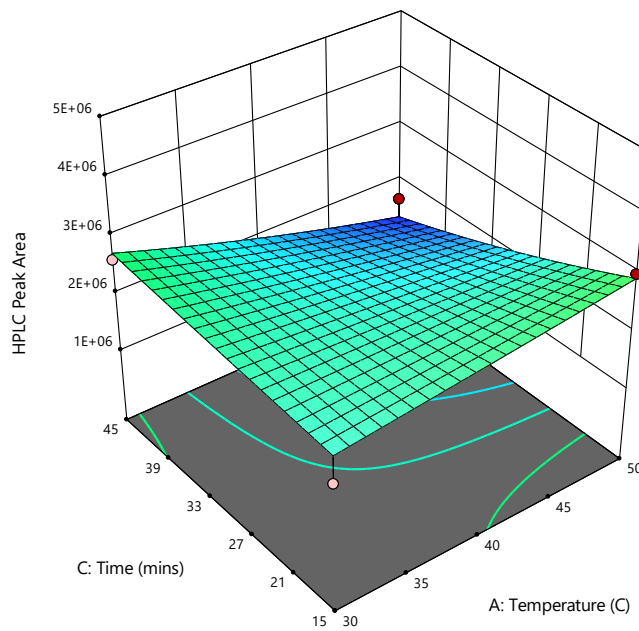


Figure 3.11 The effect of time and temperature (at 100mM NaOH concentration) on the removal efficiency of thyroxine from polyaniline. The contour plot shows very small changes in the removal with different temperature and time conditions

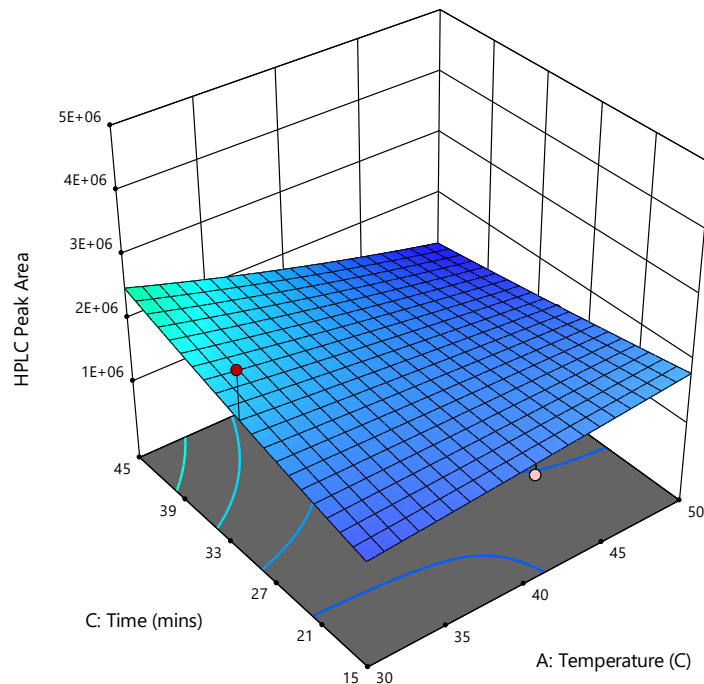


Figure 3.12 The effect of time and temperature (at 125mM NaOH concentration) on the removal efficiency of thyroxine from polyaniline. The contour plot shows negligible change in the removal with different temperature and time conditions

The figures 3.13 - 3.15 shows effect of time and concentration of sodium hydroxide when temperature is constant. The HPLC peak area (corresponds to removal of thyroxine) was found to be maximum when temperature was 30⁰C. The response reduces slightly above this temperature but increases at 50⁰C. The contours plots for all the response are shown in figure 3.13 - 3.15.

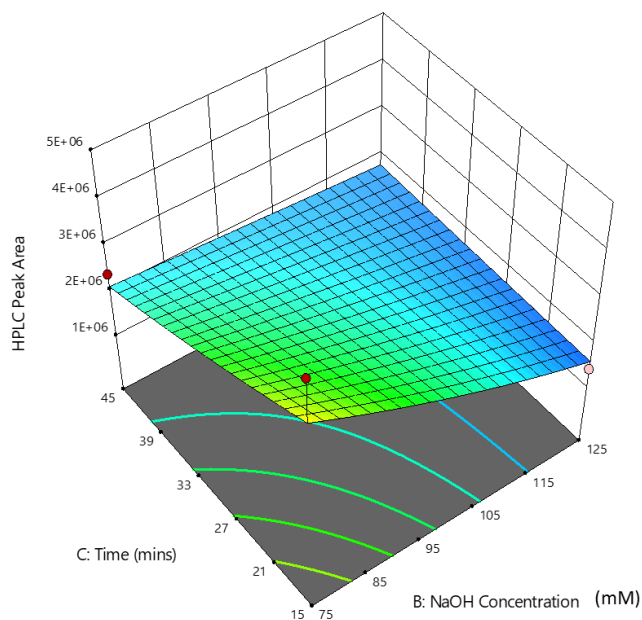


Figure 3.13 The effect of time and NaOH concentration (at 30°C) on the removal efficiency of thyroxine from polyaniline. The contour plot shows maximum removal at low concentration (75mM) and less time (15 mins)

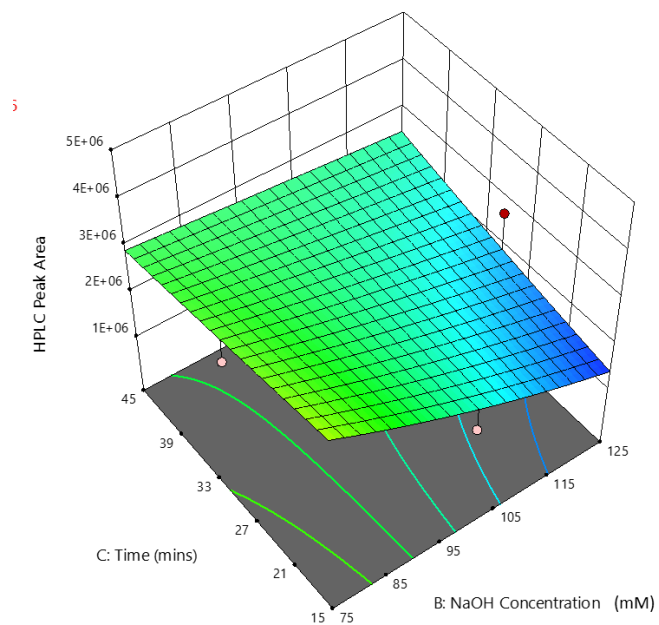


Figure 3.14 The effect of time and NaOH concentration (at 40°C) on the removal efficiency of thyroxine from polyaniline. The contour plot shows maximum removal at low concentration (75mM), but time has almost negligible effect

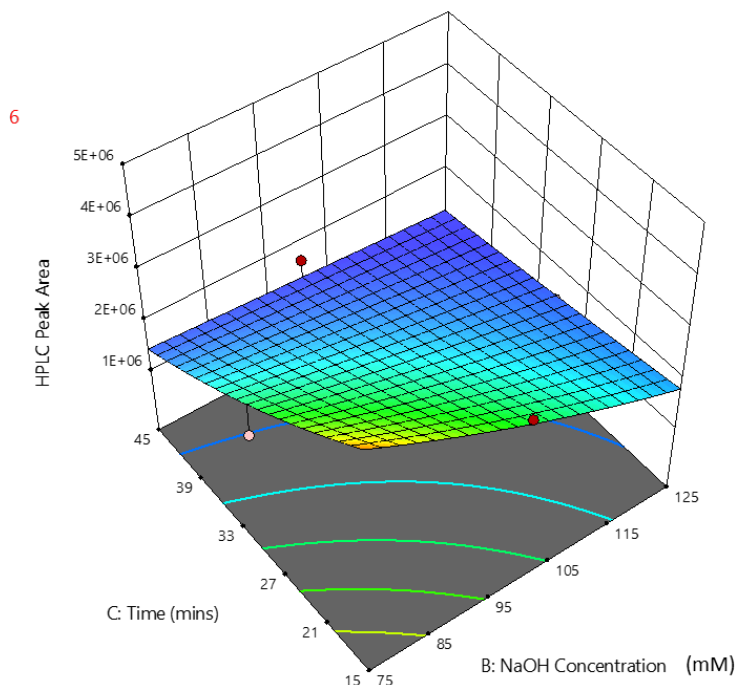


Figure 3.15 The effect of time and NaOH concentration (at 50⁰C) on the removal efficiency of thyroxine from polyaniline. The contour plot shows maximum removal at low concentration (75mM) and less time (15 mins)

After studying, all the responses from contour plots, it was observed that maximum removal of thyroxine was obtained at low NaOH concentration (75mM) and lesser time (15 mins) and temperature has negligible effect on the removal. Moreover, the conditions with best response were NaOH concentration (75mM), temperature (40⁰C) and less time (15 mins). At these conditions the removal of thyroxine was maximum (peak area mentioned in table 3.3). Imprinted polyaniline matrix (without thyroxine) was characterized further by FT-IR, AFM and contact angle. The rebinding studies were also performed to study the imprinting factor.

3.3.4. Rebinding studies

The binding property of MIP and NIP towards thyroxine was evaluated by calculating the imprinting factor (IF) using the equation 3.2 (Lafarge et al., 2020).

$$IF = \frac{B (MIS) \times F (NIS)}{F (MIS) \times B (NIS)} \quad \text{Equation 3.2}$$

- F: the free concentration of T₄ (ppm) in the supernatant

- B: the amount of T₄ bound (adsorbed) by polyaniline (mg of T₄/g of polyaniline) calculated by the difference in the initial T₄ concentration (ppm) and F.

High performance liquid chromatography (HPLC) chromatogram shows peaks for 3 different samples. First is 50µg/mL solution of T₄, second is supernatant collected after mixing NIP with 50µg/mL solution of T₄ for 3 hours and third supernatant collected after mixing MIP with 50µg/mL solution of T₄ for 3 hours. The reduction of thyroxine in the supernatant in case of MIP is evidence of the binding of thyroxine with the imprinted polymer.

The value of imprinting factor signifies better specific interactions with the polymer. Using the chromatogram obtained in figure 3.16, the imprinting factor obtained was 1.98 (Lafarge et al., 2020).

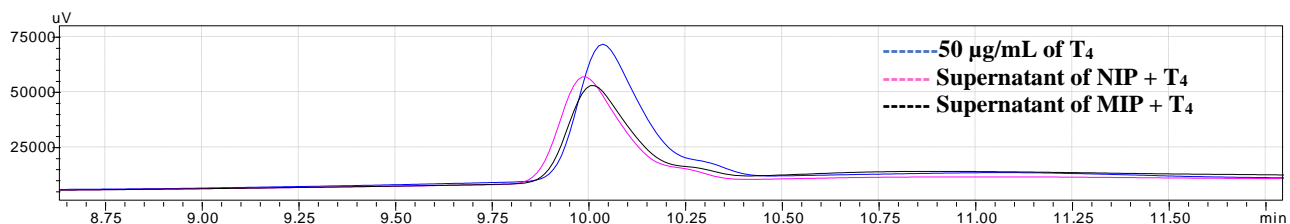


Figure 3.16 HPLC chromatogram for calculation of imprinting factor for MIP

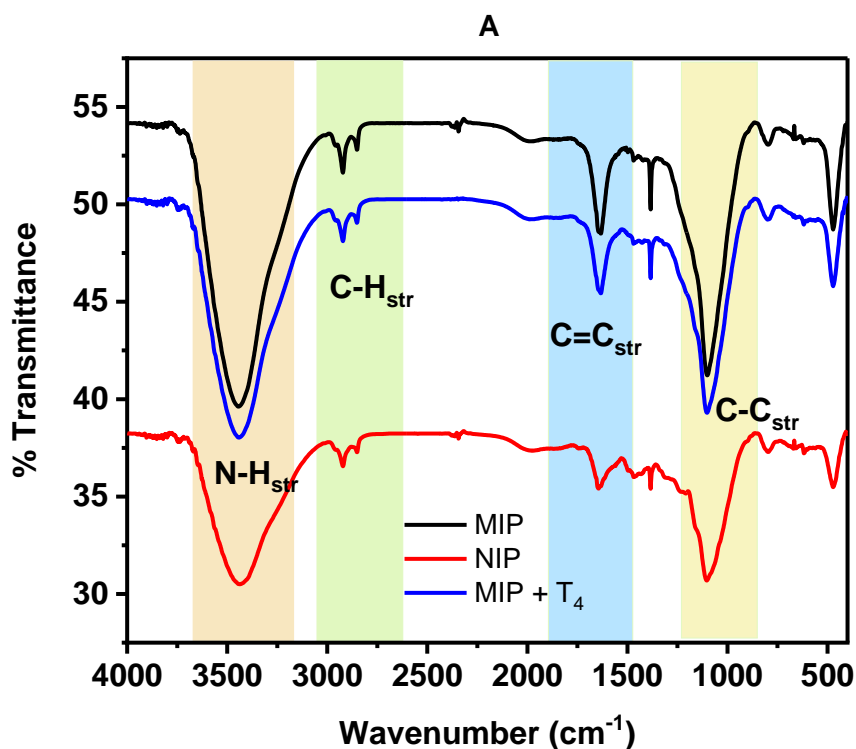
3.3.5. Characterization studies

The cavities formed in polyaniline matrix were characterized using FT-IR spectroscopy, AFM, and contact angle studies.

FT-IR characterization (figure 3.17) studies for MIP, NIP, polyaniline with thyroxine shows the characteristic peaks of polyaniline. 3460cm⁻¹ peak denotes N-H vibrational stretching, peak at 1630cm⁻¹ denotes C=C vibrational stretching frequency and peak at 1180cm⁻¹ denotes C-C vibrational stretching frequency. In figure 3.17b, the range between 1000 - 500cm⁻¹ has been highlighted to show the

changes between imprinted and non-imprinted polymer. It is well known thyroxine structure has 4 carbon-iodine bonds (C-I bonds) which show a characteristic absorption peak around 670cm^{-1} - 680cm^{-1} . As NIP does not have any thyroxine molecule, hence, there is a dip observed near 670cm^{-1} (Shao et al., 2012).

When T_4 is bound to MIP, the band disappears near 670cm^{-1} . However, after extracting thyroxine from polymer, the spectra show the C-I band again at same wavenumber. The absorption of C-I bond may be involved in neutralizing the dip at 670cm^{-1} . The FT-IR data indicates that thyroxine is present in polyaniline matrix in product I (MIP + T_4) and is absent in MIPs



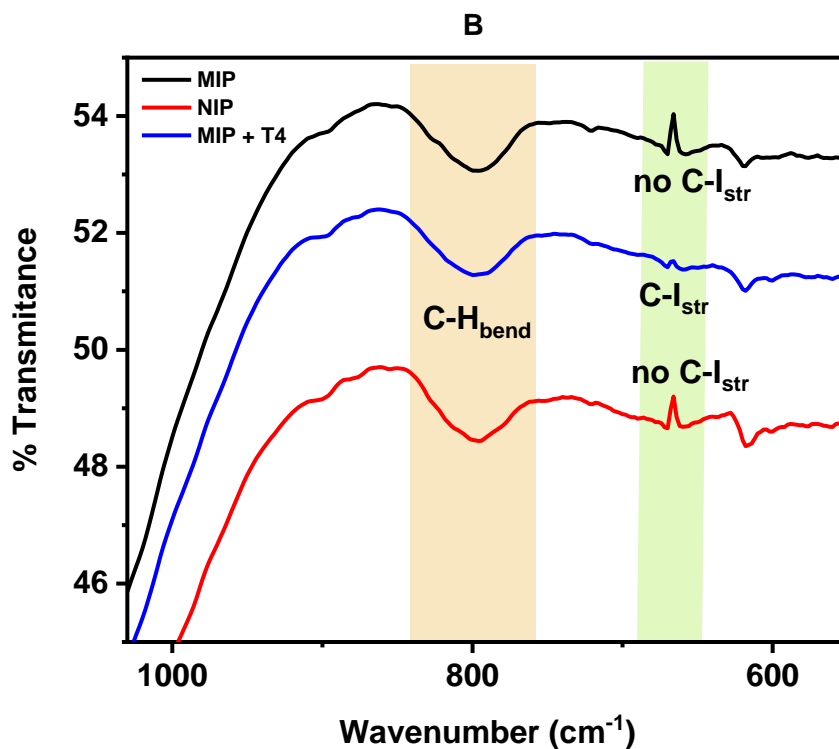


Figure 3.17 (A) shows the scan range of 4000-400 cm⁻¹ MIP, NIP and thyroxine rebound MIP (MIP+T₄) and (B) shows zoomed FT-IR scan of range 1100cm⁻¹-400 cm⁻¹ for MIP, NIP and thyroxine rebound MIP (MIP+T₄)

HPLC data compliments FT-IR data as after sonication of product I, thyroxine is removed from polyaniline matrix and is expected to be present in the solvent. The solid MIP doesn't show C-I bond in FT-IR and the solvent shows the presence of thyroxine when observed in HPLC. This strongly suggests that the thyroxine is removed from the polymer and the cavities were generated. Further, AFM analysis and contact angle studies compliment this claim (next sections).

The surface roughness through AFM studies (figure 3.18) was found to be 1.02nm for NIP and 5.04 nm for MIP respectively. The increase in roughness can be attributed due to the removal of thyroxine molecule from MIP. These AFM results compliments well with HPLC and FT-IR observations.

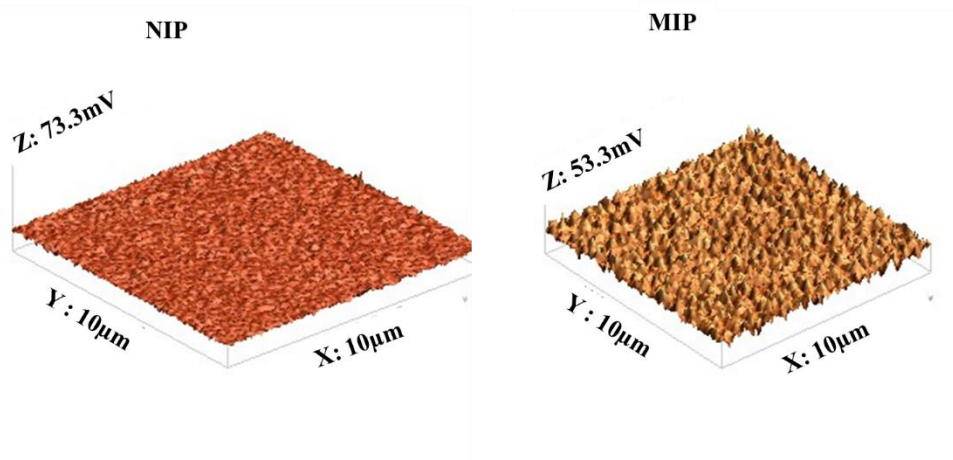


Figure 3.18. AFM images of MIP and NIP at 10µm x 10µm resolution

Contact angle (figure 3.19) of NIP with water (polar) and ethylene glycol (less polar) was found to be 54.2° and 27.3° as compared to 80.7° and 62.2° for MIP. The formation of cavities results in the roughness of polyaniline surface due to which the contact angle is higher in case of MIP as compared to NIP.

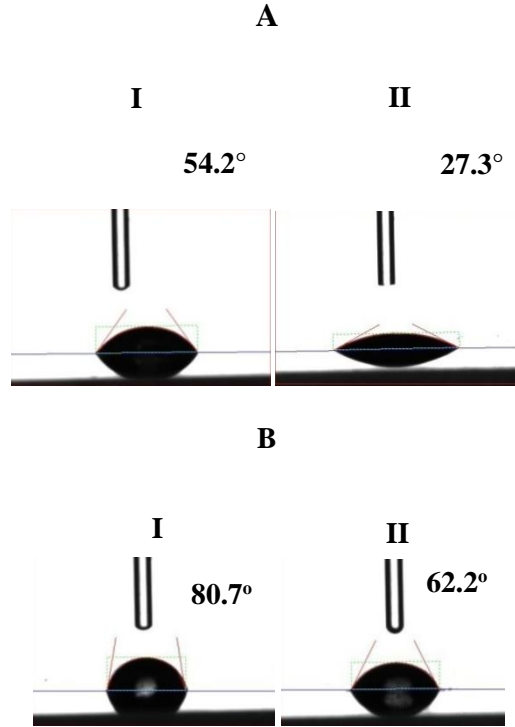


Figure 3.19 a. Contact angle for NIP with water (I) and ethylene glycol (II) and b. Contact angle for MIP with water (I) and ethylene glycol (II)

Using Fowkes equation given in equation 3.3 (Roy et al. 2021), the surface energies of MIP and NIP films was calculated (Table 3.4).

$$1 + \cos \theta = 2\sqrt{\gamma_s^d} \left(\frac{\sqrt{\gamma_1^d}}{\gamma_1} \right) + 2\sqrt{\gamma_s^p} \left(\frac{\sqrt{\gamma_1^p}}{\gamma_1} \right) \quad \text{Equation 3.3}$$

θ = contact angle at solid-liquid interface

γ_s^d = dispersive component of solid surface energy

γ_s^p = polar component of solid surface energy

γ_1^d = dispersive component of liquid surface energy

γ_1^p = polar component of liquid surface energy

γ_1 = total liquid surface energy

The polar and dispersive components of water are 51.00 mJ/m² and 21.80 mJ/m² respectively. The polar and dispersive components of ethylene glycol these values are 18.91 mJ/m² and 29.29 mJ/m² respectively. Total liquid surface energy for water and ethylene glycol is 72.80 mJ/m² and 48.20 mJ/m², respectively. By substituting these values in equation 3.3, the solid surface energies of MIP and NIP were calculated (table 3.5). The total surface (γ_s) of NIP was found to be higher than that of MIP. Due to formation of thyroxine cavities in the MIP the contact angle was higher than NIP and the surface energy was subsequently lower (Roy et al. 2021).

Table 3.5. Polar, dispersive and total solid surface energy of NIP and MIP calculated using water and ethylene glycol contact angles

S. No	Solid Surface	Contact Angle (Water)	Contact angle (Ethylene Glycol)	γ_s^p (mJ/m ²)	γ_s^d (mJ/m ²)	γ_s (mJ/m ²)
1	NIP	54.2°	27.3°	62.2	-1.01	61.1
2	MIP	80.7°	62.2°	34.8	-0.64	34.16

The results obtained with FT-IR, HPLC, AFM and contact angle confirm the formation of thyroxine imprinted cavities. Further, this imprinted polymer will be used for the selective estimation of thyroxine (Chapter 4).

3.4. Conclusion

This chapter discusses the synthesis and optimization of molecularly imprinting polymer for thyroxine. The synthesis was carried out using aniline as functional monomer. After oxidative polymerization around 600mg of polymer was formed. The template (thyroxine) was removed by sonication with dilute sodium hydroxide as solvent. The template removal conditions were optimized using the design of experiments approach where temperature, concentration of sodium hydroxide and sonication time were selected as critical parameters. The response was studied using the supernatant fraction collected after sonication and analyzed with HPLC. The peak area obtained in HPLC chromatogram was proportional to the thyroxine removed from the polyaniline matrix. The optimized conditions were found to be 75mM NaOH concentration, 40⁰C temperature and 15 mins of sonication time. Rebinding studies showed that the imprinting factor for synthesized MIPs was 1.98. MIPs were characterized using AFM, FT-IR and contact angle analysis. Finally, the synthesized molecularly imprinted polymer was stored in a cool dry place at room temperature. These MIPs served as recognition element for developing electrochemical biosensor for thyroxine.

Chapter 4

Molecularly Imprinted

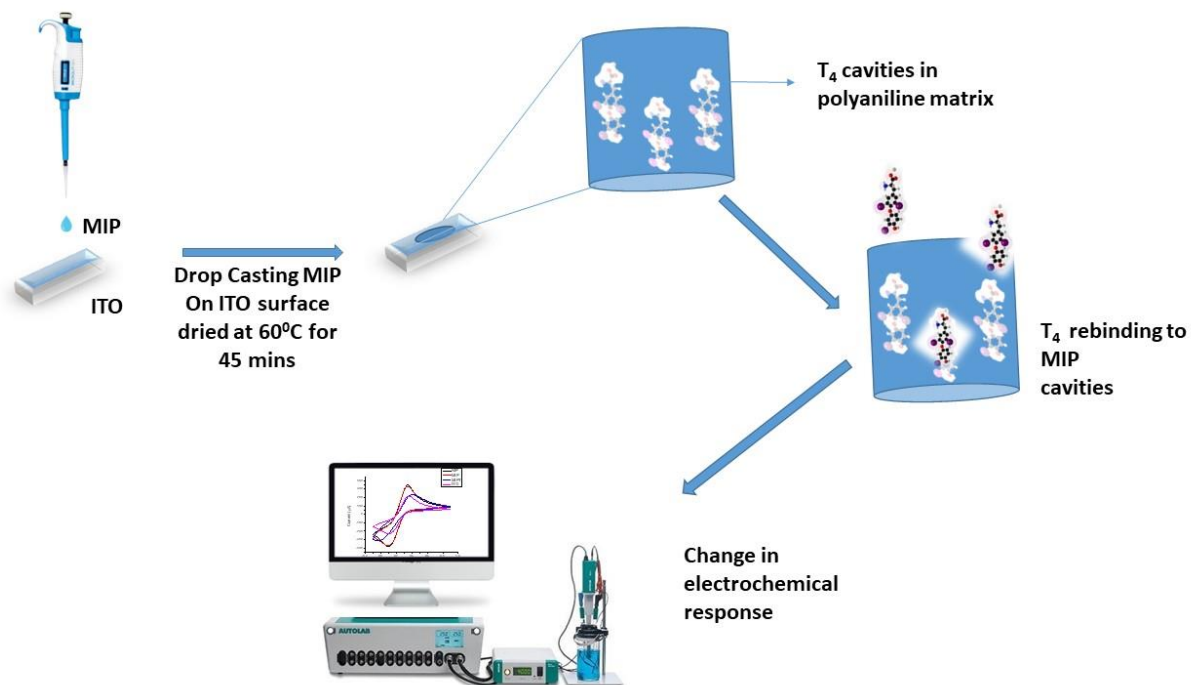
Polymers based

Electroanalytical Biosensor

for the estimation of

Thyroxine

Graphical abstract



Abstract

To prevent potentially fatal conditions, thyroid abnormalities must be diagnosed and treated promptly. Thyroxine is the most common biomarker used for the diagnosis of thyroid disorders. Presently available diagnostic techniques are time consuming, need skilled manpower and require costly instruments. An early, accurate and efficient diagnosis of thyroid disorders and regular monitoring of thyroxine is important for proper treatment of patients. In this work, molecularly imprinted polymer for thyroxine was coated on the surface of indium tin oxide (ITO) electrode for the electrochemical estimation of thyroxine. The sensor was calibrated within T₄ concentration range of 5pg/mL - 50 pg/mL, with the limit of detection as 6.16 pg/mL. Repeatability studies show the relative standard deviation of 2.45%. The interference of structurally similar molecules such as liothyronine, tyrosine and phenylalanine were negligible. To investigate the true matrix effect, 50 pg/mL was spiked in saliva; the recovery of thyroxine ranged from 96 to 115.2%. The developed electrochemical sensor exhibits high sensitivity and selectivity and offering it great potential for use in cutting-edge point-of-care applications in the future.

4.1. Introduction

Thyroxine (T_4) is considered as one of the most important indicators for diagnosing thyroid disorders. Despite the high frequency of thyroid disorders, the scientific community has not given thyroxine biosensors much attention. T_4 levels are important to be maintained to avoid health complications.

Several transducers have been used for signal measurement in a biosensor including surface plasmon resonance (SPR), colorimetric, electrochemical *etc.* Electrochemical sensors have been most accurate and reliable (Grieshaber et al., 2008). Moreover, they can easily be converted to a miniaturized point of care device. In electrochemical biosensor, bio-recognizing elements are one of the key components which are immobilized on the working electrode. MIPs stand out as bio-recognizing when compared with other materials as they have advantage of better environmental stability and shelf life. MIPs are the synthetic receptors which are used as an alternative to natural antibodies. They have high chemical stability and are resistant to harsh environmental and operational conditions such as high temperatures, pH and humidity. MIP-based methods have shown success in selective estimation of compounds in different biological matrices. Due to high sensitivity and selectivity, they have been used by researchers in biosensors for quantifying biomarkers of many diseases such as heart diseases, metabolic disorders *etc* (Cho et al., 2020). Polyaniline and polypyrrole are two common polymers which are used for developing biosensors as they are conductive. The presence of alternate pie bond frame work helps in the delocalization of electrons which is considered to be the reason of their conductive nature (Hamzah et al., 2007).

Very few studies were found in literature for estimating thyroxine using molecular imprinted technique. In 2010, B Prasad et al., developed MIP based biosensing technique for thyroxine. In their study, the group pre-concentrated thyroxine from blood samples using solid phase extraction before sensing the thyroxine molecule (Prasad et al., 2010). Recently, in 2024, another study by Seo and group (Germany)

developed the biosensor for thyroxine using imprinted mesoporous organic silica for selective sensing of thyroxine. The group claimed that by adding certain additives the re-binding of thyroxine was enhanced (Seo et al., 2024). These are the only two studies which employed MIPs for thyroxine molecule.

In this work, previously synthesized molecularly imprinted polyaniline was immobilized on indium tin oxide (ITO) electrode for sensing the electrochemical response to thyroxine (Singh et al., 2023). The response was studied with different thyroxine concentrations which cover the normal range of this hormone in human blood. Interference with structurally similar biomolecules such as tyrosine, phenylalanine and liothyronine was also studied to ensure the selectivity of the response. The accuracy of response was also checked by spiking known concentration of thyroxine in human saliva. The developed biosensor showed excellent sensitivity and selectivity for the determination of thyroxine.

4.2. Experimental

4.2.1 Materials

Thyroxine sodium (MW: 888.92 Da, > 97% using HPLC) was procured from Macleods Pharmaceuticals Limited, India. Liothyronine (MW: 672.96 Da, \geq 95% using HPLC), phenylalanine and tyrosine were purchased from Merck (Darmstadt, Germany). HPLC grade methanol was procured from Rankem (India) and ultrapure water (resistivity \sim 18.2 Ω cm at 298 K) was used from the in-house water purification system (Milli-Q system Millipore Bedford, MA, USA). Potassium dihydrogen phosphate (KH_2PO_4 ; MW: 136.08 Da \geq 99%) and di-sodium hydrogen phosphate (Na_2HPO_4 ; MW 141.9 Da, \geq 99%) were procured both from Rankem (India). Phosphate buffer saline (pH = 7) was prepared with these salts and sodium chloride as per Indian Pharmacopoeia (2007). Stock solution of thyroxine was prepared in 0.1N sodium hydroxide solution and dilutions were prepared in ultrapure water. Potassium ferrocyanide trihydrate (MW: 422.38 Da, \geq 99%) and potassium ferricyanide (MW: 329.24 Da, \geq 99%) were procured from Rankem (India). 10mM of potassium ferro-ferri cyanide solution prepared in phosphate

buffer saline (1 mM, pH 7.4) was used as a redox probe for electrochemical studies. All chemical used for the study are of analytical grade. All standard solutions of thyroxine were prepared freshly before electrochemical sensing.

4.2.2. Instruments and Electrodes

Instruments: Dropsens electrochemical potentiostat (uStat i-400, Metrohm, Switzerland) and analytical weighing balance (Shimadzu AT series, Japan).

Electrodes: Indium tin oxide coated glass electrodes were used as working electrodes (dimensions 10 mm x 7 x 1.1mm) with resistivity $\leq 10 \Omega/\text{sq.}$ and ITO film thickness 1800-2000 Å. For molecular imprinted polymer-based detection of thyroxine, silver-silver chloride electrode was used as reference electrode and platinum wire as counter electrode (Figure 4.1).

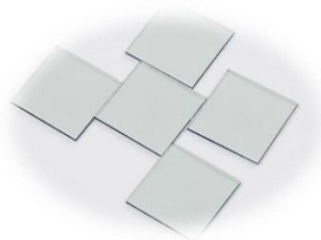


Figure 4.1. ITO coated glass electrodes of dimensions 10 mm x 7 x 1.1mm

4.2.3. Methodology

ITO coated glass was cut uniformly with dimensions 10 mm x 7mm x 1.1mm. These electrodes were washed with water and acetone before being used as working electrode for the study. The synthesized MIPs were coated onto ITO electrode by drop cast technique. 5 mg of MIPs were suspended by mixing finely powdered solid in 1 mL of distilled water and sonicated for 15-20 mins. 5 μL of this mixture was drop casted onto the ITO electrode and was kept in a hot air oven at 60°C for 45 mins. Electrodes were then gently rinsed with water and air dried at room temperature before using for electrochemical study. Approximately 40 ITO electrodes were coated with MIP and 5 electrodes were coated with NIP. These electrodes were used further for the electrochemical study.

Three electrode set-up was used for the electrochemical study with silver-silver chloride (Ag-AgCl) electrode as the reference electrode, coiled platinum wire as the counter electrode and surface modified ITO glass as working electrode. Potassium ferrocyanide-ferricyanide (10mM) in phosphate buffer saline (10mM) was used as a redox probe.

Electrochemical studies were performed using cyclic voltammetry and electrochemical impedance spectroscopy. Electrochemical analysis includes testing response of NIP, MIP, MIP+T₄ coated on electrode surface, study of scan rate, linearity, interference studies, repeatability and recovery from saliva.

Cyclic voltammetry was performed in the range -0.1 – 0.9V. For EIS, the frequency scan was performed between 10 kHz - 1 MHz. Randel's circuit simulation of impedance spectra was done using Zview software.

CV and EIS response of NIP, MIP, MIP+T₄ was studied by coating these materials on ITO electrode. Scan rate study was performed for a range of 10mV/s to 180mV/s. Calibration (linearity) plot was formed at potential corresponding to peak anodic current. Freshly prepared standard thyroxine solutions in the range of 5-50pg/mL was used for calibration plot. Several MIP coated ITO electrodes were prepared and incubated with different concentrations of thyroxine in the range of 5-50pg/mL. 5µL standard solution was added onto the MIP coated ITO and incubated for 10 min at RT. Repeatability studies were performed by incubating 50pg/mL on 5 independent MIP coated ITO electrodes and testing the response using CV. Before electrochemical analysis, all the electrodes were rinsed with distilled water to prevent non-specific binding of thyroxine.

Phenylalanine, tyrosine and liothyronine were used for interference studies due to their structural similarity with thyroxine. The concentration of these molecules for interference studies was taken as 100µg/mL for tyrosine and phenylalanine, and 5ng/mL for liothyronine. The levels of free liothyronine are almost 100 times less than T₄, hence, a lower concentration was used for interference study. The selected liothyronine concentration would be relevant for studying interference in case the

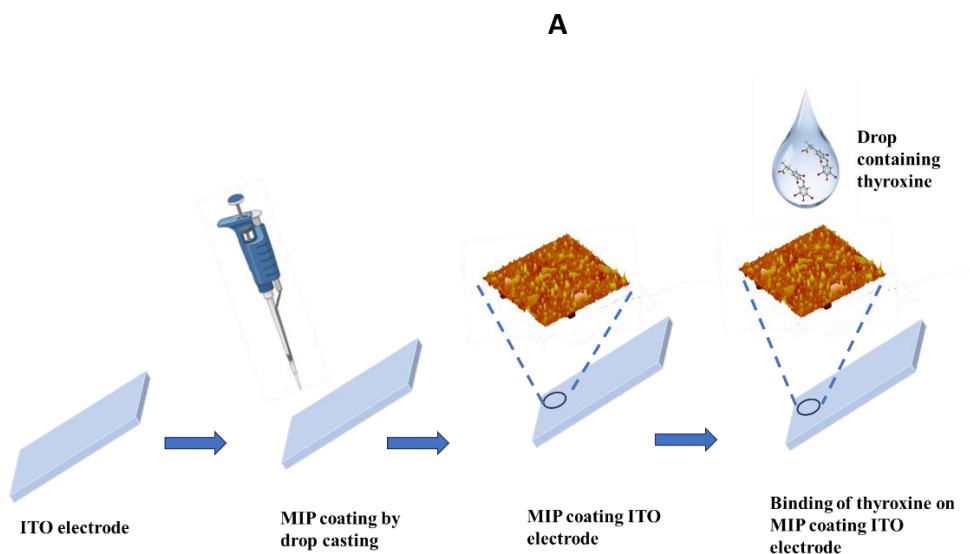
method is used for assay of thyroxine in thyroxine tablets. Liothyronine is a common degradation product found in thyroxine tablets (Neu et al., 2013).

4.3. Results and Discussion

4.3.1. Response on different stages of fabrication

The cyclic voltammetric and impedance spectra showed difference in responses at various stages of MIP sensor fabrication (figure 4.2).

The change in peak anodic current (I_{pa}) current and impedance for bare ITO, NIP, MIP and MIP + T₄ coated ITO was observed in CV scan. Bare ITO exhibits a peak anodic current (I_{pa}) response of $\sim 200 \mu\text{A}$ at 0.36V. On its modification with MIP a significant increase in $I_{pa} \sim 350 \mu\text{A}$ was observed. This increase is due to the presence of a conducting thin polyaniline film. The peak anodic current (I_{pa}) for MIP was almost similar to NIP which shows that there is very small change in conductance due to formation of cavities.



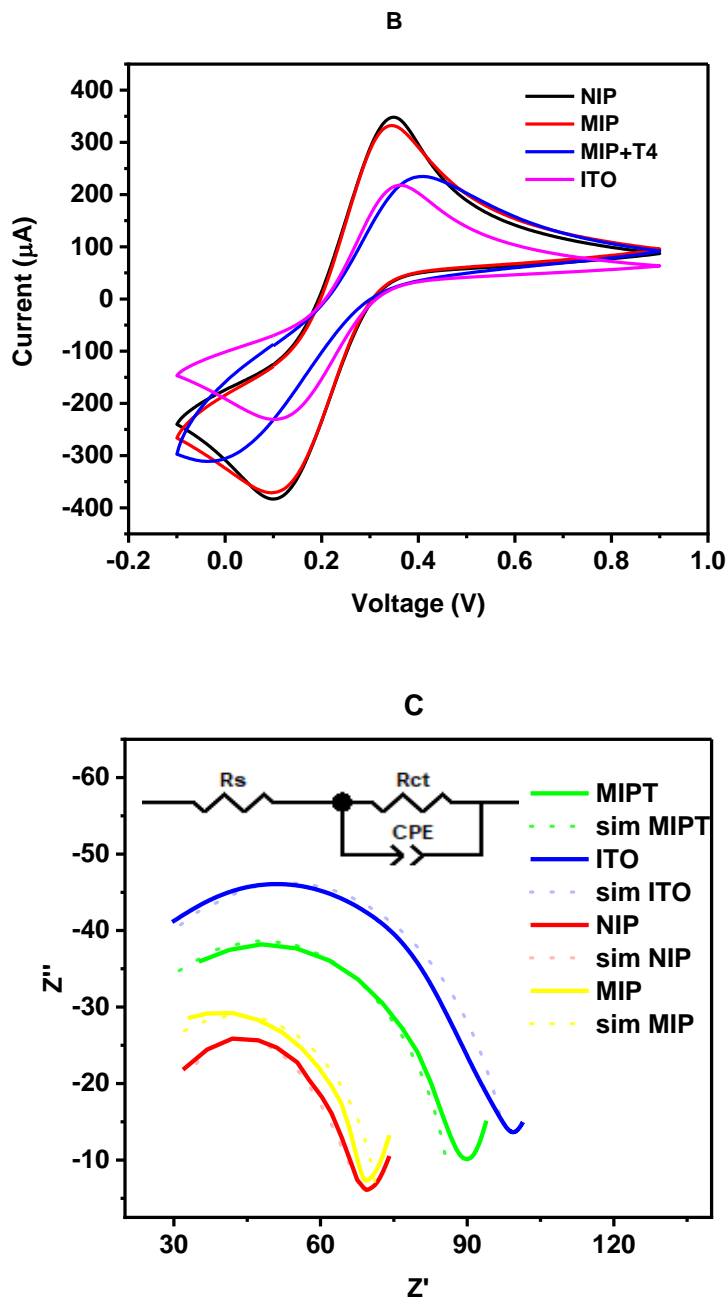


Figure 4.2 (A) Stages of fabrication of biosensor. (B) Current and voltage profile for NIP, MIP, MIP +T4 and ITO. (C) Nyquist plot for Bare ITO, NIP, MIP and T4 rebound MIP. The dotted lines show the simulated plots obtained using Zview software. Randle's circuit is shown in the inset.

However, on addition of 50 pg/mL of thyroxine solution on MIP coated ITO electrode, I_{pa} decreases to $\sim 210 \mu\text{A}$. The similar results were obtained by Park et al

2020, in which they found reduction in peak current response (in cyclic voltammetry) on addition of thyroxine to the working electrode (Park et al. 2020).

The EIS spectra in Fig 4.2c complements the voltammograms of Fig. 4.2b. High charge transfer resistance (R_{ct}) was observed when T_4 was bound to MIP. R_{ct} comparatively decreases after T_4 is removed (in case of MIP). Interface kinetics at various sensor fabrication stages are represented with the help of circuit simulation of Randle's equivalent model, shown in Fig. 4.2c inset. The movement of redox probe from the bulk to the modified ITO electrode interface (NIP, MIP, MIP+ T_4) with changing frequency gives enhanced insights of the charge transfer process. Table 4.1 shows the simulated values for circuit elements.

Table 4.1. Simulated values of circuit elements incorporated for modelling the sensor electrolyte interface, for MIP and NIP

Surface	Series Resistance R_s (k Ω)	Charge Transfer Resistance R_{ct} (k Ω)	Constant Phase Element CPE (F)
NIP	19	50	3.9×10^{-8}
MIP	13	57	6×10^{-8}

The NIP coated ITO exhibits a low $R_{ct} \sim 50$ k Ω , as compared to MIP ($R_{ct} \sim 57$ k Ω). This could be attributed to the fact polyaniline is conductive and generation of cavities may have hindered the flow of electrons on the electrode surface. MIP has an. T_4 bound to polyaniline exhibits significant $R_{ct} \sim 78$ k Ω . Such high R_s may be attributed to the hindrance offered by thyroxine in polyaniline matrix to the electron transfer process. Rebinding of thyroxine to the cavities in MIP cause impedance in the electron transfer at electrode interface which results in reduced current. Hence, it indicates that thyroxine does not contribute to the conductivity of the working electrode (Roy et al. 2021). These results are consistent with the CV responses obtained with modified ITO electrodes. Moreover, the different responses with different materials on ITO compliments the characterization data obtained with FT-IR, AFM and contact angle studies (chapter 3).

4.3.2. Scan rate study

Increase in current was observed on increasing the scan rate from 10 mV/s to 180 mV/s with the response saturating at the latter value. The electroactive surface area of MIP coated ITO was determined by examining the current response at various scan rates (figure 4.3).

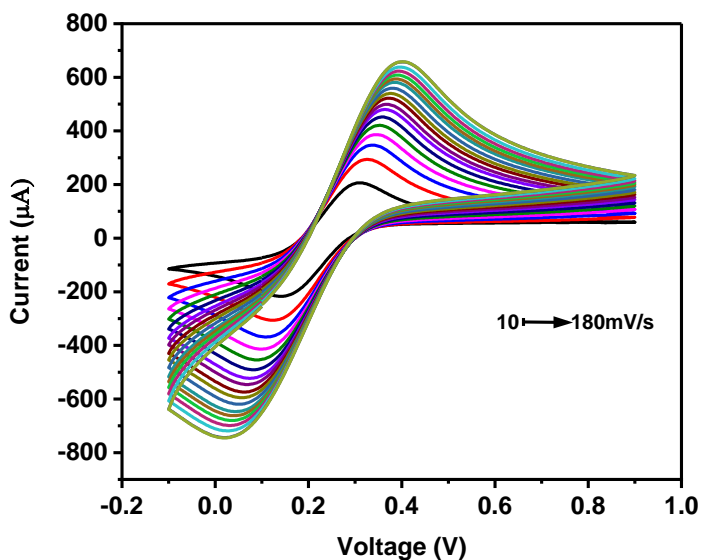


Figure 4.3. Study of scan rate vs current response from 10 mV/s to 180 mV/s

The voltametric profile of the ferri-ferrocyanide redox probe was found to be preserved even at higher scan rates. This indicates the electrochemical stability of electrode within a vast scan rate range. Figure 4.4 establishes linear relation of peak anodic (I_{pa}) and peak cathodic (I_{pc}) current with square root of scan rate (v) as shown in equation 4.1 and 4.2. This relation corresponds to the Randle's-Sevick (R-S) behaviour. The electroactive surface area was therefore calculated using Randle's-Sevick equation and found to be 0.011 cm^2 .

The electrode process was found to be diffusion controlled between scan rate 50mV/s to 180mV/s as the anodic peak current (I_{pa}) increased linearly with square root of scan rate (Prasad et al., 2010).

$$I_{pa} (\mu A) = 19.02 + 1744v^{1/2} (V/s) r^2 = 0.99 \quad \text{Equation 4.1}$$

$$I_{pc} (\mu A) = 44.02 + 1750v^{1/2} (V/s) r^2 = 0.992 \quad \text{Equation 4.2}$$

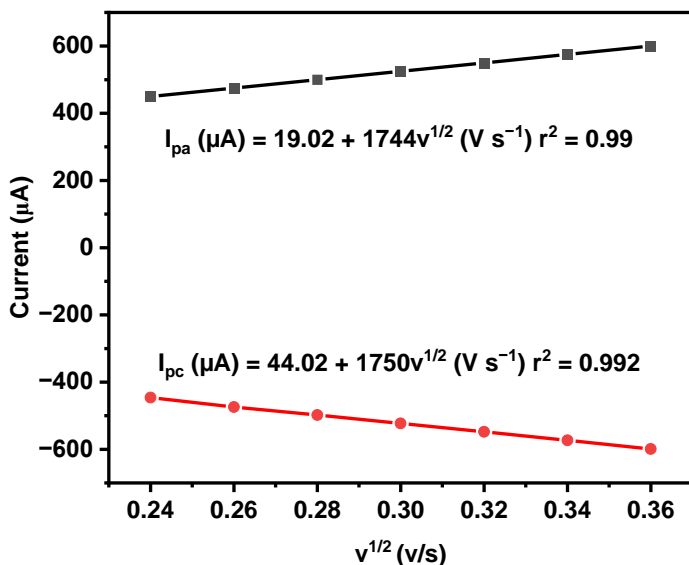


Figure 4.4. Change of peak anodic current (I_{pa}) with $v^{1/2}$

4.3.3. Linearity and Interference Studies

In cyclic voltammetry, variation of the peak anodic current (I_{pa}) with different concentration of thyroxine solution was observed at 0.36V. The I_{pa} decreases from 500 μA to 400 μA (figure 4.5a) as T_4 concentration is increased from 5 $\mu g/mL$ to 50 $\mu g/mL$ due to partial surface passivation which results in significant impedance to the interfacial electron transfer. The calibration plot shows a linear relationship between the two variables *i.e.*, concentration and current response at potential of 0.36V. The linear relationship can be represented by equation: $y = -1.978x + 537.03$ and $r^2 = 0.9978$. A strong relationship between these two parameters is established as the r^2 value is almost close to 1 (figure 4.5b). The current response beyond the concentration range of 5 $\mu g/mL$ – 50 $\mu g/mL$ did not show linearity. This range also covers the physiological range of thyroxine in the blood and saliva.

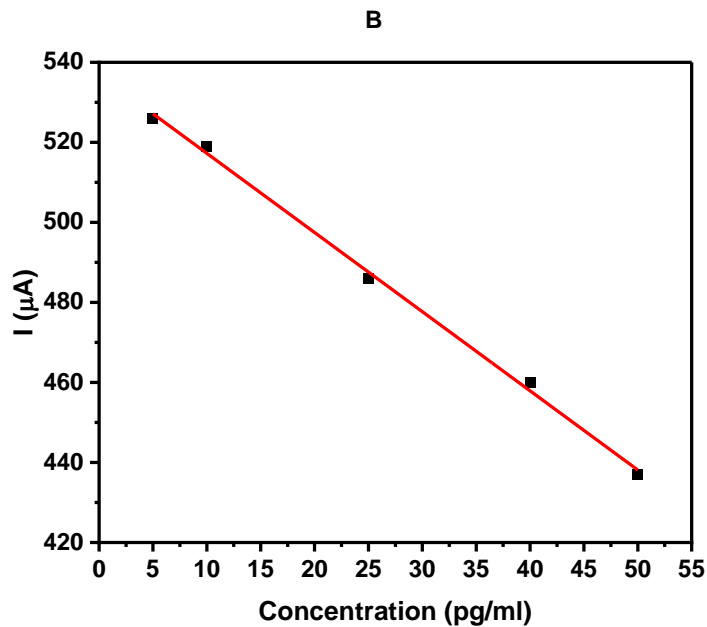
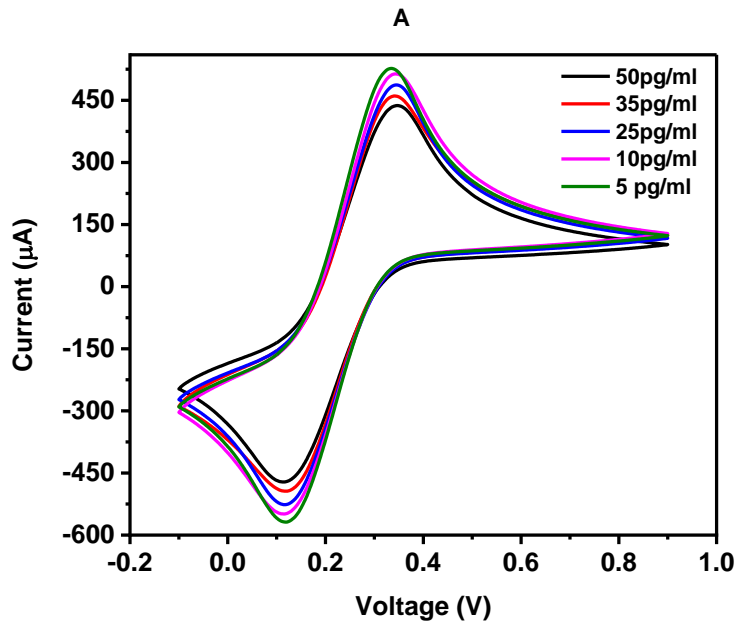


Figure 4.5. A. CV profile for different concentration of thyroxine solutions and B. calibration plot between peak anodic current (I) and concentration

The Limit of Detection (LoD) was calculated using equation 4.3.

$$\text{LOD} = 3(\text{SD}/m)$$

Equation 4.3

where SD is the standard deviation of the response and “m” is the slope of linear curve (Poggialini et al., 2023). LoD found to be 6.16 pg/mL (0.079nM). Repeatability studies were performed with 50 pg/mL concentration of thyroxine. The result shows a relative standard deviation of 2.45%. The method was found to be more sensitive than other developed thyroxine biosensors as shown in table 4.2.

Table 4.2. Different studies for development of thyroxine biosensors

Electrode	Materials used	Method	LOD (nM)	Reference
Screen Printed Electrode	Carbon nanotubes, graphene, and gold nanoparticles	Differential pulse voltammetry	30	(David et al., 2022)
Renewable mercury film silver-based electrode	Renewable mercury film	Cyclic voltammetry	18	(Smajdor et al., 2016)
Carbon paste electrode	Graphite powder in paraffin oil	Cyclic voltammetry	6.5	(Hu et al., 2004)
Gold Microgap electrode	Thyroxine DNA aptamer/ rhodium nanoplate heterolayer	Cyclic voltammetry	0.01	(Park et al., 2020)
Modified copper disk and PVC tube	Reduced graphene oxide containing gold nanoparticles attached with beta cyclodextrin	Amperometry	1	(Muñoz et al., 2016)
T₄-imprinted mesoporous organic silica	Molecular imprinted mesoporous organic silica	Fluorescence	0.47	(Seo et al., 2024)
Indium tin oxide coated glass	Molecularly Imprinted Polyaniline	Cyclic voltammetry	0.0079	Present study

Interference studies were performed using biomolecules structurally like thyroxine. The molecules selected for the study were phenylalanine, tyrosine and liothyronine. The results showed that none of these molecules were affecting the response significant. (figure 4.6) This shows that the developed biosensor is selective towards thyroxine molecule.

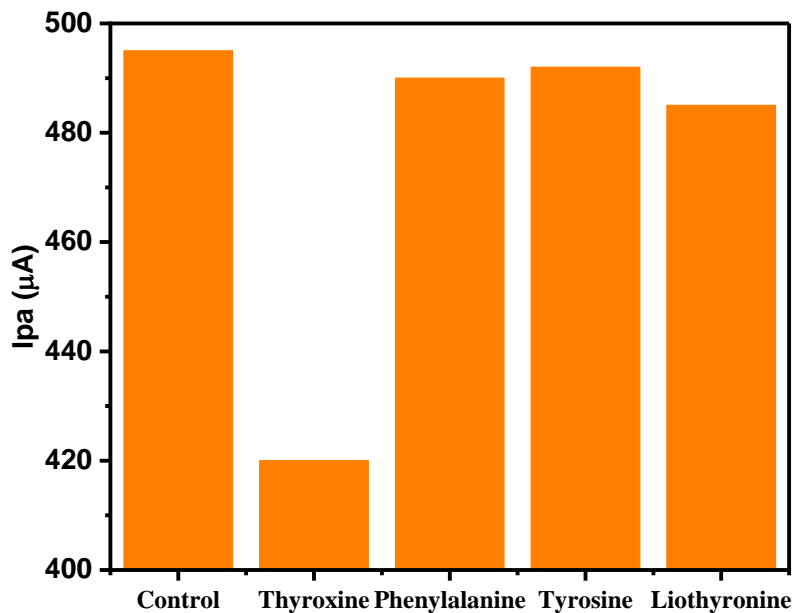


Figure 4.6. Effect of potential interfering substances on the response of molecularly imprinted PANI sensor towards the detection of T₄. Water is taken as a control.

4.4 Estimation of Thyroxine in Saliva: Spiking study

Thyroxine hormone is present in different biological matrices in the body. It is present in blood, saliva, tears, hairs, nails etc. It exists in two forms (*i*) bound form in which it is bound to proteins and (*ii*) free form. The levels of bound and free thyroxine vary in all these matrices. Different methods have been employed to find the levels of thyroxine hormone in these matrices. The levels of thyroxine in different sample matrices are shown in the following table 2.3 (chapter 2). Saliva is a better matrix to determine levels of thyroxine as free thyroxine is relatively higher in concentration as compared to blood. Also, it is a non- invasive matrix and contains relatively fewer interfering substances as compared to blood.

Sample collection

There are different methods for the collection of saliva including the draining method, the suction method, spitting method, and the swab method (Bhattarai et al., 2018; Navazesh, 1993). After saliva collection, it is recommended to be stored at -20°C (Chiappin et al., 2007). In this study, spitting method was used to collect saliva.

Human saliva was taken by directly spitting into a test tube. Before sample collection, the mouth was rinsed with water. 1mL of collected sample was diluted with 5mL of water. The samples were then filtered using $0.22\mu\text{m}$ syringe filter and stored at 4°C . The procedure is described in figure 4.7. The ethical approval for this study was taken from the institutional ethics committee (IEC) (Annexure I).

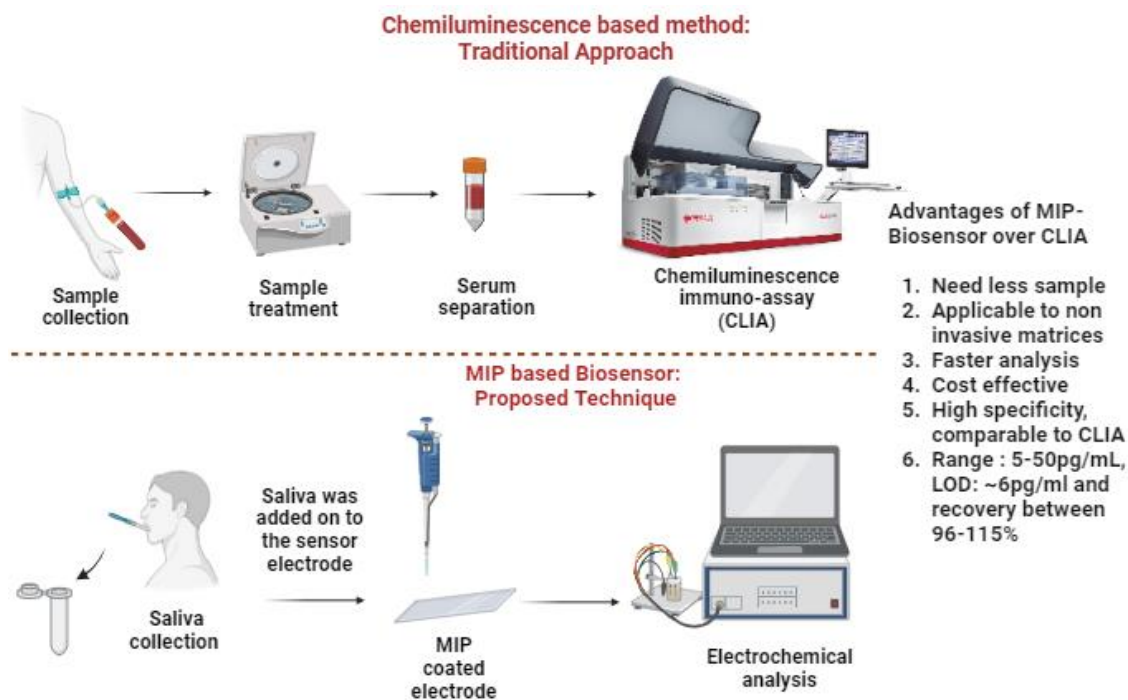


Figure 4.7. Comparison of determination of thyroxine using Chemiluminescence (CLIA) analyzer and MIP based biosensor

The calibration plot was developed again with thyroxine solution between a concentrations range of 5pg/mL - 50pg/mL. The equation represents the relation between current, and concentration is $y = -1.428x + 401.4$ with $r^2 = 0.98$. LOD was found to be 7.12pg/mL (figure 4.8a and 4.8b).

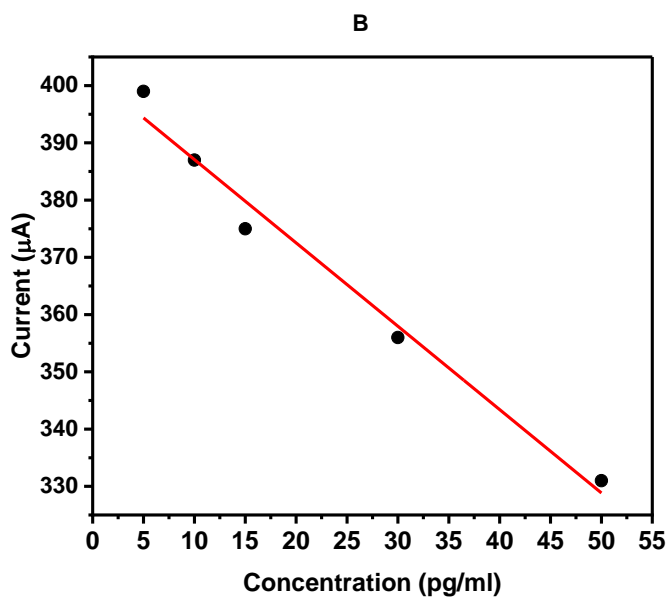
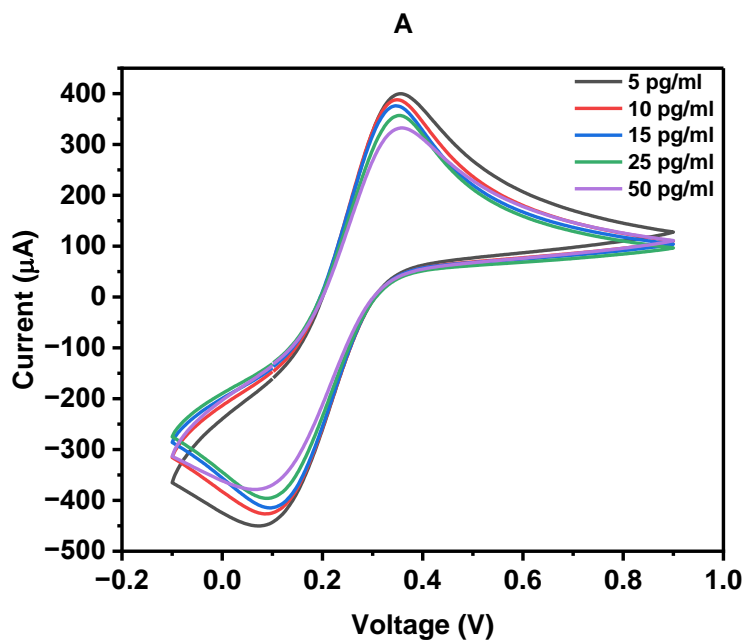


Figure 4.8. A. Effect of concentration and current response and B. Calibration plot between peak anodic current (I) and concentration

The spiked saliva samples were analyzed (in triplicate) using cyclic voltammetry and the response showed 96 - 115.2% of recovery with a relative standard deviation

of 0.98%. The slight increase in the recovered percentage of thyroxine could be due to the natural presence of thyroxine. The recovery results showed that the developed biosensor can also be used for analyzing thyroxine in saliva for diagnostic purposes. The promising analytical sensor performance therefore highlights the potential of the developed platform to be translated towards clinical applications in a point-of-care scenario, for increased patient compliance.

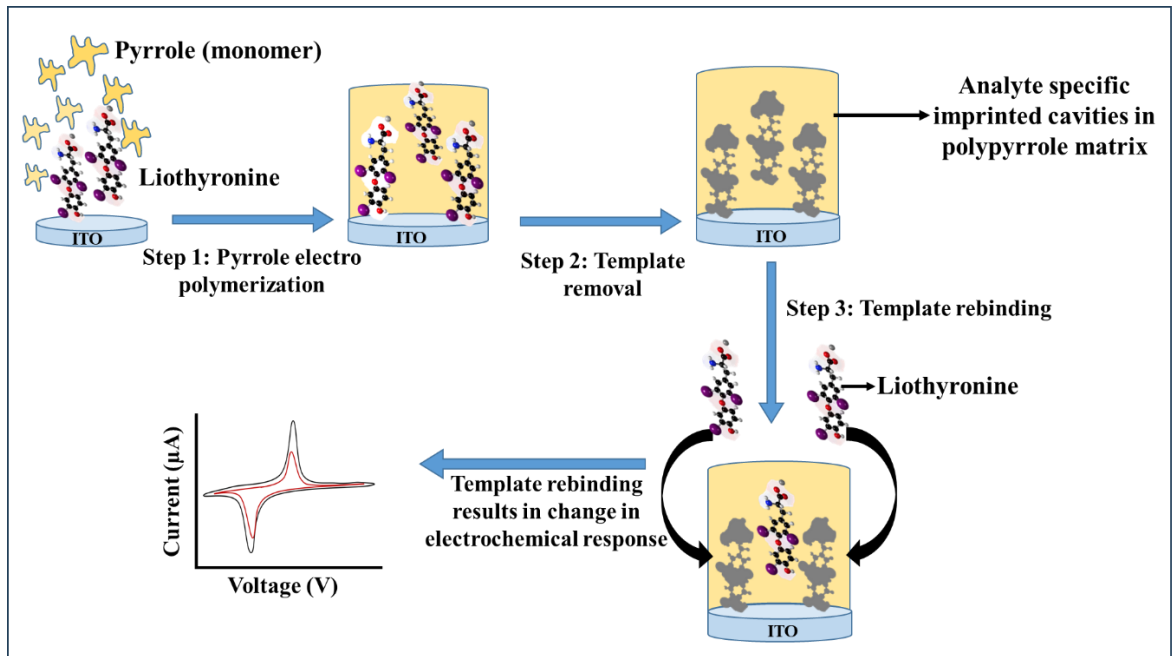
4.5. Conclusion

This chapter discuss the development of thyroxine biosensor with molecular imprinted polymer coated ITO electrode. The fabricated sensor was analyzed electrochemically for linearity, interference, repeatability, and biological matrix study. The sensor was calibrated within T₄ concentration range of 5pg/mL-50 pg/mL, with limit of detection of 6.16 pg/mL. Repeatability studies showed a percentage relative deviation of 2.45. The studies were also performed by spiking thyroxine in diluted saliva. Recovered thyroxine after spiking saliva was between 96 and 115.2%. The developed MIP-based electroanalytical sensor was found to exhibit a high degree of selectivity against various interferants. Due to high sensitivity and selectivity, the developed biosensor has huge prospects toward futuristic point-of-care applications.

Chapter 5

Electrochemical synthesis of Molecularly Imprinted Polymers for Development of Electroanalytical Biosensor to estimate Liothyronine

Graphical Abstract



Abstract

Liothyronine (T_3) is a thyroid hormone which is frequently administered alongside thyroxine in the treatment of hypothyroidism. However, several market withdrawals have been called for due to persistent quality issues with liothyronine tablets. Given its narrow therapeutic index, maintaining optimal liothyronine levels is imperative, highlighting the criticality of ensuring quality both during manufacturing and at the patient's bedside. In this study, we introduce a pioneering electroanalytical biosensor designed for liothyronine estimation using molecularly imprinted poly-pyrrole (MIP-Ppy). Notably, the sensor demonstrates linear response within the concentration range of 50-300 pg/mL ($r^2 = 0.986$) with a remarkable limit of detection (LOD) of 80 pg/mL. Interference studies were performed to validate the sensor's robustness, with negligible response alterations. This method was used for the assay of liothyronine tablets and was compared with the traditional HPLC method. The MIP-Ppy biosensor showed 90.7% recovery with a minimal relative standard deviation of 0.093 whereas HPLC showed 92.7% recovery with RSD 0.054. These findings underscore the biosensor's potential as a cost-effective alternative to sophisticated chromatographic methods for liothyronine estimation in pharmaceutical tablets. This advancement lays the groundwork for the development of a user-friendly point-of-care device.

5.1. Introduction

Liothyronine (T_3) is a hormone secreted by the thyroid gland that regulates human metabolism. It is another important biomarker which is used along with thyroxine for diagnosis of thyroid disorders. Liothyronine is also used as a therapeutic compound for hypothyroid patients. The sodium salt of T_3 is given in combination with thyroxine for hypothyroid patients who do not respond to thyroxine treatment alone (Jonklaas et al., 2021). The usefulness of T_3 is not limited to hypothyroid patients as it is also used for other conditions such as improving hair growth and treating dermal heat loss. (Bjerkreim et al., 2021; Safer et al., 2001)

The amount of T_3 in tablets is as low as $5\mu\text{g}$ which is less than 0.01% of the total weight of tablet. Due to very low amount, liothyronine tablets have high chance of compromised product quality in terms of content uniformity and assay. Many product recalls were observed in the last few years for T_3 mainly due to reduced potency in the tablet (Food and Drug Administration, 2018). Even in human blood, the levels of free liothyronine are in a very narrow range *i.e.*, between 2pg/mL - 4pg/mL (J. Jonklaas et al., 2016). The quality of the product can severely affect the levels of liothyronine in blood after ingestion which can result in partial treatment for the patients. Food and Drug Administration (FDA) has recommended that dose titration of liothyronine is necessary to avoid any serious adverse effects (Food and Drug Administration, 2022). Hence, it is important to maintain and monitor the levels of T_3 in the pharmaceutical formulations.

Pharmaceutical industries mainly relies on high performance liquid chromatography (HPLC) for quality control analysis, including assay, dissolution and stability studies (Collier et al., 2011). HPLC instrument requires skilled professionals, costly solvents, and prolonged testing time. Alternatively, biosensing techniques are emerging for estimation of analytes present in very low amounts. These techniques are selective, cost effective and have high specificity. The detection method is based on either electrochemical, optical, piezoelectric, and mass. Electrochemical methods are the most versatile and most used detection

methods. For electrochemical sensors, biorecognition targets such as antibodies, aptamers, enzymes, and imprinted polymers are required for selective estimation of a target molecule in a solution containing mixture of compounds.

For electrochemical analysis of T_3 , antibodies have been explored as bio-recognizing targets in some reports. Although antibodies show high specificity for the analyte molecule but have several drawbacks such as shorter shelf life, low chemical stability, high cost and require special storage conditions (Byrne et al., 2009). As an alternate, molecularly imprinted polymers (MIPs), also known as synthetic antibodies, overcome these drawbacks. The MIP approach allows for the customization of biomimetic materials, which gives them high selectivity comparable to antibodies. Pyrrole and aniline are the two most used functional monomers (Alonso-Lomillo et al., 2023; BelBruno, 2019; Özcan et al., 2008; Ratautaite et al., 2022). They are preferred due to their simple synthesis, high electrical conductivity, suitable redox properties, good biocompatibility, environmental stability, electrochemical properties, and easier polymerization process (Muhammet et al., 2009; Rajendraprasad, 2022; Regasa et al., 2020; Setiyanto et al., 2017). Several companies in the world commercially develop molecularly imprinted polymers for biosensing application such as Ligar (New Zealand), MIP Discovery (United Kingdom) *etc.*

To date, no molecularly imprinted polymer has been developed for sensing of T_3 molecule. Here, we present the first molecular imprinting poly-pyrrole (MIP-Ppy) based T_3 biosensor which can be used for ultrasensitive estimation of T_3 in pharmaceutical dosage forms. The developed biosensor shows high specificity, sensitivity, and stability for up to 28 days. The method was applied to estimate liothyronine in liothyronine tablets and a recovery of around 90.7% was observed. This biosensor can be used as an alternative for monitoring the quality of T_3 tablets by pharmaceutical industries. It is a step forward for the determination of liothyronine in blood levels. This study will also help to miniaturize and develop a point-of-care device for estimating the amount of T_3 in tablets even at home.

However, further improvement in sensitivity will enable this method to be used for estimation of liothyronine in other biological fluids.

5.2. Experimental

5.2.1. Materials

Liothyronine (MW: 672.96 Da, $\geq 95\%$ using HPLC) and tyrosine were purchased from Merck (Darmstadt, Germany). Glucose (MW: 180.15 Da, $\geq 99\%$), ascorbic acid (MW: 176.12 Da, $\geq 99\%$), potassium ferrocyanide trihydrate (MW: 422.38 Da, $\geq 99\%$) and potassium ferricyanide (MW: 329.24 Da, $\geq 99\%$), potassium dihydrogen phosphate (KH_2PO_4 ; MW: 136.08 Da, $\geq 99\%$) and di-sodium hydrogen phosphate (Na_2HPO_4 ; MW 141.9 Da, $\geq 99\%$), sodium chloride were procured from Rankem, India. Liothyronine tablets (Linorma 5 μg , Abbott) were purchased from local pharmacy store (India). Ultrapure water (resistivity $\sim 18.2 \Omega \text{ cm}$ at 298 K) from water purification system (Milli-Q system Millipore Bedford, MA, USA) was used in all HPLC experiments. All the chemicals procured were of the highest analytical grade and did not require further purification. Freshly prepared working solutions were used for electrochemical sensing.

5.2.2. Electrodes and Instruments

Electrodes: Indium tin oxide coated glass electrodes were used as working electrodes (dimensions 10 mm x 10 x 1mm) with resistivity $\leq 10 \Omega/\text{sq.}$ and ITO film thickness 1800-2000 Å. For molecular imprinted polymer-based detection of thyroxine and liothyronine, silver-silver chloride electrode was used as reference electrode and platinum wire as counter electrode.

Instruments: Dropsens electrochemical potentiostat (uStat i-400, Metrohm, Switzerland), high performance liquid chromatography (HPLC) (Shimadzu Prominence-i LC-2030C 3D Plus, Japan), consisted of a Shimadzu C-18 column (250mm \times 4.6mm, 5 μm), quaternary pump, an automatic injector, variable wavelength detector, and a column oven. SEM (Evo-18, Zeiss) was used to find the deposited polymer coating layer thickness. Data was collected using Lab solutions software. Atomic Force Microscope (AFM) (Nanosurf AG, Switzerland), Particle

size analyzer (Zen 1690, Malvern instruments Ltd.), Fourier Transform Infrared spectrometer (Perkin Elmer), Drop shape analyser (DSA25Kruss, Germany), analytical weighing balance (Shimadzu AT series, Japan).

5.2.3. Methodology

5.2.3.1. Preliminary studies

Solubility studies of liothyronine were performed using water, dimethyl sulfoxide (DMSO), dilute sodium hydroxide and dilute hydrochloric acid. The identification test of liothyronine was performed using UV-spectrometer as per certificate of analysis given by the manufacturer. FT-IR and HPLC was also performed to check the purity of liothyronine as per Indian Pharmacopoeia 2018. The characteristic peaks obtained in UV scan and FT-IR spectra were matched with the reported data in the literature.

For UV-scan, 50 ppm of liothyronine solution was prepared in 0.1N sodium hydroxide solution as mentioned in the certificate of analysis. The solution was scanned in the range of 260-400nm.

For FT-IR analysis, around 2 mg of liothyronine was mixed uniformly with KBr, and a pellet was formed. This pellet was analyzed with FT-IR in the range of 4000cm^{-1} - 400cm^{-1} . Number of scans were 16 and resolution was 4 cm^{-1} .

HPLC analysis was done to check the purity of liothyronine. The 20ppm solution was prepared in dilute sodium hydroxide using ultrapure milliQ water. A gradient reverse phase (C-18) method was used for the analysis of liothyronine with a run time of 20 mins. HPLC parameters for analyzing liothyronine are given in table 5.1 (Collier et al., 2011).

Table 5.1. HPLC parameters for testing the purity of liothyronine

Conditions	Parameters
Conditions	Parameters
Column	Reverse phase C-18 column, 4.6mm x 250 mm and 5 μ m particle size
Mobile phase	Methanol - Solvent A Phosphate buffer (1mM, pH 3) - Solvent B
Gradient	45 - 20% solvent A in 5 mins 20% Solvent A for 9 mins
Injection volume	20 μ L
Flow rate	1 mL/min

5.2.3.2 Synthesis of MIPs on ITO electrode

MIP-Ppy was synthesized electrochemically using pyrrole as monomer. The monomer solution was prepared by adding 27 μ L of pyrrole in 19.973mL of phosphate buffer (pH 6). T₃ (1.0 mg) was added to the pyrrole solution. The mixture was ultrasonicated for 10 mins for uniform mixing. Electrochemical deposition was performed further in this solution using three-electrode set-up with ITO electrode as working electrode (1cm x 1cm), platinum wire as counter electrode, and silver-silver chloride as reference electrode. The potential was varied from -1.15V to +1 V (vs. SCE) at a scan rate of 0.05 V/s (S. Kim et al., 2016). After deposition, the electrodes were then washed with distilled water. The template (T₃) removal was performed by ultrasonication in 0.1N sodium hydroxide solution for 30 mins. The detailed synthesis scheme is as summarized (figure 5.1).

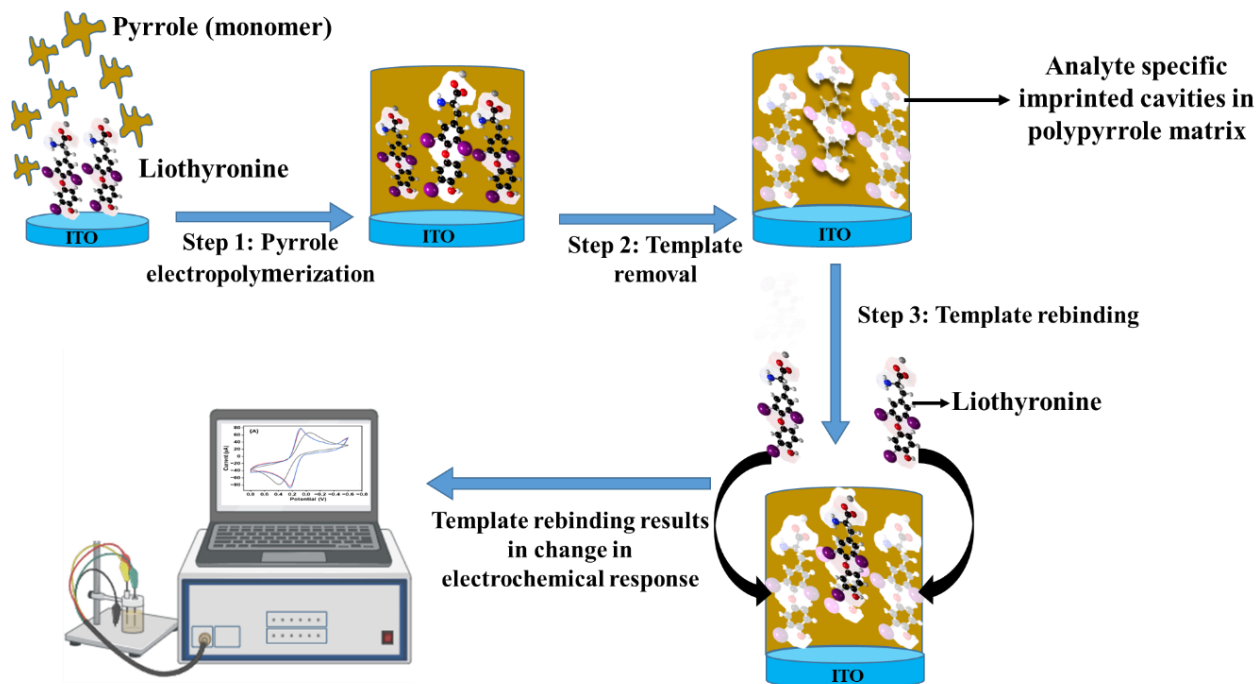


Figure 5.1. Schematic representation of molecular imprinting process of polypyrrole with liothyronine (T₃) and subsequent sensing with cyclic voltammetry

5.2.3.3. Characterization studies of MIPs and NIPs

Structural characterization of NIP and MIP surfaces was done using FT-IR, AFM, and CV. The samples were analysed from 400cm⁻¹ - 4400cm⁻¹ range. AFM (Nanosurf AG, Switzerland) scan was performed on 10 μm x 10μm surface. The coating thickness was found using SEM at 5Kx magnification and image was analyzed using smartSEM software. The scans were performed for both non imprinted polypyrrole and MIP-Ppy on ITO surface. Electrochemical (cyclic voltammetry) analysis was performed for MIP-coated ITO, MIP + liothyronine coated ITO and bare ITO as the working electrode while, Ag/AgCl and Pt served as reference and counter electrodes, respectively. All electrochemical studies were performed in potassium ferro-ferricyanide solution (10mM) prepared in phosphate buffer saline (1mM, pH 7.4). Electrochemical conditions were set between -0.8 to +1 V at a scan rate of 0.05 V/s.

5.2.3.4 Analytical sensor performance: Scan rate, linearity, interference, and stability studies

Scan rate study was performed to find the active surface area of the working electrode potential range of -0.8 to $+1$ V starting from 10mV/s till 90mV/s . It helped to ensure electrode stability and to check if the electrodes follow the Randel's-Sevick (R-S) behavior of the electrodes.

Linearity studies were performed using freshly prepared solutions of liothyronine for concentrations between 50pg/mL to 300pg/mL . Several MIP coated ITO electrodes were prepared and kept at room temperature (RT) before use. The sample ($5\mu\text{L}$) was added onto the MIP coated ITO and incubation was done at room temperature for 10 min. Interference studies were performed using biomolecules such as dextrose, tyrosine, ascorbic acid, and phosphate buffer (pH 7.4).

Stability of electrodes was studied with respect to time and pH. For pH stability, the MIP-Ppy coated electrodes were kept in different pH solutions from 3 to 11 and the CV response was observed. To study the effect of time, the CV response for MIP-Ppy coated electrodes was performed at different intervals of time. These electrodes were stored in desiccator till further use.

5.2.3.5. Estimation of Liothyronine in Pharmaceutical Tablets

MIP-Ppy method: The sample pharmaceutical tablet of liothyronine sodium USP ($5\mu\text{g}$) was crushed in pestle mortar and dissolved in 0.1M sodium hydroxide. The sample was diluted to 200pg/mL and analyzed in potential range of -0.8 to $+1$ V using MIP-Ppy coated ITO electrodes similar to the standard solution.

The concentration of sample was analyzed using the calibration plot developed in the range of 50pg/mL - 300pg/mL. The sample was analyzed in triplicate and relative standard deviation (RSD) was calculated.

HPLC method: Liothyronine standard solutions were prepared in a range of 1-5µg/mL. 500 µL was added into HPLC vials. Sample pharmaceutical tablet of liothyronine sodium USP (5µg) was crushed in pestle mortar and dissolved in 0.1M sodium hydroxide. The sample was diluted to obtain a concentration of 2µg/mL. The HPLC analysis was performed using parameters given in table 5.1. All readings were taken in triplicate. An equilibration time of 20 mins was given before each run.

5.3. Results and Discussion

Liothyronine was found to be freely soluble in 0.1N sodium hydroxide solution. The UV spectra (figure 5.2) showed a lambda max of 297nm which corresponds to the value mentioned in literature (Gregorini et al., 2013).

The FTIR spectra (figure 5.3) showed characteristic stretching frequency peaks of liothyronine were similar to thyroxine as the structure is almost similar. The observed peaks include characteristics stretching frequencies of C-I around 680cm⁻¹, C=O around 1650cm⁻¹, O-H around 3500cm⁻¹, C-C around 1100cm⁻¹etc (Shao et al., 2012). The HPLC chromatograph shows a single peak of liothyronine at 7.3 mins (figure 5.4).

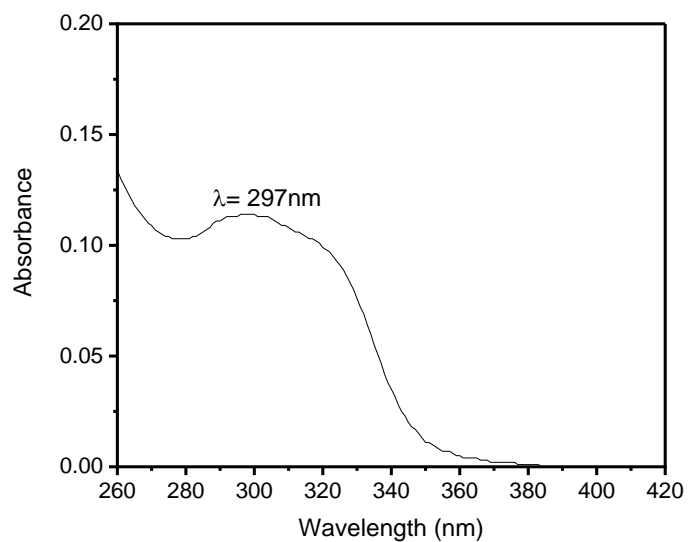


Figure 5.2. UV scan of liothyronine solution taken between 260nm to 400nm. The maximum absorbance is observed at 297nm.

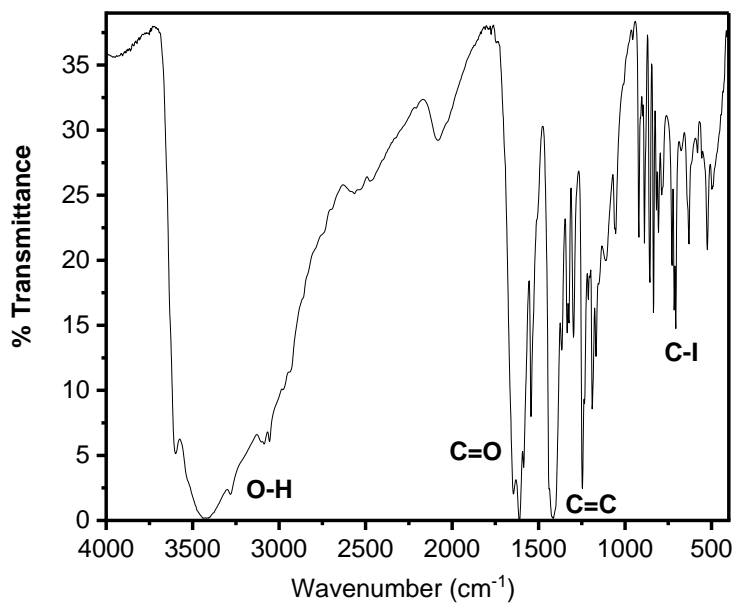


Figure 5.3. FT-IR spectra of liothyronine

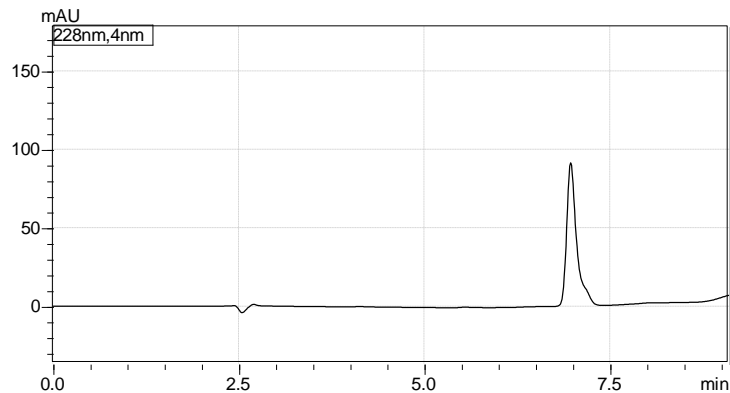


Figure 5.4. HPLC chromatogram of liothyronine

5.3.1. Synthesis and Characterization

A thin greenish-black layer of polymer was electrodeposited onto ITO electrodes (Kim et al., 2016). The dimensions of the deposited layer were $1.0 \times 0.5 \pm 0.1$ cm. Optimization of number of scans for polymer deposition showed that after the third scan there was not much change in current. Hence, for coating the polymer layer, three scans were performed. The coating thickness found using SEM was around 750 nm. Figure 5.5A and 5.5B shows polypyrrole layer coated onto ITO electrodes and SEM image for coated polypyrrole on ITO glass. MIP-Ppy on ITO was formed after template removal by sonicating in 0.1N sodium hydroxide. FT-IR, AFM and cyclic voltammetry confirmed the synthesis of MIP.

A



B

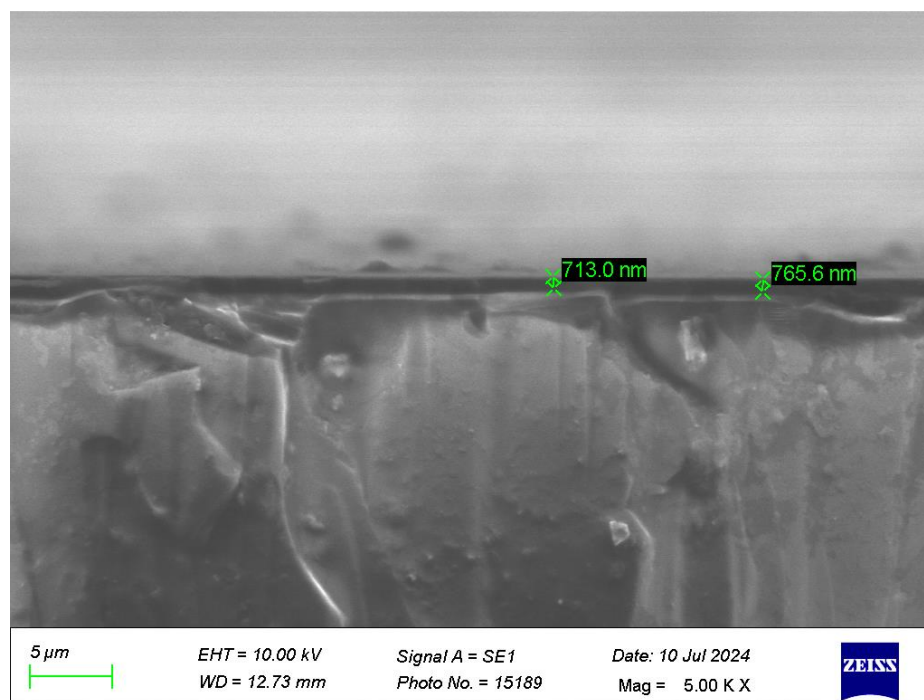


Figure 5.5. A. ITO electrode with and without coating of polypyrrole B. SEM image of polypyrrole coated on ITO glass (3 cycles). The thickness of polypyrrole layer is around 1000nm

FT-IR spectra shows characteristic peaks of polypyrrole (figure 5.6), peak at 3300cm^{-1} indicates N-H stretching, 1640cm^{-1} indicates C=C stretching, and peak around 1200cm^{-1} indicates C-C stretching. The spectra indicate the presence of polypyrrole structural moiety (Yussuf, et al., 2018). Some of the other peaks show that polypyrrole has undergone over-oxidation. Over-oxidation is common phenomenon in electrochemical synthesis of polypyrrole. FT-IR spectra shows a peak at 1800cm^{-1} which confirms carbonyl group (C=O stretching) and a broad peak between $2400 - 3200\text{cm}^{-1}$ confirms O-H stretching of carboxylic group. Based on the FT-IR spectra, the ring opening might have occurred and there is a formation of carboxylic group in some of the pyrrole rings as a side reaction in the polypyrrole matrix due to overoxidation (Debiemme-Chouvy et al., 2008). On comparison, the

difference in the broad peak between 2400 cm^{-1} - 3200 cm^{-1} in MIP, NIP and MIP + Liothyronine signifies that -OH group of carboxylic acid may be involved in binding to liothyronine as the peak intensity of -OH group is significantly reduced in case of MIP + Liothyronine but the intensity of unbound MIP and NIP was found to be significantly higher.

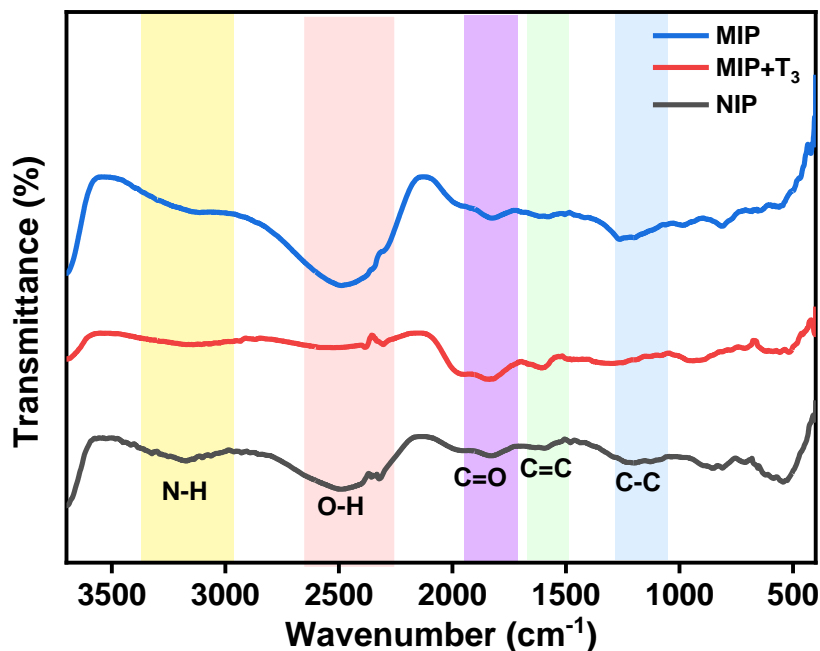


Figure 5.6. FT-IR spectra for MIP, NIP and MIP + Liothyronine

AFM analysis (figure 5.7) showed the surface topology and 3D surface profile. The result shows significant change in surface morphology of NIP and MIP. The surface roughness of MIP was calculated using WSxM software and was found to be 1.91nm. The roughness can be due to small scale variations in the height of electrodeposited polymers. The surface roughness in MIP is higher which could be due to the formation cavities whereas in case of NIP the surface was relatively smooth due to absence of cavities.

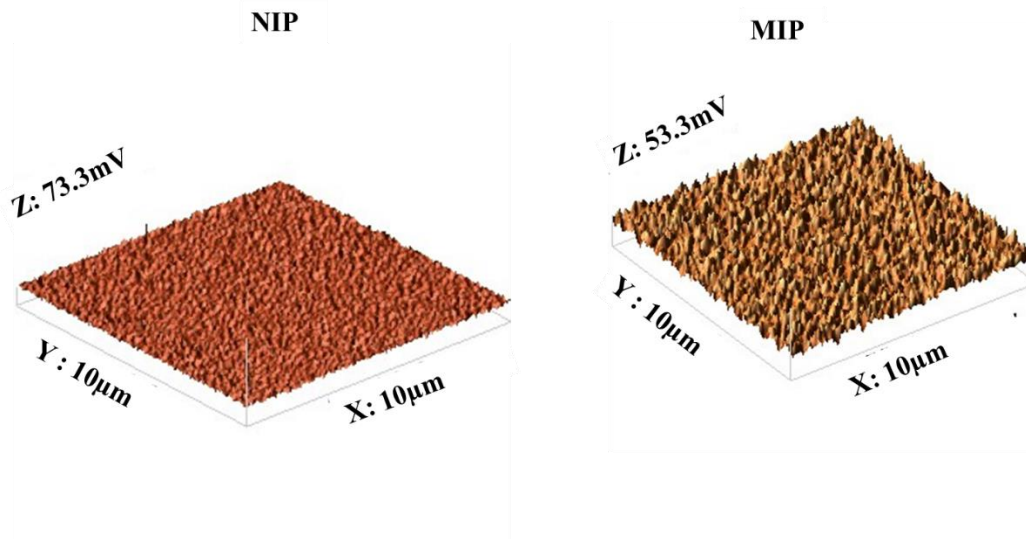


Figure 5.7. AFM image of NIP surface and MIP surface

Electrochemical characterization result shows the difference in the anodic peak current (I_{pa}) for NIP, MIP, MIP+T₃ and bare ITO (figure 5.8).

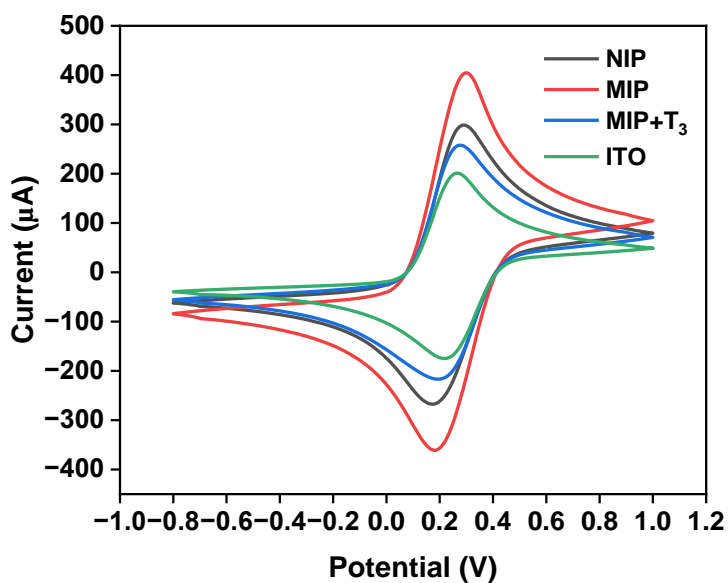


Figure 5.8. CV scan for NIP, MIP, MIP + Liothyronine, and bare ITO

Bare ITO surface exhibits a peak anodic current $I_{pa} \sim 200 \mu\text{A}$ (figure 5.8). However, its modification with the imprinted polypyrrole film results in an increase in $I_{pa} \sim 325 \mu\text{A}$ which is higher than that observed in pristine ITO and can be attributed

to the presence of a conducting thin polymeric film (Ateh et al., 2006). On addition of liothyronine (200pg/mL) to the polypyrrole matrix, the current decreases to $I_{pa} \sim 200 \mu A$. The results also showed that rebinding of liothyronine to the imprinted polypyrrole matrix causes significant decrease in current. A similar trend was observed when thyroxine (a structural analog of liothyronine) binds to its cavities. The distinct response at each stage of sensor fabrication observed in CV shows a successful fabrication of molecularly imprinted polypyrrole-based sensor for the selective recognition of liothyronine. The results obtained by FT-IR, AFM and cyclic voltammetry prove that T₃ was imprinted in the polypyrrole matrix.

5.3.2 Sensor Performance: Scan rate, linearity, interference, and stability

The electroactive surface area of T₃ templated polypyrrole electrodes was found by studying the current response at different scan rates (figure 5.9).

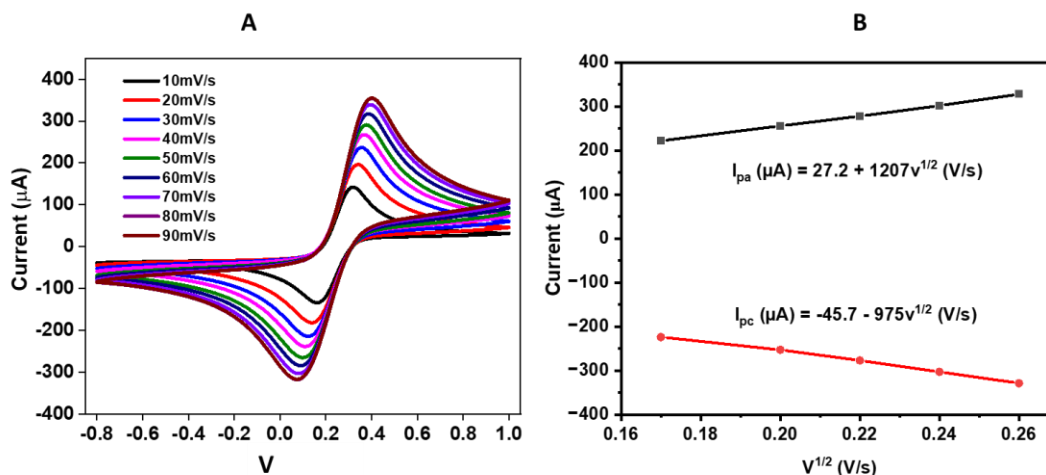


Figure 5.9. (A) Study of scan rate vs current response from 10 mV/s to 90 mV/s. (B) Linearity between peak anodic and cathodic current with square root of scan rate

The peak anodic and cathodic currents increase as the scan rate is increased from 10 – 90 mV/s (figure 5.9a), with the response saturating at the latter value. Wilson et al. observed a similar increase in peak anodic current for polypyrrole (Wilson et al., 2015). A direct proportionality of I_{pa} and I_{pc} (equation 5.1 and 5.2) with square root of scan rate (v) corresponds to the well-known Randel's-Sevick (R-S) behavior. The electroactive surface area was found to be 0.52 cm² using the R-S equation.

$$I_{pa} (\mu A) = 27.2 + 1207v^{1/2} (V/s), r^2 = 0.988 \quad \text{Equation 5.1}$$

$$I_{pc} (\mu A) = - 45.7 - 975v^{1/2} (V/s), r^2 = 0.993 \quad \text{Equation 5.2}$$

Between scan rate 30 mV/s to 70 mV/s the electrode process was found to be diffusion controlled as the anodic peak current (I_{pa}) and peak cathodic current (I_{pc}) increased linearly with square root of scan rate (figure 5.9b) (Prasad et al., 2010; P. Zhu et al., 2019). Scan rate of 50mV/s was selected for the cyclic voltammetric analysis.

The analytical response of the developed MIP-Ppy sensor at various T_3 concentrations was studied using CV. It can be observed that the I_{pa} decreases from 340 μ A to 231 μ A as T_3 concentration is elevated from 50 pg/mL to 300 pg/mL (figure 5.10). This can be attributed to the formation of partial surface passivation, at higher T_3 concentrations, resulting in significant impediments to the interfacial electron transfer. The developed sensor was calibrated at 0.38 V (Fig 5.11). A linear relation between I_{pa} (at 0.38V) and T_3 concentration was observed. The linear equation was found to be $y = -0.423x + 363.7$ and $r^2 = 0.993$.

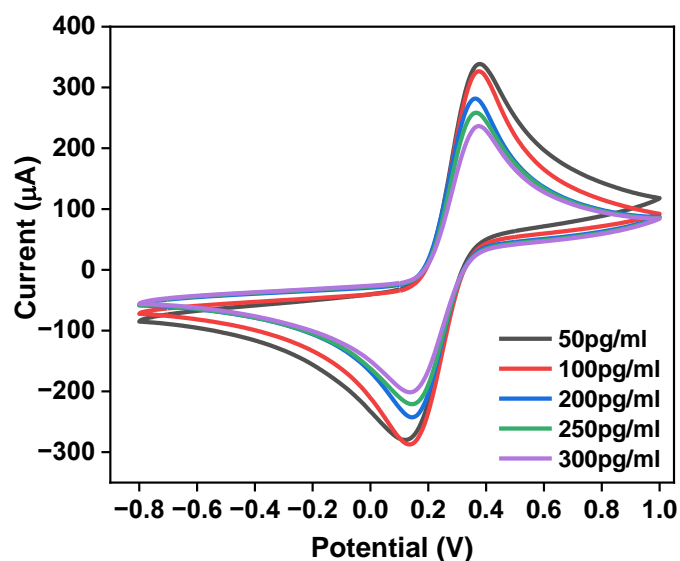


Figure 5.10. CV scans for different concentration of T_3 solutions from 50pg/mL - 300pg/mL

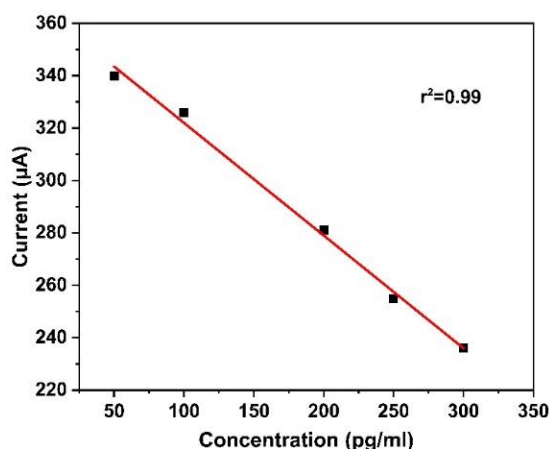


Figure 5.11. Calibration plot shows linearity in the range 50pg/mL-300pg/mL concentration for liothyronine using developed biosensor

The Limit of Detection (LoD) was calculated using the 3σ rule and was found to be 80pM. The sensor parameters of developed MIP-based platform were compared with few previously reported studies, as highlighted in Table 5.2. The method was found to be better than reported in literature.

Table 5.2. Comparison of sensitivity other techniques for determination of T₃

Electrode/ Technique	Materials used	Method	Linearity Range	Reference
Gold Electrode	Gold nanoparticles coated with anti-T ₃ antibodies	Impedance Spectroscopy	10 - 10 ⁵ pg/mL $r^2 = 0.946$	(Nguyen et al., 2020)
Carbon paste electrode	Enzyme modified carbon paste	Amperometry	340 - 17x10 ³ pg/mL $r^2 = 0.997$	(Aboul-Enein et al., 2002)
Glassy carbon electrode	Fe ₃ O ₄ @graphene nanocomposite coated with anti-PDIA3	Differential pulse voltammetry	10-200 µM $r^2 = 0.997$	(Baluta et al., 2023)
Microcolumn coated with T₃	Anti-Triiodothyronine monoclonal antibody	Flow fluorimeter	0.1 - 30ng/mL	(Wani TA et al., 2016)
Indium tin oxide coated glass	Molecularly Imprinted Polypyrrole	Cyclic voltammetry	50–300 pg/mL $r^2 = 0.993$	Present study

The developed MIP-Ppy sensor was further subjected to various potential interfering molecules, and the corresponding response was obtained using CV technique. The CV response of T_3 in presence of tyrosine (Tyr), glucose, ascorbic acid was observed for the interference studies. The relative reduction percentage response due to interfering substances is shown in figure 5.12.

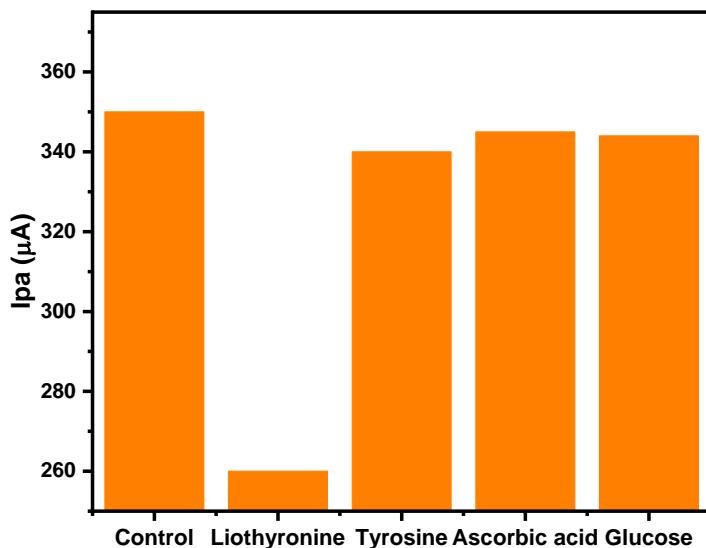


Figure 5.12. Bar graph showing the effect of potential interfering substances (tyrosine, ascorbic acid, glucose) on the response of MIP-Ppy based sensor towards the detection of T_3 . Water is taken as a control.

It was observed that the interfering substances have insignificant binding capabilities in the templated polypyrrole matrix as indicated by the % binding values mentioned above, which justifies the presence of T_3 -specific cavities. The promising analytical sensor performance therefore highlights the potential of the developed platform to be used for selective estimation of T_3 in different samples.

Effect of pH (figure 5.13) showed that the biosensor was stable around pH 7. The response decreases significantly above pH 7.5 and below pH 5. At slight acidic pH, the amine nitrogen can get protonated and at higher pH the acidic group of

overoxidized polypyrrole gets deprotonated. Hence, the response works well for sample with pH around 7 (Tsugita, et al. 2022).

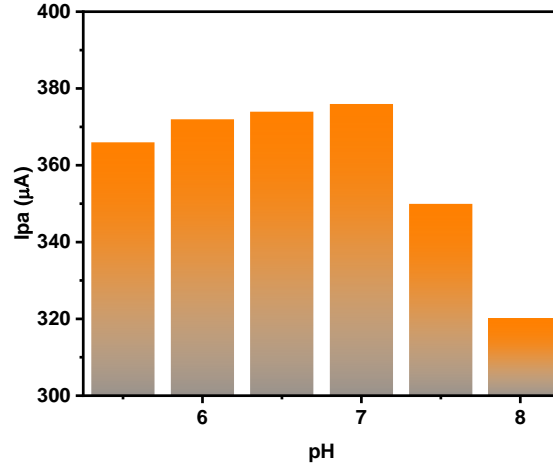


Figure 5.13. Bar graph showing the effect of pH on the biosensor response

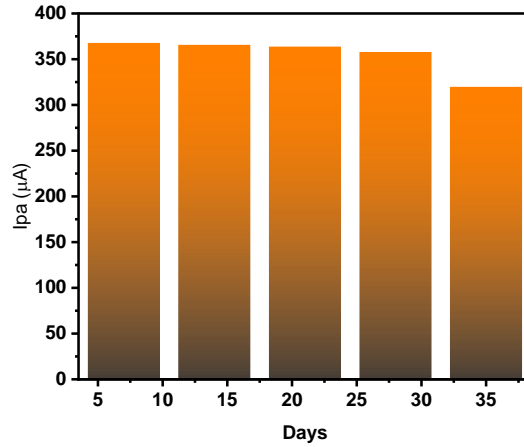


Figure 5.14. Bar graph showing the effect of time on the biosensor response

Below pH 2, the layer of MIP-Ppy tends to dissolve completely. The response showed almost negligible change till 28 days but there was a significant decrease after 32 days (figure 5.14). Hence, the electrode shows shelf life of 4 weeks.

5.3.3. Estimation of liothyronine in Liothyronine Tablet

The developed method was used to find the amount of liothyronine in the tablets figure 5.15.



Figure 5.15. Liothyronine tablets (Linorma) manufacture by Abbott

The calibration plot showed linearity of response between current and concentration (as shown in figure 5.16) in the range of 50-300pg/mL (equation as $y = -0.423x + 363.7$ and $r^2 = 0.993$). The diluted tablet samples with concentration of 200pg/mL (triplicate) showed an average recovery of 90.7%.

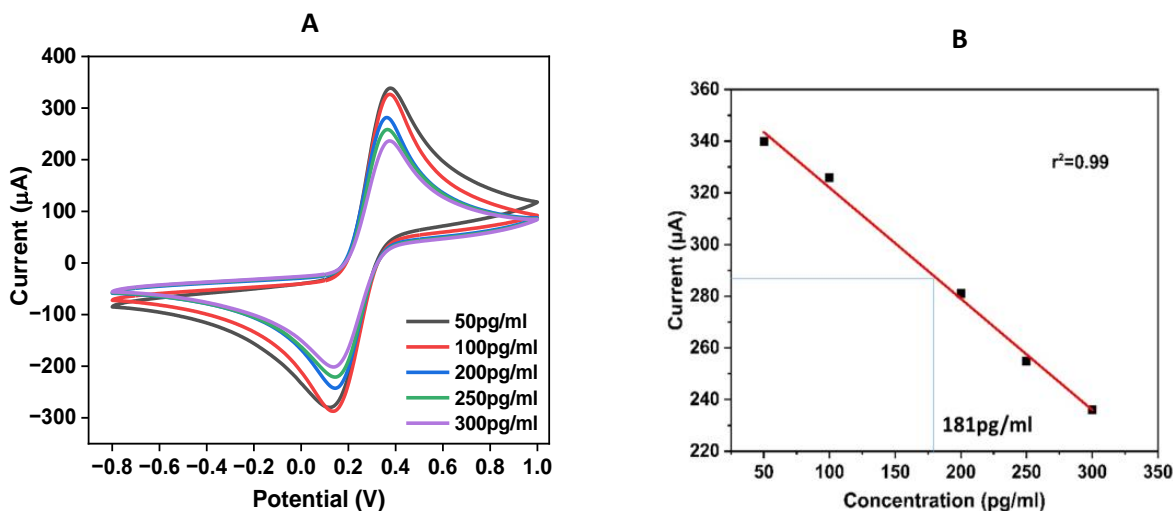


Figure 5.16. A. The plot shows a change in CV response with different concentrations. B. Calibration plot between current and concentration of liothyronine in the range of 50-300pg/mL

showed a peak around retention time of 7.3 mins as shown in figure 5.17. A small peak around 2.6 mins could be due to some unwanted impurity in the HPLC

column. The chromatogram of the sample obtained from the tablet ($2\mu\text{g/mL}$) showed liothyronine peak around retention time of 7.3 mins which can be correlated with the liothyronine peak obtained with pure liothyronine standard. Several other peaks observed in the chromatogram may be due to the excipients present in the tablets (figure 5.17). The peak areas were calculated for different concentrations of liothyronine.

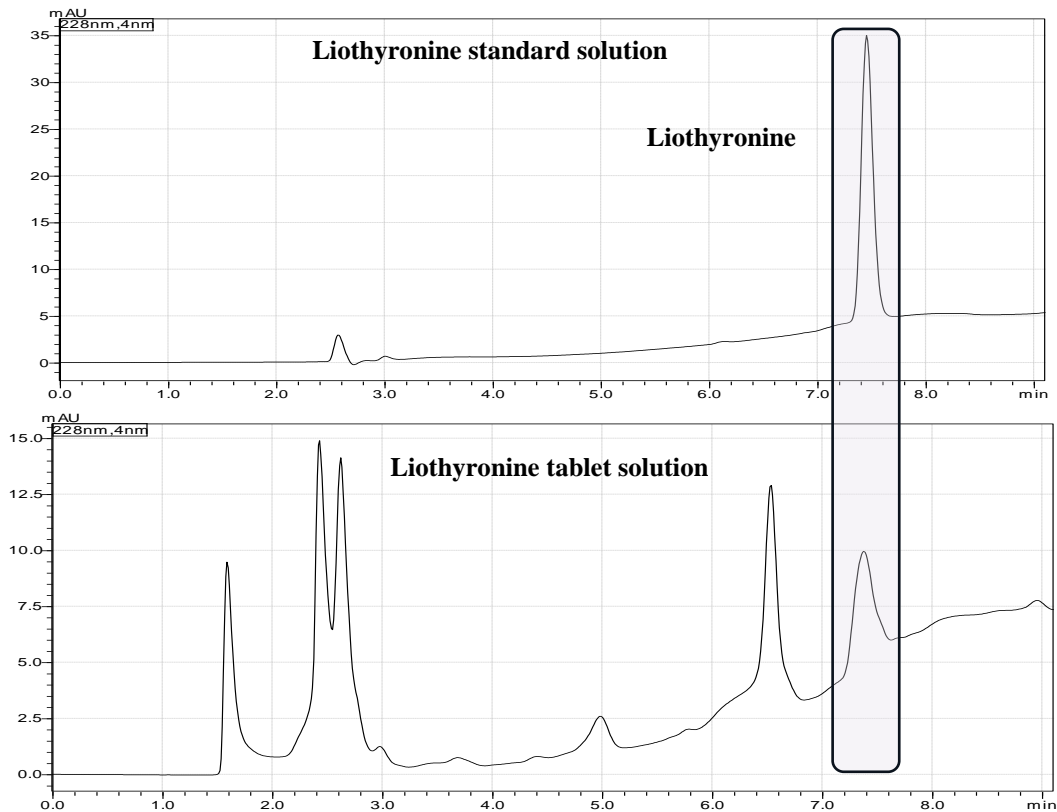


Figure 5.17 Chromatogram of pure liothyronine (above). Chromatogram of solution prepared using liothyronine tablet (below)

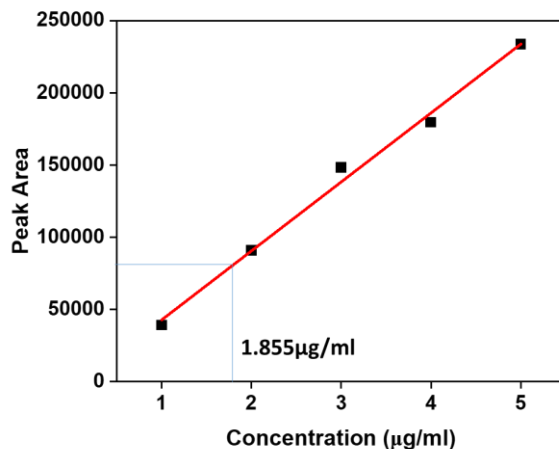


Figure 5.18 Calibration plot between current and concentration of liothyronine in the range 1-5µg/mL

The calibration plot was developed using HPLC method showed linearity within a range of 1-5 µg/mL (equation as $y = 47970x - 5785.3$ and $r^2 = 0.9926$) as shown in figure 5.18. The diluted tablet sample showed a recovery of 92.75%. The results obtained using biosensor and HPLC are summarized in table 5.3.

Table 5.3. Summary of results obtained for liothyronine tablets using MIP-Ppy biosensor and HPLC method

Method	Concentration analyzed (n=3, triplicate)	Concentration found in diluted sample	Recovery percentage	Relative standard deviation (RSD)	Amount found in the tablet (5 µg)
MIP based biosensor	200pg/mL	181.4±16.6 pg/mL	90.7%	0.093	4.53 µg
HPLC	2 µg/mL	1.855±0.1 µg/mL	92.75	0.054	4.64 µg

5.4. Conclusion

In this present work, we have pioneered a molecularly imprinted polymer-based method for T₃ estimation, offering a promising alternative to the established HPLC technique. Demonstrating remarkable linearity within the clinically relevant range of 50-300 pg/mL (with an impressive $r^2 = 0.993$) and exceptional selectivity, our biosensor represents a paradigm shift in accuracy and efficiency. With shelf life of four weeks at room temperature, it promises good stability. Moreover, its performance in estimating liothyronine levels in tablets rivals that of HPLC, opening avenues for broader applications such as quality control assays. This pioneering study marks a significant stride towards the development of a user-friendly point-of-care biosensor, revolutionizing liothyronine estimation in commercially available tablets.



Chapter 6

Development of

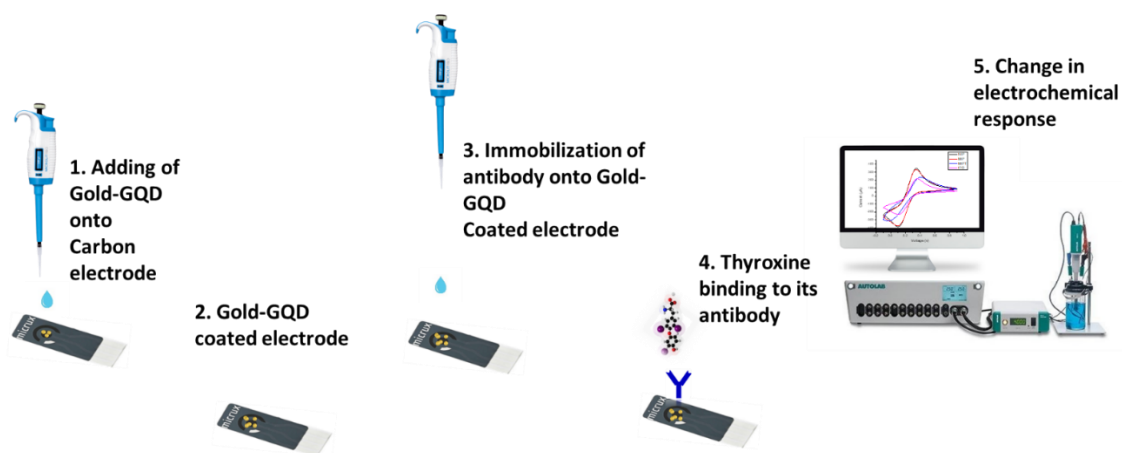
Electrochemical

Immunosensor for the

Ultrasensitive estimation of

Thyroxine

Graphical Abstract



Abstract

Thyroxine is one of the most important hormones involved in the metabolic process of the human body. Monitoring its levels in the human body is important to avoid any serious implications such as depression, cardiac disorders *etc.* In this chapter, we present the antibody based electrochemical biosensor for the estimation of thyroxine. Gold-Graphene Quantum Dots (Au-GQD) were used for immobilizing anti-thyroxine antibodies. The characterization studies for Au-GQD were performed with UV, FT-IR, Scanning Electron Microscope (SEM) and particle size analyzer. The sensor was fabricated by coating with Au-GQD following by immobilization of antibody. The characterization of sensor was done using FT-IR and cyclic voltammetry. Optimization of antibody concentration was done for optimal response. The sensor demonstrated a linear response towards T₄ concentrations in the range of 5pg/mL - 50pg/mL with $r^2 = 0.986$ and the limit of detection as 8.3pg/ml. Interference studies were performed with tyrosine, ascorbic acid, creatinine and dextrose, and no significant change in response was observed with these interfering substances. The sensor shows high sensitivity which enables it to be used for determination of thyroxine in biological matrices.

6.1. Introduction

Immunosensor is a type of biosensor which shows change in signal on interaction of target molecule (antigen) and the capturing agent (antibody) (Patil et al., 2023). Immunosensors are different from immunoassays as in case of immunoassays the interaction between antigen and antibody is measured by a separate platform, however, in immunosensors the formation of immunocomplex and the measurement happens on the same platform. (Mollarasouli et al., 2019) Immunosensors are of different types and are classified into three major categories including optical (luminescence) immunosensors, electrochemical (amperometric, potentiometric, impedance) immunosensors, and piezoelectric immunosensors. Among them, the electrochemical immunosensors are the most simplified type of biosensors as the analysis with them gives the most rapid and reliable signals. In electrochemical immunosensors, fabrication of electrode is done via the immobilization of a recognition element (antibody) on the electrode surface. The change in current resulting from the interaction between recognition element (antibody) and antigen is measured (Ghindilis et al., 1997). Despite the challenge with their shelf life, they are still widely used for their excellent sensitivity and selectivity.

Chemically, antibodies are glycoproteins, and these are of 5 different types *i.e.*, IgG, IgA, IgM, IgD, and IgE. Out of all the antibodies, IgG is the most widely used in immunosensors. It has “Y” shaped molecules which comprise of two identical light chains and two heavy chains linked together by –S-S- (disulfide) linkage and non-covalent interactions (such as hydrogen bonds). Antibodies are bivalent which allows them to bind with two specific antigens according to the shape, size, and compatibility. The Ag-binding site is called the “paratope”, and the complementary region on the Ag is called the “epitope” (Chiu et al., 2019). They provide selectivity to the quantitative electroanalytical method.

The antibodies are usually immobilized on the solid support via either physical adsorption or covalent bonding (Sueda, 2022). Several nanomaterials have been

used for immobilization of antibodies. Carbon based nanomaterials, gold nanomaterials, silica nanomaterials are the ones which are most used. In carbon nanomaterials, graphene quantum dots have a unique structure where carbon atom is sp^2 -hybridized and has a perpendicular unhybridized π -bonds (Lara et al., 2018). This provides semiconductor properties to graphene nanostructures and makes them highly photoluminescence, catalytic and high conductive. The other most commonly used class of nanoparticles are gold nanoparticles (Hammami et al., 2021). Gold nanoparticles are of great interest to the researchers because of their high conductivity, biocompatibility, ease in preparation, surface modification and high surface area to volume ratio (Mradula et al., 2020). Further, if gold nanoparticles are combined with Graphene Quantum Dots (GQD), there is a significant enhancement in electron mobility and chemical stability of nanoparticles (Wadhwa et al., 2020).

In the present study, the gold and GQD composite is used as a solid support for the immobilization of anti-thyroxine antibody. This chapter describes the development of the electrochemical biosensing platform using anti-thyroxine antibody immobilized on Au-GQD nanoparticles for the estimation of thyroxine. The immobilized antibodies onto the nanomaterial coated on working electrode (screen printed carbon electrodes) provide the selectivity to the target analyte response and nanomaterial used helps in the conduction of signal. The change in current on addition of different concentration of analyte (antigen) solution is measured using cyclic voltammetry. The developed calibration plot covers the normal range of thyroxine in blood and saliva.

6.1. Experimental

6.1.1. Materials

Thyroxine sodium (MW: 888.92 Da, > 97% using HPLC) was procured from Macleods Pharmaceuticals Limited, India. Liothyronine sodium (MW: 672.96 Da, \geq 97% using HPLC), phenylalanine, creatinine and tyrosine were purchased from Merck (Darmstadt, Germany).

Glucose (MW: 180.15 Da, \geq 99%, Rankem, India), tri-sodium citrate (MW: 258.06 Da, \geq 99%, Rankem, India) and gold chloride trihydrate ($\text{HAuCl}_4 \cdot 3\text{H}_2\text{O}$; MW 393.85, \geq 49.0% Au basis, Merck) were used for the synthesis of gold-GQD nanomaterial. Anti-thyroxine antibody (Serpina7 antibody, Polyclonal) with concentration of 1mg/mL was purchased from Geno Technology Inc. (USA) with molecular weight of 46kDa. Ascorbic acid (MW: 176.12 Da, \geq 99%), potassium ferrocyanide trihydrate (MW: 422.38 Da, \geq 99%), potassium ferricyanide (MW: 329.24 Da, \geq 99%), potassium dihydrogen phosphate (KH_2PO_4 ; MW: 136.08 Da, \geq 99%), di-sodium hydrogen phosphate (Na_2HPO_4 ; MW 141.9 Da, \geq 99%), sodium chloride were procured from Rankem, India. Ultrapure water (resistivity \sim 18.2 Ω cm at 298 K) from the water purification system (Milli-Q system Millipore Bedford, MA, USA) was used for all solutions. All the chemicals procured were of the highest analytical grade and did not require further purification. Freshly prepared working solutions were used for electrochemical sensing.

Phosphate buffer saline (pH = 7) was prepared with potassium dihydrogen phosphate (KH_2PO_4) and dipotassium hydrogen phosphate (K_2HPO_4) both from Rankem. Stock solution of thyroxine was made in 0.1N sodium hydroxide solution and dilutions were prepared in ultra-pure water. Electrochemical studies were performed in potassium ferro-ferricyanide solution (10 mM) prepared in phosphate buffer saline (1 mM, pH 7.4). All the chemicals procured were of highest analytical grade and did not require further purification. Freshly prepared working solutions for electrochemical sensing were used.

6.2.2. Electrodes and Instruments

Instruments: Dropsens electrochemical potentiostat (uStat i-400, Metrohm, Switzerland), analytical weighing balance (Shimadzu AT series, Japan), UV spectrometer (UV-Vis 1900, Shimadzu, Japan), Particle size analyzer (Zen 1690, Malvern instruments Ltd.), Field emission scanning electron microscope (FE-SEM) (JSM 7800F, JEOL, Japan).

Electrodes: Screen printed electrode (Drop SensC110), with carbon as working electrode, silver as reference electrode silver, carbon as counter electrode.

6.2.3. Methodology

6.2.3.1. Synthesis and characterization of gold-GQD composite

Gold-GQD nanocomposite was synthesized to be used as a nanomaterial for immobilizing the anti-thyroxine antibodies. The synthesis was performed using the procedure followed by Wadhwa et al. 2020. In the synthesis process, three solutions were prepared. Solution A: 5.6 g of D-glucose was dissolved in 50 mL of DI water. Solution B: 0.15 g of tri-sodium citrate was dissolved in 50 mL of DI water (0.01 M tri-sodium citrate solution). Solution C: 2 mg of Gold (III) chloride trihydrate was dissolved in 1 mL of DI water (7 mM Chloroauric acid solution). Solution A was irradiated in microwave power range 100 W for 5 minutes resulting in a sticky yellow paste. This corresponds to the formation of grapheme quantum dots (GQD). To this solution stabilizing citrate solution was slowly added with constant stirring. Finally, solution C was added with constant stirring to prepare Au-GQD nano composite. The resulting solution shows a reddish color which confirms the formation of Au-GQD (Wadhwa et al., 2020).

Characterization studies for Au-GQD were done using UV spectrometer, FT-IR, particle size analyzer and SEM. UV analysis was done by diluting the sample 5 times and analyzing it in the range of 200nm - 780nm. FT-IR analysis was done by forming a KBr pellet and scanning between 4000cm^{-1} - 400cm^{-1} with 16 scans and resolution of 4 cm^{-1} . SEM analysis was performed to understand the particle shape

and size. Suspended nanoparticles were drop casted on the solid surface for SEM analysis (under 100nm resolution).

5.2.3.2. Sensor fabrication

Cyclic voltammetry was used to study the response of thyroxine with antibody. In this study, screen printed carbon electrodes were used as working electrodes. Previously synthesized Au-GQD solution (2 μ l) was added onto the electrodes and dried in the oven for 60 mins at 50⁰C. 2 μ l of anti-thyroxine antibody (1000ng/ml) was immobilized onto the Au-GQD nanocomposite coated electrodes. The electrodes were kept for 45 mins at room temperature for complete binding. The stages of fabrication are shown in figure 6.1. The modified electrodes were stored in a desiccator for further studies. The fabricated sensor surface was characterized using FT-IR and cyclic voltammetry.

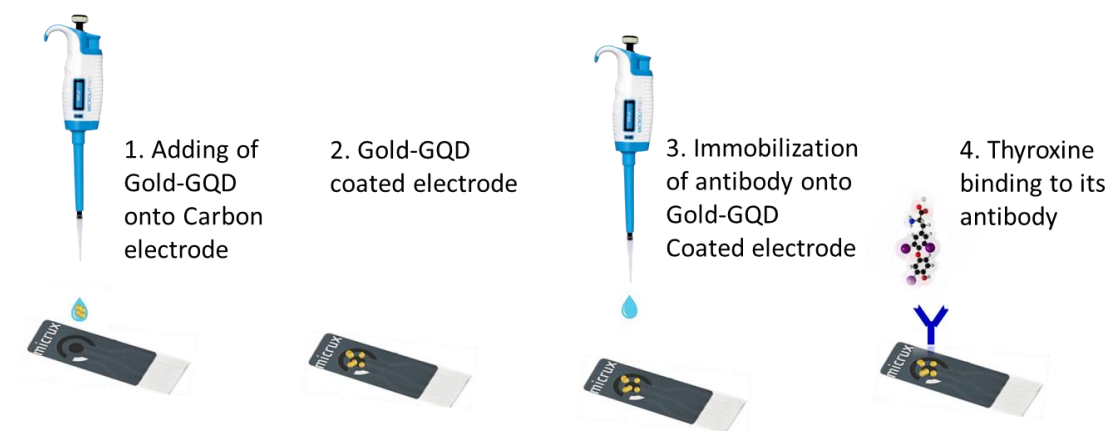


Figure 6.1. Electrode fabrication steps for the development of electrochemical biosensor of thyroxine

6.2.3.3. Electrochemical Studies

Cyclic voltammetric (CV) studies were performed for the fabricated biosensor in the range of -0.4V - 0.7V. The CV response for different stages of fabrication of biosensor was performed for Au-GQD, Au-GQD + Ab and Au-GQD + Ab + T₄ coated electrodes respectively. 50 μ L of potassium ferro-ferricyanide solution (10mM) was used as a redox probe. The set up is shown in figure 6.2. This study

helps to ensure proper binding on the electrode surface. The sensor performance was also checked through scan rate study, effect of antibody concentration, effect of pH, linearity studies and interference studies.

To ensure optimal concentration of antibody on electrode surface, the cyclic voltammetric response was studied with different antibody concentrations in the range of 500ng/mL to 2000ng/mL. 2 μ L of different antibody concentration were added respectively onto different working electrodes coated with Au-GQD. Incubation was done after addition of antibodies for around 45 mins at room temperature before using it for electrochemical study. The concentration range of antibodies was selected based on factors including analyte concentration, effective surface binding *etc.*

The pH range was studied from 6 - 7.5. This pH was selected as it covers the pH of different biological fluids including blood and saliva *etc.* Phosphate buffer (10mM) was used to make solutions of different pH between 6 - 7.5. Scan rate study was performed to study the electroactive surface area and electrode stability in the range of 10mV/s – 130 mV/s.

Linearity studies were performed by comparing the peak anodic current response at voltage of +0.2 V for different concentration of thyroxine in the range of 5pg/mL - 50pg/mL (prepared in phosphate buffer saline pH 7). Interference studies were performed using 10 μ g/mL solutions of liothyronine, creatinine, tyrosine, and ascorbic acid. For all electrochemical studies, 50 μ l potassium ferro-ferricyanide solution was used as a redox probe (10mM).

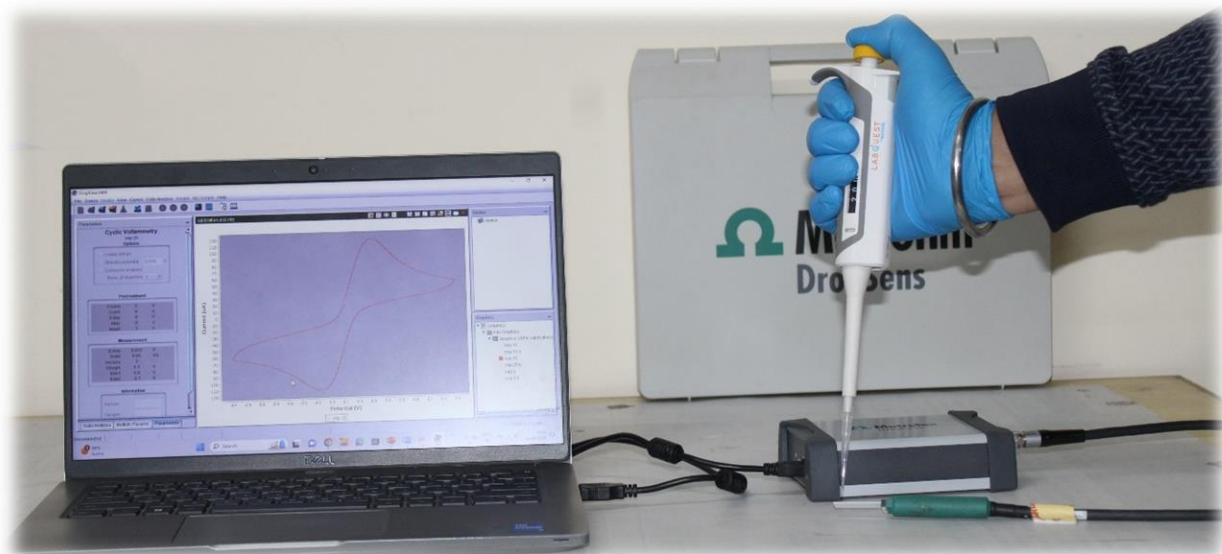


Figure 6.2. Portable electrochemical analyzer with surface modified working electrode for analysis of thyroxine

6.3. Results and Discussions

6.3.1. Synthesis and characterization of Au-GQD

The Au-GQD nanomaterial was synthesized, and the mixture showed red color due to formation of Au-GQD (figure 6.3 islet). This red color of the solution confirms the synthesis of Au-GQD. In UV spectra, both characteristic peaks of Gold and GQD were observed at 530nm and 280nm respectively as shown in figure 6.3. (Botteon et al., 2021; Gozali Balkanloo et al., 2023). The color of the solution and UV spectra indicates the synthesis of Au-GQD.

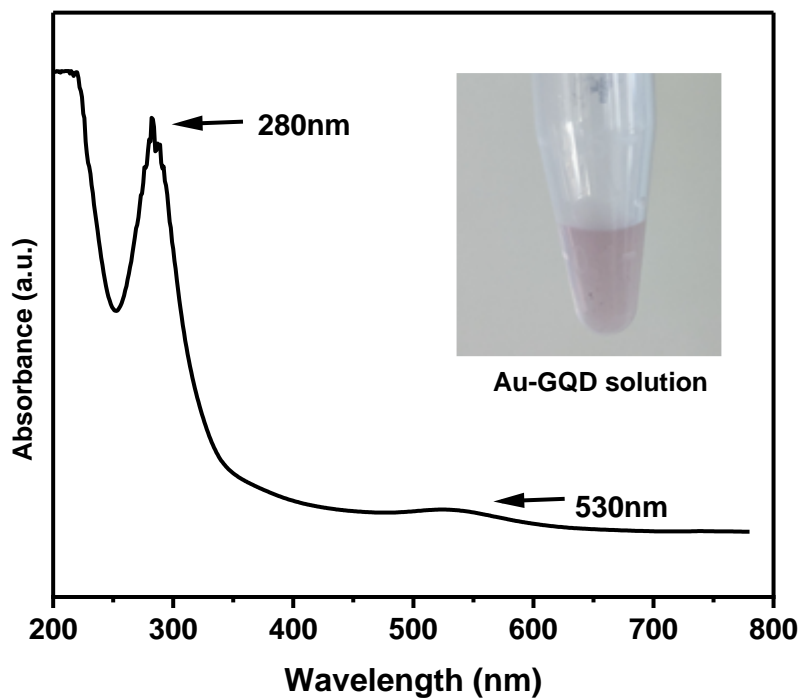
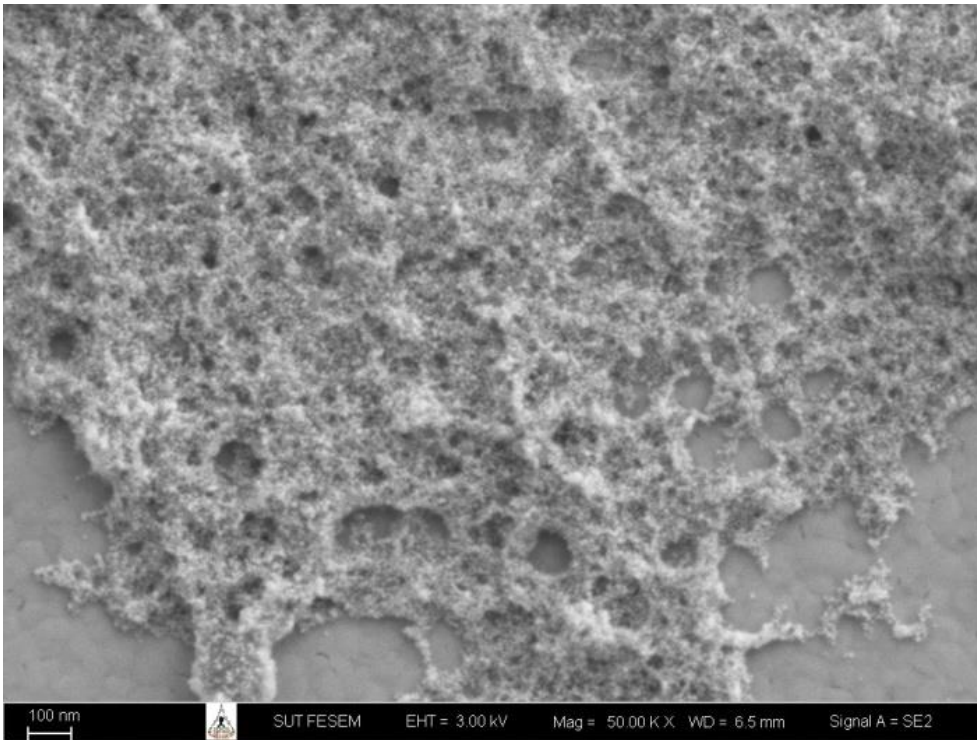


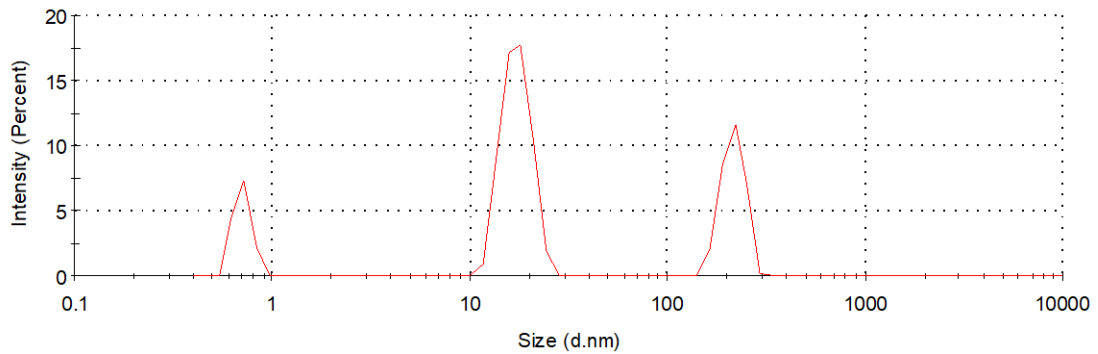
Figure 6.3. UV spectra of Au-GQD in the wavelength range of 200-780nm against absorbance (au)

Particle size of Au-GQD was found using particle size analyzer and SEM (figure 6.4). Particle size analyzer shows three peaks at 1 nm, 14nm and 198nm. Typically, the reported particle size of graphene quantum dots is less than 20nm (Gozali Balkanloo et al., 2023). The peaks at higher size could be due to aggregation of Au-GQD nanoparticles. The SEM data also compliments the particle size analyzer data. The shiny small white spots in SEM image are due to Au-GQD and the highlighted particles could be the aggregated forms.



A

Size Distribution by Intensity



B

Figure 6.4. A. SEM image of Au-GQD. B. Particle size pattern for Au-GQD

FT-IR spectra also shows characteristic peaks of graphene quantum dots (GQD) as shown in figure 6.5. As GQD contains O-H, C=C, C-H and C-C, stretching frequency peaks corresponding to these bonds can be observed in the spectra. Peak at 3500cm^{-1} corresponds O-H bond stretching, peak around 3000cm^{-1} corresponds

to C-H stretch. Peaks around 1600cm^{-1} and 1100 cm^{-1} corresponds to C=C stretch and C-C stretch respectively (Rodwihok et al., 2022).

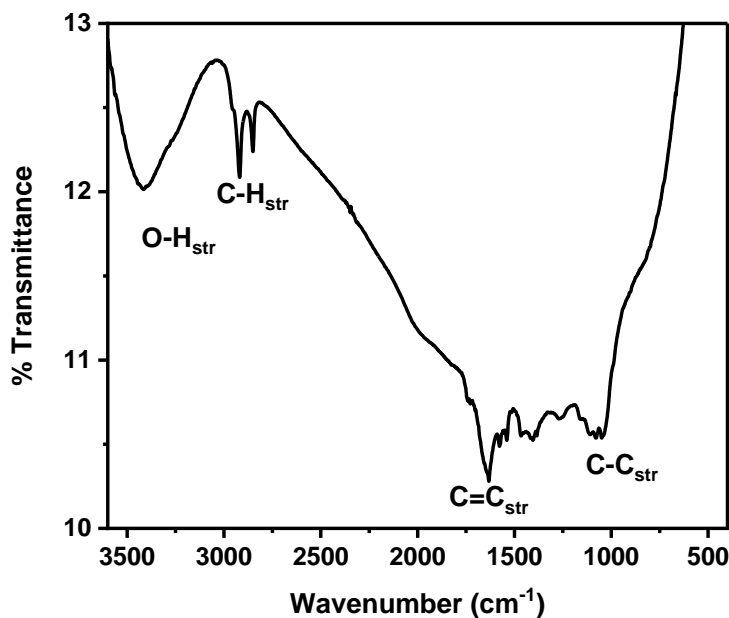


Figure 6.5. FT-IR spectra of Au-GQD in the range of 4000 cm^{-1} - 400cm^{-1} against percentage transmittance

6.3.2. Sensor Performance: Electrochemical studies

FT-IR spectra for different stages of biosensor development were performed to characterize the material(s) coated on the surface of the electrodes (figure 6.6). The FT-IR shows the characteristic peaks Au-GQD stabilized by citrate. A comparison was made between FT-IR spectra of nanomaterial with and without antibody and analyte. On comparing FT-IR spectra of Au-GQD, with Ab immobilized Au-GQD, it can be noted that peak around 1620cm^{-1} becomes more prominent which could be due to C=O group of amino acids which is a structural feature of antibodies. The FT-IR spectra of T₄-Ab - Au-GQD, shows a characteristic peak of C-I at 670cm^{-1} which is absent in other two spectra. This peak is due to the binding of thyroxine onto the antibody as thyroxine contain 4 C-I bonds (Singh et al., 2023). This peak was observed in the MIP study also (chapter 3).

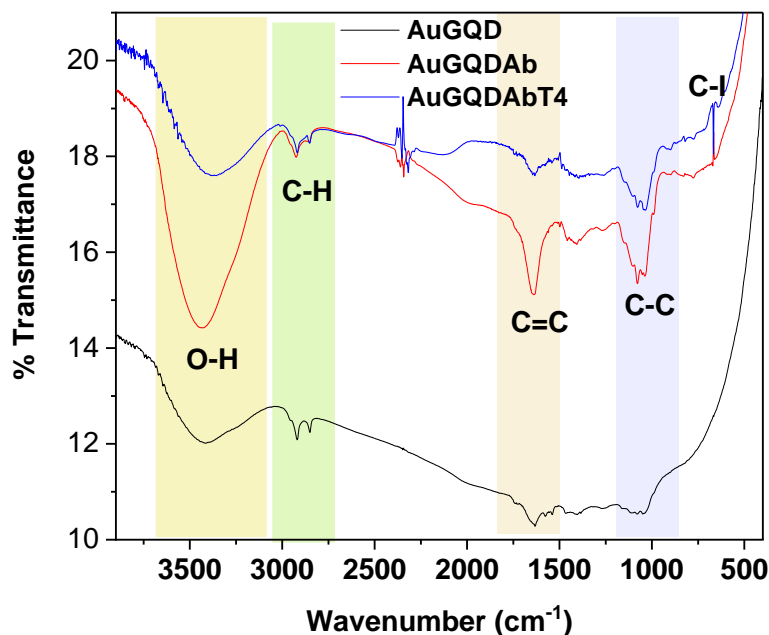


Figure 6.6. FT-IR spectra of Au-GQD, Au-GQD immobilized Ab and Au-GQD-Ab with thyroxine

Cyclic voltammetric response was studied for different stages of fabrication of biosensor. On comparing the cyclic voltammetric response for different stages of biosensor fabrication, a variation in peak anodic current response was observed at +0.2V (figure 6.7). The peak anodic current (I_{pa}) slightly decreases when Au-GQD was coated on the electrode. This could be due to the relatively low conduction of electrons by nanomaterial as compared to bare ITO. I_{pa} was slightly higher when antibody was immobilized on the nanomaterial as antibodies. The increase in anodic peak current response may be related to the fact that the antibody structure on the electrode surface is more conducive to electron conduction on the electrode surface. In the last step, the binding of thyroxine causes further decrease of I_{pa} . A similar response was observed by Mradula et al. while developing immuno-sensor for thyroxine (Mradula et al., 2021)

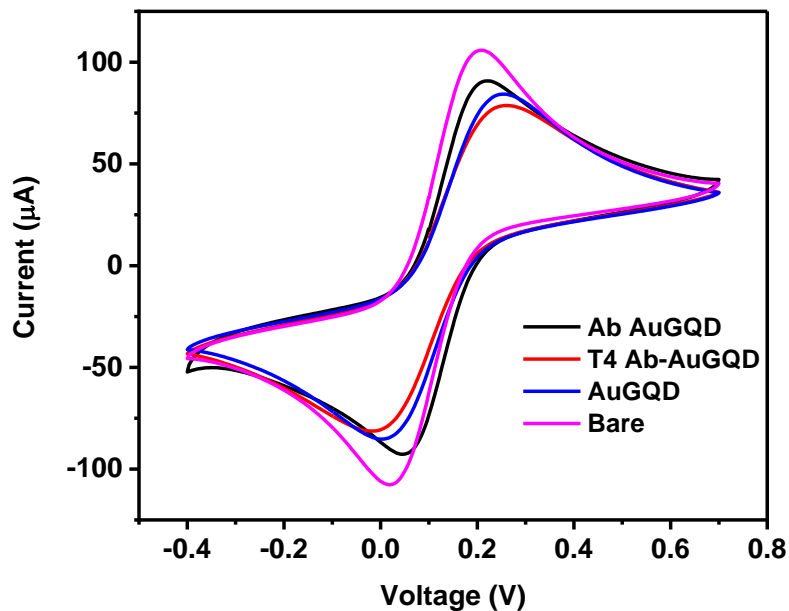
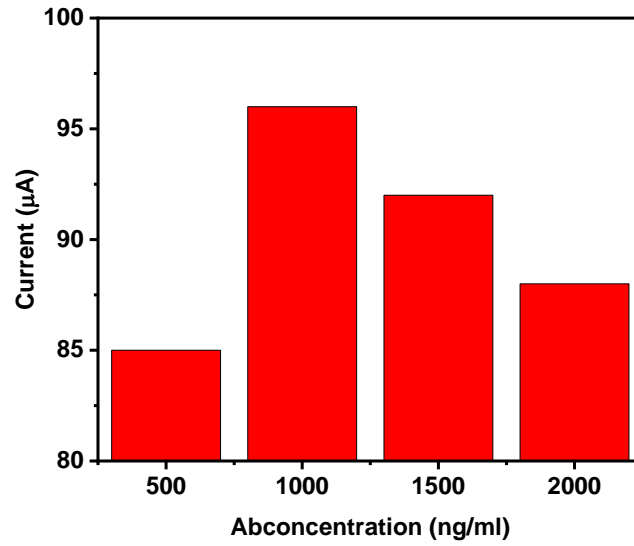


Figure 6.7. Cyclic voltammetric curves for different stages of biosensor fabrication

It is reported in literature that several factors affect the response of antibody based biosensor including pH, antibody concentration, redox probe *etc* (Busch et al., 2019). The effect of pH and antibody concentration are two important factors while developing a sensor especially when it is intended to be used for measurement of a biomolecule in biological fluid. The pH affects the stability of the electrode and antibody concentration is critical to ensure sufficient binding sites for the analyte (Ruiz et al., 2019).

A



B

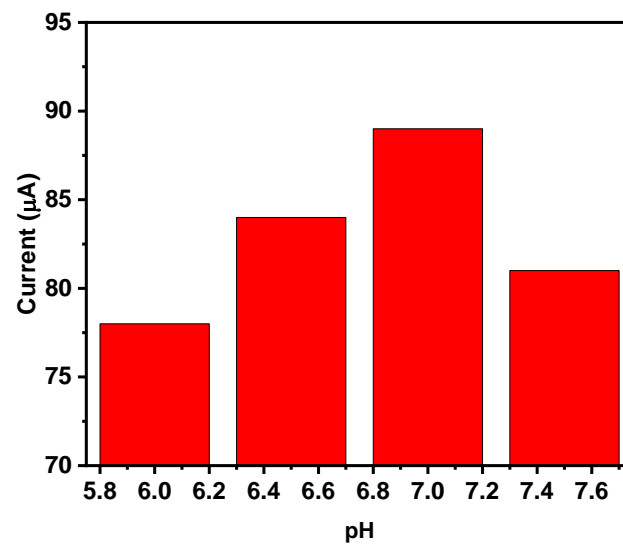


Figure 6.8. (A) Effect of antibody concentration on current response (B) Effect of pH on current response

The optimal antibody concentration was found to be 1000ng/mL and the optimal pH was found to be 7 (figure 6.8a). This could be due to saturation of antibodies on the electrode surface above this concentration resulting in reduction in current response. The biosensor shows highest stability at pH 7 and the response reduces drastically above 7.5 and below 6.5 (figure 6.8b). The results were in accordance with the studies in literature (M. Mradula et al., 2021; Singh et al., 2023).

Scan Rate study: The peak anodic and cathodic currents increase as the scan rate is increased from 10mV/s - 130 mV/s, with the response saturating at the latter value. It can also be observed from Fig. 6.9 that the voltammetric profile (using potassium ferro-ferricyanide as redox probe) is preserved at higher scan rates, thereby indicating the electrochemical stability within a vast scan rate range. Fig.6.10 establishes a direct proportionality (equation 6.1 and 6.2) of peak anodic current (I_{pa}) and peak cathodic current (I_{pc}) with square root of scan rate (v) between 20mV/s - 90mV/s, which corresponds to the well-known Randel's-Sevick (R-S) behaviour. The electroactive surface area was therefore found to be 0.031 cm² using the R-S equation.

Between scan rate 20mV/s to 90mV/s, the electrode process was found to be diffusion controlled as the anodic and cathodic peak current increased linearly with square root of scan rate (Prasad et al., 2010).

$$I_{pa} (\mu A) = 16.02 + 406v^{1/2} (V/s) \quad r^2 = 0.996 \quad \text{Equation 6.1}$$

$$I_{pc} (\mu A) = -14.02 - 402.2v^{1/2} (V/s) \quad r^2 = 0.998 \quad \text{Equation 6.2}$$

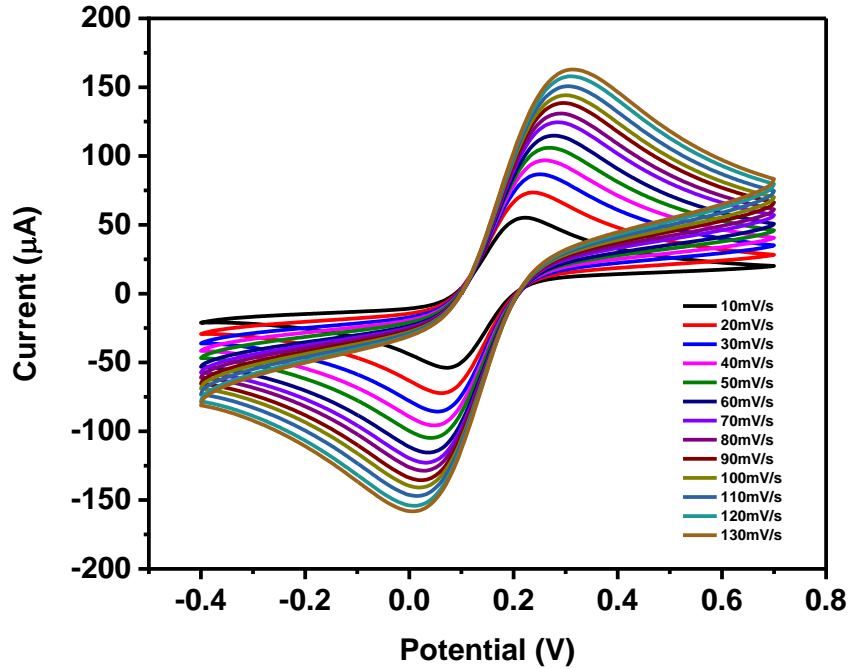


Figure 6.9. Variation of Current with change in scan rate from (10mV/s - 130mV/s)

In cyclic voltammetric scans, the variation of the peak anodic current (I_{pa}) with different concentration of thyroxine solution was observed at 0.2V. The I_{pa} decreases from 118 μA to 76 μA (figure 6.11a) as T_4 concentration is increased from 5 pg/mL to 50 pg/mL . This could be due to interaction between antibody and thyroxine which cause non-conductive electron transfer process on the surface of biosensor, hence, resulting in the reduction in current response.

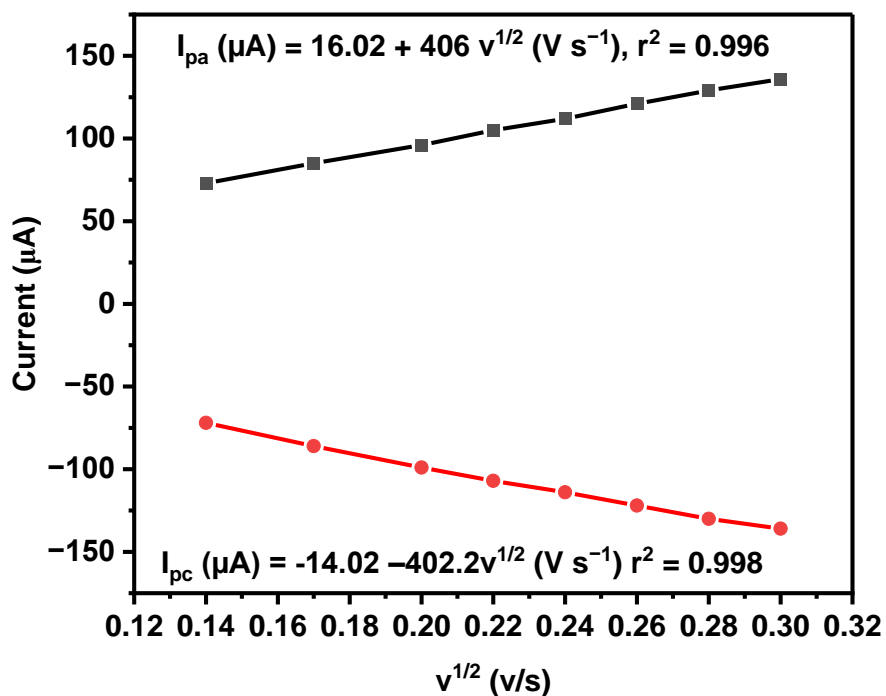


Figure 6.10. Change of peak anodic current (I_{pa}) with $v^{1/2}$ in the range of 20mV/s – 90mV/s

The calibration plot shows a linear relationship between the two variables *i.e.*, concentration and current response. The linear equation is $y = -0.591x + 113.08$ and $r^2 = 0.986$. r^2 value is close to 1, which denotes strong relationship between these two variables (figure 6.11b). The current response beyond the concentration range of 5pg/mL - 50 pg/mL did not show linearity. This range also covers the normal concentration of thyroxine in the blood and saliva. The Limit of Detection (LoD) was calculated using the 3 (SD/m) rule where SD is the standard deviation of the

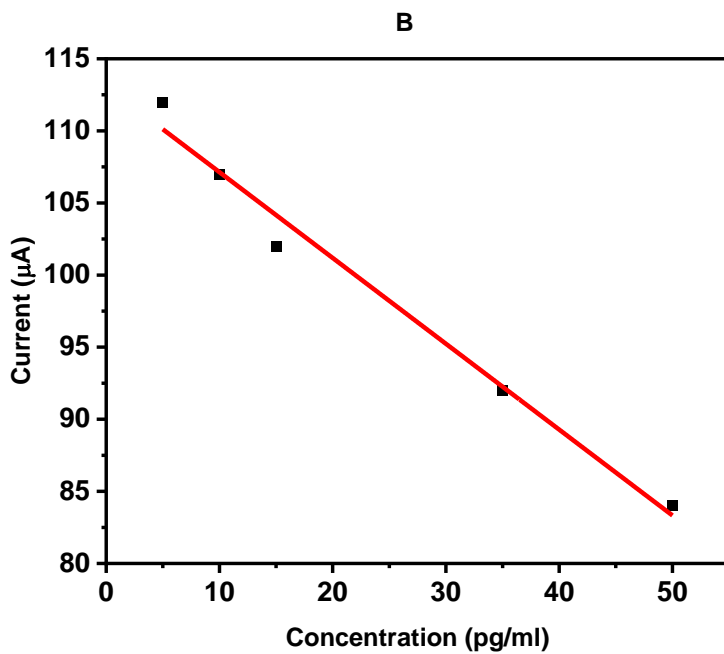
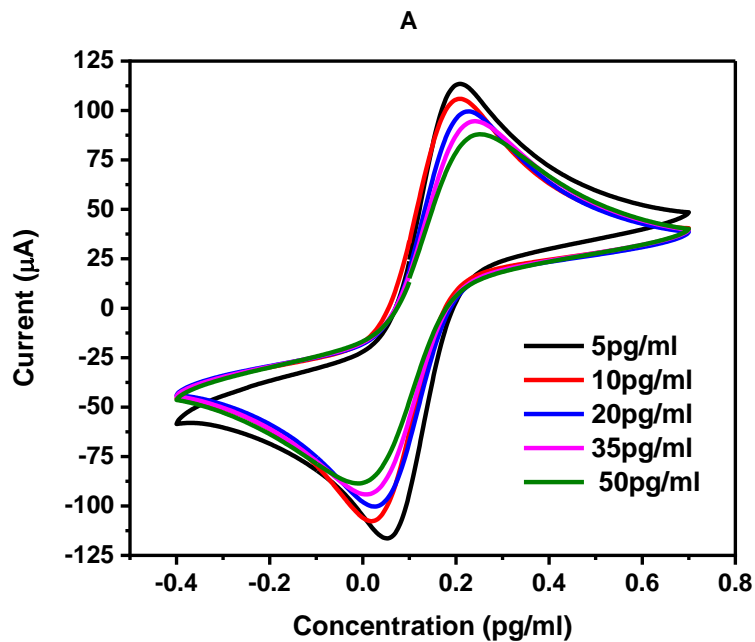


Figure 6.11. A. The plot shows a change in CV response with different concentrations. B. Calibration plot between current and concentration of thyroxine in the range of 5-50pg/mL

response and “m” is the slope of linear plot (Poggialini et al., 2023). Limit of detection was found to be 8.3pg/mL.

Interference studies showed insignificant change in current response with common biomolecules having similar structural features as of thyroxine (figure 6.12). The significant peak anodic current (I_{pa}) response decreased with thyroxine only from around 115 μ A to 80 μ A.

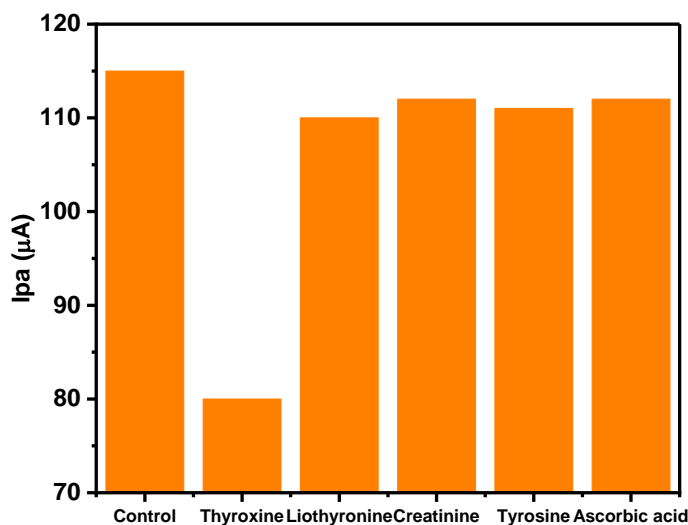


Figure 6.12. The effect of interference by liothyronine, creatinine, tyrosine, ascorbic acid, water (as control).

The interference studies showed that the method is selective for thyroxine. On comparison with other methods (table 6.1) this method is sensitive than other antibody-based methods given in the literature.

Table 6.1. Different reported biosensing techniques for the estimation of thyroxine biosensors

Electrode	Materials used	Method	LOD (nM)	Reference
Screen Printed Electrode	Carbon nanotubes, graphene, and gold nanoparticles	Differential pulse voltammetry	30	(David et al., 2022)
Mercury film silver-based electrode	Renewable mercury film	Cyclic voltammetry	18	(Smajdor et al., 2016)
Carbon paste electrode	Graphite powder in paraffin oil	Cyclic voltammetry	6.5	(Hu et al., 2004)
Gold Micro electrode	Thyroxine DNA aptamer/ rhodium nanoplate heterolayer	Cyclic voltammetry and Electrochemical Impedance spectroscopy	0.01	(Park et al., 2020)
Modified copper disk and PVC tube	Reduced graphene oxide containing gold nanoparticles attached with beta cyclodextrin	Amperometry	1	(Muñoz et al., 2016)
Screen printed carbon electrode	Antibody immobilized on Au-GQD	Cyclic voltammetry	~0.01	Present work

6.4. Conclusion

Antibody based biosensor was developed for thyroxine using antibody immobilized on Au-GQD nanoparticles. The developed sensor showed linearity in the range of 5pg/mL - 50pg/mL with $r^2 = 0.986$ and was found to be highly selective. The antibody concentration was optimized to ensure sufficient antibodies for binding of thyroxine. The biosensor showed pH stability in the range of 6 - 7. The sensitivity of the developed biosensor enables it to be used for estimation of T₄ in biological matrices. This study will help to develop a point-of-care biosensor for thyroxine which can be used for diagnosis of thyroid disorders.



Chapter 7

Conclusion and Future

Outlook

7.1. Conclusion

In this work, electrochemical biosensors were developed for estimation of thyroxine and liothyronine using molecularly imprinted polymer and antibody as biorecognition elements. The developed biosensors show high sensitivity and selectivity towards thyroxine and liothyronine respectively.

For thyroxine, biosensors were developed by MIP and antibody-based approaches, and it was found that MIP-based technique was better with respect to processing conditions and shelf-life. However, the sensitivity for both these techniques were almost similar. The concentration of thyroxine in the human body is in the range of picograms/mL. The limit of detection for thyroxine using both MIP and antibody technique was found to be sufficient for estimation of the levels of thyroxine in biological matrices such as saliva and blood. Thyroxine spiked saliva was used to study the recovery of the developed biosensor. The results showed a recovery of over 90%. Hence, the developed biosensor for thyroxine can be used as an alternative for the measurement of thyroxine in saliva.

Liothyronine estimation using MIP based biosensor also showed promising results. Although the limit of detection was higher than the levels of liothyronine in the body, but the method can be used to estimate the levels of liothyronine in pharmaceutical tablets.

Table 7.1. Summary of results of different method for analysis of thyroid hormones (T₄/T₃)

Technique	Analyte	LOD (pg/ml)	Range
MIP	Thyroxine in buffer	6.16	5-50pg/ml
Antibody	Thyroxine in buffer	8.3	5-50pg/ml
MIP	Liothyronine in buffer	80	50-300pg/ml

7.2. Future Outlook

According to reports, the global thyroid gland disorders treatment market size was valued around 2.37 billion USD in 2022. It is further expected to grow to 3.14 USD billion by 2031. This data highlights the prevalence of thyroid disorders and indicates the need for a rapid and reliable diagnostic technique for early detection of these disorders.

In this study, we have developed biosensors which can be used for spot analysis of thyroid hormones either in biological matrix (thyroxine) or in pharmaceutical tablets (liothyronine). The developed biosensors can be translated into miniaturized portable electrodes which can be easily attached to the portable potentiostat (Figure 7.1). The change in current due to binding of analyte will show the concentration with the help of already installed algorithm obtained using current and concentration relation. The application of this device will enhance patient compliance for diagnosis as well as quality control for thyroid hormones. Table 7.1 summarizes the results of all the studies performed for detection of thyroxine and liothyronine.

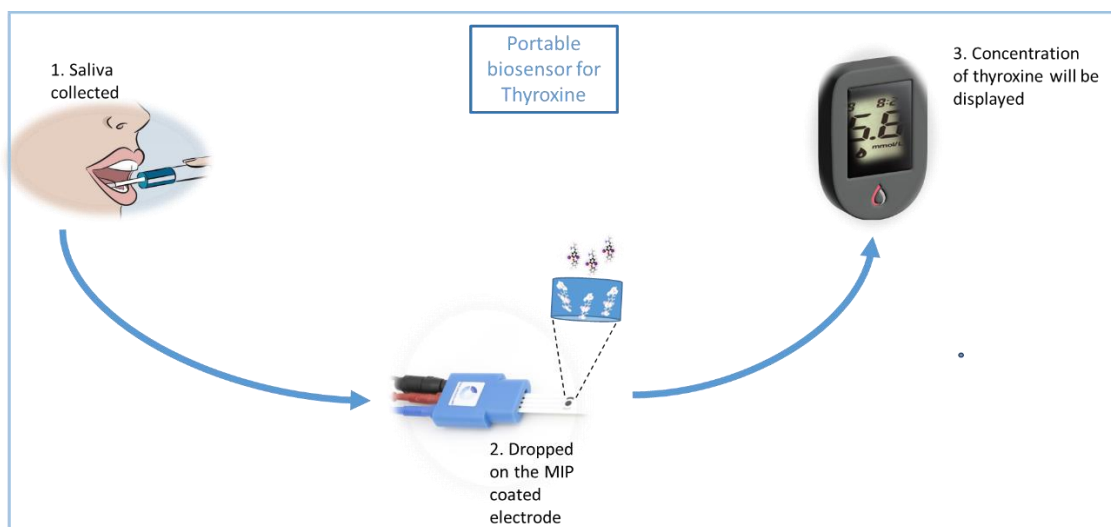


Figure 7.1 Schematic of parts of portable biosensor for determination of thyroxine

Considering the frequent quality issues faced by pharmaceutical companies with respect to liothyronine, our methods can be a better alternative for testing the quality of pharmaceutical tablets of liothyronine. It was found that the developed method shows comparable recovery of liothyronine from liothyronine tablets to that obtained with HPLC. This study opens new avenues for the development of point-of-care quality control testing. As pharmaceutical industry struggles with the quality of these molecules due to their environmental instability, the developed methods can be useful to monitor and maintain the quality of pharmaceutical dosage forms containing these hormones.

Even at the patient level, such a point of care device will be useful for a patient to determine if the medication contains the labelled amounts or not. In last few years, several adulterated and substandard medicines have been found and it becomes difficult for the patient to identify authentic medicine. Through point of care home testing, the patients will be empowered to know what is being taken.

To summarize, in this project alternative analytical methodology has been proposed in detail for the estimation of thyroxine in biological matrices and liothyronine in pharmaceutical matrices.

References

- Aboul-Enein, H. V., Stefan, R. I., Litescu, S., & Radu, G. L. (2002). Biosensor for the enantioselective analysis of the thyroid hormones (+)-3,3',5-triiodo-L-thyronine (T₃) and (+)-3,3',5,5'-tetraiodo-L-thyronine (T₄). *Journal of Immunoassay and Immunochemistry*, 23(2), 181-190.
- Abu-Thabit, N. Y. (2016). Chemical oxidative polymerization of polyaniline: A practical approach for preparation of smart conductive textiles. *Journal of Chemical Education*, 93(9), 1606-1611.
- Alonso-Lomillo, M. A., & Domínguez-Renedo, O. (2023). Molecularly imprinted polypyrrole based electrochemical sensor for selective determination of ethanethiol. *Talanta*, 253, 123936.
- Anthony, P. Z., & Geever, J. E. (1958). An identity test for iodinated derivatives of tyrosine and thyronine, particularly triiodothyronine and thyroxine. *Journal of the American Pharmaceutical Association*, 47(6), 394-395.
- Ariani, M. D., Zuhrotun, A., Manesiotis, P., & Hasanah, A. N. (2024). Dummy template molecularly imprinted polymers as potential sorbents in the separation and purification of active compounds in natural products. *Polymers for Advanced Technologies*, 35(1), e6201.
- Arshavsky-Graham, S., Heuer, C., Jiang, X., & Segal, E. (2022). Aptasensors versus immunosensors-Which will prevail? *Engineering in Life Sciences*, 22(3-4), 319-333.
- Ateh, D. D., Navsaria, H. A., & Vadgama, P. (2006). Polypyrrole-based conducting polymers and interactions with biological tissues. *Journal of the Royal Society Interface*, 3(11), 741-752.

- Baluta, S., Romaniec, M., Halicka-Stępień, K., Alicka, M., Pieła, A., Pala, K., & Cabaj, J. (2023). A novel strategy for selective thyroid hormone determination based on an electrochemical biosensor with graphene nanocomposite. *Sensors*, *23*(2), 602.
- Barros, R., De Azevedo, W., & M. de Aguiar, F. (2003). Photo-induced polymerization of polyaniline. *Materials Characterization*, *50*, 131-134.
- Beckskereki, G., Horvai, G., & Tóth, B. (2021). The selectivity of molecularly imprinted polymers. *Polymers*, *13*(11), 1781.
- BelBruno, J. J. (2019). Molecularly imprinted polymers. *Chemical Reviews*, *119*(1), 94-119.
- Berkes, B. B., Bandarenka, A. S., & Inzelt, G. (2015). Electropolymerization: Further insight into the formation of conducting polyindole thin films. *The Journal of Physical Chemistry C*, *119*(4), 1996-2003.
- Bhattarai, K. R., Kim, H. R., & Chae, H. J. (2018). Compliance with saliva collection protocol in healthy volunteers: strategies for managing risk and errors. *International Journal of Medical Sciences*, *15*(8), 823-831.
- Bjerkreim, B. A., Hammerstad, S. S., Gulseth, H. L., Berg, T. J., Lee-Ødegård, S., Rangberg, A., Jonassen, C. M., Budge, H., Morris, D., Law, J., Symonds, M., & Eriksen, E. F. (2021). Effect of liothyronine treatment on dermal temperature and activation of brown adipose tissue in female hypothyroid patients: a randomized crossover study. *Frontiers in Endocrinology*, *12*, 785175.
- Botteon, C. E. A., Silva, L. B., Ccana-Ccapatinta, G. V., Silva, T. S., Ambrosio, S. R., Veneziani, R. C. S., Bastos, J. K., & Marcato, P. D. (2021). Biosynthesis and characterization of gold nanoparticles using Brazilian red propolis and evaluation of its antimicrobial and anticancer activities. *Scientific Reports*, *11*(1), 1974.
- Busch, R. T., Karim, F., Weis, J., Sun, Y., Zhao, C., & Vasquez, E. S. (2019). Optimization and structural stability of gold nanoparticle-antibody bioconjugates. *ACS Omega*, *4*(12), 15269-15279.

- Byrne, B., Stack, E., Gilmartin, N., & O'Kennedy, R. (2009). Antibody-based sensors: principles, problems and potential for detection of pathogens and associated toxins. *Sensors*, *9*(6), 4407-4445.
- Byun, H. S., Youn, Y. N., Yun, Y. H., & Yoon, S. D. (2010). Selective separation of aspirin using molecularly imprinted polymers. *Separation and Purification Technology*, *74*(1), 144-153.
- Chiamolera, M. I., & Wondisford, F. E. (2009). Thyrotropin-releasing hormone and the thyroid hormone feedback mechanism. *Endocrinology*, *150*(3), 1091-1096.
- Chiappin, S., Antonelli, G., Gatti, R., & De Palo, E. F. (2007). Saliva specimen: a new laboratory tool for diagnostic and basic investigation. *Clinica Chimica Acta*, *383*(1-2), 30-40.
- Chiovato, L., Magri, F., & Carlé, A. (2019). Hypothyroidism in Context: Where we've been and where we're going. *Advances in Therapy*, *36*(2), 47-58.
- Chiu, M. L., Goulet, D. R., Teplyakov, A., & Gilliland, G. L. (2019). Antibody structure and function: the basis for engineering therapeutics. *Antibodies*, *8*(4), 55.
- Cho, I. H., Kim, D. H., & Park, S. (2020). Electrochemical biosensors: perspective on functional nanomaterials for on-site analysis. *Biomaterials Research*, *24*(1), 6.
- Cinquanta, L., Fontana, D. E., & Bizzaro, N. (2017). Chemiluminescent immunoassay technology: what does it change in autoantibody detection? *Auto Immunity Highlights*, *8*(1), 9.
- Collier, J. W., Shah, R. B., Bryant, A. R., Habib, M. J., Khan, M. A., & Faustino, P. J. (2011). Development and application of a validated HPLC method for the analysis of dissolution samples of levothyroxine sodium drug products. *Journal of Pharmaceutical and Biomedical Analysis*, *54*(3), 433-438.
- Collier, J. W., Shah, R. B., Gupta, A., Sayeed, V., Habib, M. J., & Khan, M. A. (2010). Influence of formulation and processing factors on stability of levothyroxine sodium pentahydrate. *AAPS PharmSciTech*, *11*(2), 818-825.

- Colucci, P., Yue, C. S., Ducharme, M., & Benvenga, S. (2013). A review of the pharmacokinetics of levothyroxine for the treatment of hypothyroidism. *European Endocrinology*, 9(1), 40-47.
- Couto, R. A. S., Gonçalves, L. M., Góes, M. S., Rodrigues, C. M. P., Quinaz, M. B., & Rodrigues, J. A. (2017). SAM-based immunosensor for the analysis of thyroxine (T₄). *Journal of Electrochemical Society*, 164(4), B103.
- Crapnell, R. D., Dempsey-Hibbert, N. C., Peeters, M., Tridente, A., & Banks, C. E. (2020). Molecularly imprinted polymer based electrochemical biosensors: overcoming the challenges of detecting vital biomarkers and speeding up diagnosis. *Talanta Open*, 2, 100018.
- Cui, M., Sun, X., Liu, R., Du, M., Song, X., Wang, S., Hu, W., & Luo, X. (2022). A dual-responsive electrochemical biosensor based on artificial protein imprinted polymers and natural hyaluronic acid for sensitive recognition towards biomarker CD44. *Sensors and Actuators B: Chemical*, 371, 132554.
- D'Aurizio, F., Kratzsch, J., Gruson, D., Petranović Ovčariček, P., & Giovanella, L. (2023). Free thyroxine measurement in clinical practice: how to optimize indications, analytical procedures, and interpretation criteria while waiting for global standardization. *Critical Reviews in Clinical Laboratory Sciences*, 60(2), 101-140.
- Danzi, S., & Klein, I. (2003). Thyroid hormone and blood pressure regulation. *Current Hypertension Reports.*, 5(6), 513-520.
- David, M., Şerban, A., Enache, T. A., & Florescu, M. (2022). Electrochemical quantification of levothyroxine at disposable screen-printed electrodes. *Journal of Electroanalytical Chemistry*, 911, 116240.
- De Leo, S., Lee, S. Y., & Braverman, L. E. (2016). Hyperthyroidism. *Lancet*, 388(10047), 906-918.
- Debiemme-Chouvy, C., Tran, T.T.M. (2008) An insight into the overoxidation of polypyrrole materials. *Electrochemistry Communications*, 10, 947-50.

- Durakovic, B. (2017). Design of experiments application, concepts, examples: state of the art. *Periodicals of Engineering and Natural Sciences*, 5, 421-439.
- Elson, M. K., Morley, J. E., & Shafer, R. B. (1983a). Salivary thyroxine as an estimate of free thyroxine: concise communication. *Journal of Nuclear Medicine*, 24(8), 700-702.
- Ertuğrul Uygun, H. D., Uygun, Z. O., Canbay, E., Girgin Sağın, F., & Sezer, E. (2020). Non-invasive cortisol detection in saliva by using molecularly cortisol imprinted fullerene-acrylamide modified screen printed electrodes. *Talanta*, 206, 120225.
- Favresse, J., Burlacu, M. C., Maiter, D., & Gruson, D. (2018). Interferences with thyroid function immunoassays: clinical implications and detection algorithm. *Endocrine Reviews*, 39(5), 830-850.
- Feyssa, B., Liedert, C., Kivimaki, L., Johansson, L. S., Jantunen, H., & Hakalahti, L. (2013). Patterned immobilization of antibodies within roll-to-roll hot embossed polymeric microfluidic channels. *PLoS One*, 8(7), e68918.
- Food and Drug Administration. (2018). Westminster Pharmaceuticals, LLC. Issues Voluntary Nationwide Recall of Levothyroxine and Liothyronine (Thyroid Tablets, USP) Due to Risk of Adulteration. <https://www.fda.gov/safety/recalls-market-withdrawals-safety-alerts/westminster-pharmaceuticals-llc-issues-voluntary-nationwide-recall-levothyroxine-and-liothyronine> (accessed on 20/02/24).
- Food and Drug Administration. (2022). Draft guidance on liothyronine. https://www.accessdata.fda.gov/drugsatfda_docs/psg/PSG_010379.pdf (accessed on 20/02/24).
- Fopase, R., Paramasivam, S., Kale, P., & Paramasivan, B. (2020). Strategies, challenges and opportunities of enzyme immobilization on porous silicon for biosensing applications. *Journal of Environmental Chemical Engineering*, 8(5), 104266.

- Fröhlich, E., & Wahl, R. (2021). Physiological role and use of thyroid hormone metabolites - potential utility in COVID-19 Patients. *Frontiers in Endocrinology*, 12, 587518.
- Garg, M., & Pamme, N. (2024). Strategies to remove templates from molecularly imprinted polymer (MIP) for biosensors. *TrAC Trends in Analytical Chemistry*, 170, 117437.
- Ghindilis, A. L., Atanasov, P., & Wilkins, E. (1997). Enzyme-catalyzed direct electron transfer: fundamentals and analytical applications. *Electroanalysis*, 9(9), 661-674.
- Gietka-Czernel, M. (2017). The thyroid gland in postmenopausal women: physiology and diseases. *Prz Menopauzalny*, 16(2), 33-37.
- Gottwald-Hostalek, U., & Razvi, S. (2022). Getting the levothyroxine (LT₄) dose right for adults with hypothyroidism: opportunities and challenges in the use of modern LT₄ preparations. *Current Medical Research and Opinion*, 38(11), 1865-1870.
- Gozali Balkanloo, P., Mohammad Sharifi, K., & Poursattar Marjani, A. (2023). Graphene quantum dots: synthesis, characterization, and application in wastewater treatment: a review. *Materials Advances*, 4(19), 4272-4293.
- Gregorini, A., Ruiz, M., & Volonté, M. (2013). A derivative UV spectrophotometric method for the determination of levothyroxine sodium in tablets. *Journal of Analytical Chemistry*, 68I, 510-515.
- Grieshaber, D., MacKenzie, R., Vörös, J., & Reimhult, E. (2008). Electrochemical Biosensors - sensor principles and architectures. *Sensors*, 8(3), 1400-1458.
- Hamada, Y., Masuda, K., Okubo, M., Nakasa, H., Sekine, Y., & Ishii, I. (2015). Pharmaceutical studies of levothyroxine sodium hydrate suppository provided as a hospital preparation. *Biological and Pharmaceutical Bulletin*, 38(4), 625-628.
- Hammami, I., Alabdallah, N. M., jomaa, A. A., & kamoun, M. (2021). Gold nanoparticles: Synthesis properties and applications. *Journal of King Saud University - Science*, 33(7), 101560.

- Hamzah, M., Saion, E., Kassim, A., Yahya, N., & Mahmud, H. N. M. (2007). Conjugated conducting polymers: A brief overview. *UCSI Academic Journal: Journal for the Advancement of Science & Arts*, 2, 63-68.
- Higashi, T., Ichikawa, T., Shimizu, C., Nagai, S., Inagaki, S., Min, J. Z., Chiba, H., Ikegawa, S., & Toyo'oka, T. (2011). Stable isotope-dilution liquid chromatography/tandem mass spectrometry method for determination of thyroxine in saliva. *Journal of Chromatography: B*, 879(13), 1013-1017.
- Hu, C., He, Q., Li, Q., & Hu, S. (2004). Enhanced reduction and determination of trace thyroxine at carbon paste electrode in the presence of trace cetyltrimethylammonium bromide. *Analytical Sciences*, 20(7), 1049-1054.
- Hudson, A. D., Solà, R., Ueta, J. T., Battell, W., Jamieson, O., Dunbar, T., Macià, B., & Peeters, M. (2019). Synthesis of optimized molecularly imprinted polymers for the isolation and detection of antidepressants via HPLC. *Biomimetics*, 4(1), 18.
- Jonklaas, J., Bianco, Antonio C., Cappola, Anne R., Celi, Francesco S., Fliers, E., Heuer, H., McAninch, Elizabeth A., Moeller, Lars C., Nygaard, B., Sawka, Anna M., Watt, T., & Dayan, Colin M. (2021). Evidence-based use of levothyroxine/liothyronine combinations in treating hypothyroidism: a consensus document. *European Thyroid Journal*, 10(1), 10-38.
- Jonklaas, J., & Burman, K. D. (2016). Daily administration of short-acting liothyronine is associated with significant triiodothyronine excursions and fails to alter thyroid-responsive parameters. *Thyroid*, 26(6), 770-778.
- Karunakaran, R., & Keskin, M. (2022). Chapter 11 - Biosensors: components, mechanisms, and applications. In C. Egbuna, K. C. Patrick-Iwuanyanwu, M. A. Shah, J. C. Ifemeje & A. Rasul (Eds.), *Analytical Techniques in Biosciences*, Academic Press, 179-190.
- Kaur, N., & Suryanarayanan, R. (2021). Levothyroxine sodium pentahydrate tablets - formulation considerations. *Journal of Pharmaceutical Sciences*, 110(12), 3743-3756.

- Keefe, A. D., Pai, S., & Ellington, A. (2010). Aptamers as therapeutics. *Nature Reviews Drug Discovery*, 9(7), 537-550.
- Kendall, E. C. (1926). Chemical Constitution of thyroxine. *Nature*, 118, 65-66.
- Khadem, N., Ayatollahi, H., Vahid Roodsari, F., Ayati, S., Dalili, E., Shahabian, M., Mohajeri, T., & Shakeri, M. T. (2012). Comparison of serum levels of tri-iodothyronine (T₃), thyroxine (T₄), and thyroid-stimulating hormone (TSH) in preeclampsia and normal pregnancy. *Iranian Journal of Reproductive Medicine.*, 10(1), 47-52.
- Kim, H., Moon, S. Y., Han, K., Lee, J. H., Im, J. H., Kim, S., & Yoo, J. E. (2020). Treatment of hypothyroidism using Korean medicine: 2 case reports. *Medicine*, 99(18), e19737.
- Kim, S., Jang, L. K., Park, H. S., & Lee, J. Y. (2016). Electrochemical deposition of conductive and adhesive polypyrrole-dopamine films. *Scientific Reports*, 6(1), 30475.
- Kim, S. J., Dhesingh, R. S., Kawaguchi, T., & Miura, N. (2008). Surface plasmon resonance (SPR) based immunosensor for sensitive detection of thyroxine. *ECS Transactions*, 16(11), 55.
- Kinnamon, D., Ghanta, R., Lin, K.-C., Muthukumar, S., & Prasad, S. (2017). Portable biosensor for monitoring cortisol in low-volume perspired human sweat. *Scientific Reports*, 7(1), 13312.
- Kostoglou-Athanassiou, I., & Ntalles, K. (2010). Hypothyroidism - new aspects of an old disease. *Hippokratia*, 14(2), 82-87.
- Lafarge, C., Bitar, M., El Hosry, L., Cayot, P., & Bou-Maroun, E. (2020). Comparison of molecularly imprinted polymers (MIP) and sol-gel molecularly imprinted silica (MIS) for fungicide in a hydro alcoholic solution. *Materials Today Communications*, 24, 101157.
- Lakard, B. (2020). Electrochemical biosensors based on conducting polymers: a review. *Applied Sciences*, 10(18), 6614.
- Lara, S., & Perez-Potti, A. (2018). Applications of nanomaterials for immunosensing. *Biosensors*, 8(4), 104.

- Ledeți, I., Romanescu, M., Cîrcioban, D., Ledeti, A., Vlase, G., Vlase, T., Suciu, O., Murariu, M., Olariu, S., Matusz, P., Buda, V., & Piciu, D. (2020). Stability and compatibility studies of levothyroxine sodium in solid binary systems-instrumental screening. *Pharmaceutics*, *12*(1), 58.
- Lendoiro, E. (2022). Overview on advantages & disadvantages of alternative matrices. *Toxicologie Analytique et Clinique*, *34*(3), S16-S17.
- Leso, V., Vetrani, I., De Cicco, L., Cardelia, A., Fontana, L., Buonocore, G., & Iavicoli, I. (2020). The impact of thyroid diseases on the working life of patients: a systematic review. *International Journal of Environmental Research and Public Health*, *17*(12), 4295.
- Liu, X., & Liu, J. (2021). Biosensors and sensors for dopamine detection. *VIEW*, *2*(1), 20200102.
- Lorenzo, R. A., Carro, A., Alvarez-Lorenzo, C., & Concheiro, A. (2011). To remove or not to remove? The challenge of extracting the template to make the cavities available in molecularly imprinted polymers (MIPs). *International Journal of Molecular Sciences*, *12*, 4327-4347.
- Luka, G., Ahmadi, A., Najjaran, H., Alocilja, E., DeRosa, M., Wolthers, K., Malki, A., Aziz, H., Althani, A., & Hoorfar, M. (2015). Microfluidics integrated biosensors: a leading technology towards Lab-on-a-Chip and sensing applications. *Sensors*, *15*(12), 30011-30031.
- Luong, J. H. T., Narayan, T., Solanki, S., & Malhotra, B. D. (2020). Recent Advances of conducting polymers and their composites for electrochemical biosensing applications. *Journal of Functional Biomaterials*, *11*(4), 71.
- Mahadevan, S., Sadacharan, D., Kannan, S., & Suryanarayanan, A. (2017). Does time of sampling or food intake alter thyroid function test? *Indian Journal of Endocrinology and Metabolism*, *21*(3), 369-372.
- McConnell, E. M., Nguyen, J., & Li, Y. (2020). Aptamer-based biosensors for environmental monitoring. *Frontiers in Chemistry*, *8*, 434.
- Mollarasouli, F., Kurbanoglu, S., & Ozkan, S. A. (2019). The role of electrochemical immunosensors in clinical analysis. *Biosensors*, *9*(3), 86.

- Mostafa, A. M., Barton, S. J., Wren, S. P., & Barker, J. (2021). Review on molecularly imprinted polymers with a focus on their application to the analysis of protein biomarkers. *TrAC Trends in Analytical Chemistry*, *144*, 116431.
- Mradula, Raj, R., Devi, S., & Mishra, S. (2020). Antibody-labeled gold nanoparticles based immunosensor for the detection of thyroxine hormone. *Analytical Sciences*, *36*(7), 799-806.
- Mradula, M., Raj, R., & Mishra, S. (2021). Voltammetric immunosensor for selective thyroxine detection using Cu-MOF@PANI composite. *Electrochemical Science Advances*, *2*, 2:e2100051.
- Muhammet, S. M., Cete, S., Arslan, F., & Yaşar, A. (2009). Amperometric cholesterol biosensors based on the electropolymerization of pyrrole and aniline in sulphuric Acid for the determination of cholesterol in serum. *Artificial Cells Blood Substitutes and Immobilization Biotechnology*, *37*(6), 273-278.
- Mullur, R., Liu, Y. Y., & Brent, G. A. (2014). Thyroid hormone regulation of metabolism. *Physiological Reviews*, *94*(2), 355-382.
- Muñoz, J., Riba-Moliner, M., Brennan, L. J., Gun'ko, Y. K., Céspedes, F., González-Campo, A., & Baeza, M. (2016). Amperometric thyroxine sensor using a nanocomposite based on graphene modified with gold nanoparticles carrying a thiolated β -cyclodextrin. *Microchimica Acta*, *183*(5), 1579-1589.
- Mustafa, Y. L., Keirouz, A., & Leese, H. S. (2022). Molecularly imprinted polymers in diagnostics: accessing analytes in biofluids. *Journal of Materials Chemistry B*, *10*(37), 7418-7449.
- Naresh, S., Bitla, A., & Sachan, A. (2018). Utility of saliva for measurement of thyroid hormones. *Indian Journal of Medical Biochemistry*, *22*, 36-40.
- Nasajpour-Esfahani, N., Dastan, D., Alizadeh, A. a., Shirvanisamani, P., Rozati, M., Ricciardi, E., Lewis, B., Aphale, A., & Toghraie, D. (2023). A critical review on intrinsic conducting polymers and their applications. *Journal of Industrial and Engineering Chemistry*, *125*, 14-37.

- Navazesh, M. (1993). Methods for collecting saliva. *Annals of the New York Academy of Sciences*, 694, 72-77.
- Neu, V., Bielow, C., Schneider, P., Knut, R., Stuppner, H., & Huber, C. (2013). Investigation of reaction mechanisms of drug degradation in the solid state: a kinetic study implementing ultrahigh-performance liquid chromatography and high-resolution mass spectrometry for thermally stressed thyroxine. *Analytical chemistry*, 85, 2385-90.
- Nguyen, H. V., Go, A., & Lee, M. H. (2020). Quantitative determination of triiodothyronine by electrochemical impedance spectroscopic biosensor using gold nanoparticle-modified electrode. *Journal of Nanoscience and Nanotechnology*, 20(11), 7163-7168.
- Ning, Y., Hu, J., & Lu, F. (2020). Aptamers used for biosensors and targeted therapy. *Biomedicine and Pharmacotherapy*, 132, 110902.
- Orden, I., Pie, J., Juste, M. G., Marsella, J. A., & Blasco, C. (1987). Thyroxine in unextracted urine. *Acta Endocrinology*, 114(4), 503-508.
- Özcan, L., Sahin, M., & Sahin, Y. (2008). Electrochemical preparation of a molecularly imprinted polypyrrole-modified pencil graphite electrode for determination of ascorbic acid. *Sensors*, 8(9), 5792-5805.
- Park, S. Y., Kim, J., Yim, G., Jang, H., Lee, Y., Kim, S. M., Park, C., Lee, M.-H., & Lee, T. (2020). Fabrication of electrochemical biosensor composed of multi-functional DNA/rhodium nanoplate heterolayer for thyroxine detection in clinical sample. *Colloids Surf. B: Biointerfaces*, 195, 111240.
- Phonklam, K., Wannapob, R., Sriwimol, W., Thavarungkul, P., & Phairatana, T. (2020). A novel molecularly imprinted polymer PMB/MWCNTs sensor for highly-sensitive cardiac troponin T detection. *Sensors and Actuators B: Chemical*, 308, 127630.
- Pirzada, M., & Altintas, Z. (2021). Chapter 14 - Template removal in molecular imprinting: principles, strategies, and challenges. In A. Denizli (Ed.), *Molecular Imprinting for Nanosensors and Other Sensing Applications*, Elsevier, 367-406.

- Poggialini, F., Legnaioli, S., Campanella, B., Cocciaro, B., Lorenzetti, G., Raneri, S., & Palleschi, V. (2023). Calculating the limits of detection in laser-induced breakdown spectroscopy: not as easy as it might seem. *Applied Sciences*, *13*(6), 3642.
- Patil, P. A. V., Chuang, Y. S., Li, C., & Wu, C.C. (2023). Recent advances in electrochemical immunosensors with nanomaterial assistance for signal amplification. *Biosensors*, *13*(1), 125.
- Prasad, B. B., Madhuri, R., Tiwari, M. P., & Sharma, P. S. (2010). Layer-by-layer assembled molecularly imprinted polymer modified silver electrode for enantioselective detection of d- and l-thyroxine. *Analytica Chimica Acta*, *681*(1), 16-26.
- Pratama, K. F., Manik, M. E. R., Rahayu, D., & Hasanah, A. N. (2020). Effect of the molecularly imprinted polymer component ratio on analytical performance. *Chemical and Pharmaceutical Bulletin*, *68*(11), 1013-1024.
- Qi, P., Wang, J., Wang, L., Li, Y., Jin, J., Su, F., Tian, Y., & Chen, J. (2010). Molecularly imprinted polymers synthesized via semi-covalent imprinting with sacrificial spacer for imprinting phenols. *Polymer*, *51*, 5417-5423.
- Rahmati, Z., & Roushani, M. (2022). SARS-CoV-2 virus label-free electrochemical nanohybrid MIP-aptasensor based on Ni₃ (BTC)₂ MOF as a high-performance surface substrate. *Microchimica Acta*, *189*(8), 287.
- Rajendraprasad, N. (2022). Applications of pyrrole based molecularly imprinted polymers as analytical sensors: a review. *Portugaliae Electrochimica Acta*, *45*, 273-303.
- Rajpal, S., & Mishra, P. (2022). Next generation biosensors employing molecularly imprinted polymers as sensing elements for in vitro diagnostics. *Biosensors and Bioelectronics.: X*, *11*, 100201.
- Ramkumar, R., & Sundaram, M. M. (2016). Electrochemical synthesis of polyaniline cross-linked NiMoO₄ nanofibre dendrites for energy storage devices. *New Journal of Chemistry*, *40*(9), 7456-7464.

- Rasmussen, S. C. (2020). Conjugated and conducting organic polymers: the first 150 years. *Chempluschem*, 85(7), 1412-1429.
- Ratautaite, V., Brazys, E., Ramanaviciene, A., & Ramanavicius, A. (2022). Electrochemical sensors based on l-tryptophan molecularly imprinted polypyrrole and polyaniline. *Journal of Electroanalytical Chemistry*, 917, 116389.
- Regasa, M. B., Soreta, T. R., Femi, O. E., Ramamurthy, P. C., & Subbiahraj, S. (2020). Novel multifunctional molecular recognition elements based on molecularly imprinted poly (aniline-co-itaconic acid) composite thin film for melamine electrochemical detection. *Sensing and Bio-Sensing Research*, 27, 100318.
- Rochitta, G., Spanu, A., Babudieri, S., Latte, G., Madeddu, G., Galleri, G., Nuvoli, S., Bagella, P., Demartis, M. I., Fiore, V., Manetti, R., & Serra, P. A. (2016). Enzyme biosensors for biomedical applications: strategies for safeguarding analytical performances in biological fluids. *Sensors*, 16(6), 780.
- Rodwihok, C., Tam, T. V., Choi, W. M., Suwannakaew, M., Woo, S. W., Wongratanaphisan, D., & Kim, H. S. (2022). Preparation and characterization of photoluminescent graphene quantum dots from watermelon rind waste for the detection of ferric ions and cellular bio-imaging applications. *Nanomaterials*, 12(4), 702.
- Roland, R. M., Bhawani, S. A., & Ibrahim, M. N. M. (2023). Synthesis of molecularly imprinted polymer for the removal of cyanazine from aqueous samples. *Chemical and Biological Technologies in Agriculture*, 10(1), 92.
- Romero-Gómez, B., Guerrero-Alonso, P., Carmona-Torres, J. M., Notario-Pacheco, B., & Cobo-Cuenca, A. I. (2019). Mood disorders in levothyroxine-treated hypothyroid women. *International Journal of Environmental Research and Public Health*, 16(23), 4776.
- De Rossi, A., & Lima, V. (2018). Processed drug classification and temporal analysis by technical chemometrics for quality controlling using

- spectroscopy of FT-IR and X-Ray diffraction. *Orbital: The Electronic Journal of Chemistry*, 10, 496-502.
- Roy, S., Nagabooshanam, S., Chauhan, N., Kumar, R., Wadhwa, S., & Mathur, A. (2021). Design and development of a novel flexible molecularly imprinted electroanalytical sensor for the monitoring of diabetic foot ulcers. *Surfaces and Interfaces*, 26, 101310.
- Ruiz, G., Tripathi, K., Okyem, S., & Driskell, J. D. (2019). pH impacts the orientation of antibody adsorbed onto gold nanoparticles. *Bioconjugate Chemistry*, 30(4), 1182-1191.
- Ruuskanen, S., Hsu, B. Y., Heinonen, A., Vainio, M., Darras, V. M., Sarraude, T., & Rokka, A. (2018). A new method for measuring thyroid hormones using nano-LC-MS/MS. *Journal of Chromatography B: Analytical Technologies in the Biomedical and Life Sciences*, 1093-1094, 24-30.
- Safer, J. D., Fraser, L. M., Ray, S., & Holick, M. F. (2001). Topical triiodothyronine stimulates epidermal proliferation, dermal thickening, and hair growth in mice and rats. *Thyroid*, 11(8), 717-724.
- Seo, Y. H., Baik, S., & Lee, J. (2024). Nanopore surface engineering of molecularly imprinted mesoporous organosilica for rapid and selective detection of L-thyroxine. *Colloids and Surfaces B: Biointerfaces*, 234, 113711.
- Setiyanto, H., Rahmadhani, S., & Zulfikar, M. A. (2017). Electropolymerized of aniline as a new molecularly imprinted polymer (MIP) for determination of phenol - a study for phenol sensor. *International Seminar on Sensors, Instrumentation, Measurement and Metrology (ISSIMM), Surabaya, Indonesia*, 124-128.
- Shafqat, S. R., Bhawani, S. A., Bakhtiar, S., Ibrahim, M. N. M., & Shafqat, S. S. (2023). Template-assisted synthesis of molecularly imprinted polymers for the removal of methyl red from aqueous media. *BMC Chemistry*, 17(1), 46.
- Shao, W., Jamal, R., Xu, F., Ubul, A., & Abdiryim, T. (2012). The effect of a small amount of water on the structure and electrochemical properties of solid-state synthesized polyaniline. *Materials*, 5, 1811-1825.

- Sharma, S., Byrne, H., & O'Kennedy, R. J. (2016). Antibodies and antibody-derived analytical biosensors. *Essays in Biochemistry.*, 60(1), 9-18.
- Singh, D., Roy, S., Mahindroo, N., & Mathur, A. (2023). Design and development of an electroanalytical sensor based on molecularly imprinted polyaniline for the detection of thyroxine. *Journal of Applied Electrochemistry*, 54, 147-61.
- Smajdor, J., Piech, R., Rumin, M., Paczosa-Bator, B., & Smajdor, Z. (2016). High sensitive voltammetric levothyroxine sodium determination on renewable mercury film silver based electrode. *Journal of Electrochemical Society*, 163(7), H605-H609.
- Spencer, C. (2000). Assay of thyroid hormones and related substances. In: Feingold KR, Anawalt B, Blackman MR, et al., editors. South Dartmouth (MA): MDTText.com, Inc.; 2000. Available from: <https://www.ncbi.nlm.nih.gov/books/NBK279113/>.
- Staal, O. M., Hansen, H. M. U., Christiansen, S. C., Fougner, A. L., Carlsen, S. M., & Stavadahl, Ø. (2018). Differences between flash glucose monitor and fingerprick measurements. *Biosensors*, 8(4), 93.
- Strikić Đula, I., Pleić, N., Babić Leko, M., Gunjača, I., Torlak, V., Brdar, D., Punda, A., Polašek, O., Hayward, C., & Zemunik, T. (2022). Epidemiology of hypothyroidism, hyperthyroidism and positive thyroid antibodies in the croatian population. *Biology*, 11(3), 394.
- Strong, D. K., Decarie, D., & Ensom, M. H. (2010). Stability of levothyroxine in sodium chloride for IV administration. *Canadian Journal of Hospital Pharmacy*, 63(6), 437-443.
- Sueda, S. (2022). Antibody immobilization for immunosensing. *Analytical Sciences*, 38(1), 1-2.
- Svirskis, D., Lin, S. W., Brown, H., Sangaroomthong, A., Shin, D., Wang, Z., Xu, H., Dean, R., Vareed, P., Jensen, M., & Wu, Z. (2018). The influence of tablet formulation, drug concentration, and pH modification on the stability

- of extemporaneously compounded levothyroxine suspensions. *International Journal of Pharmaceutical Compounding*, 22(2), 164-171.
- Takikawaa, H. (1955). Physico-chemical studies on thyroid hormones. *Endocrinology Japon*, 2(1), 65-78.
- Tang, S. J., Wang, A. T., Lin, S. Y., Huang, K. Y., Yang, C. C., Yeh, J. M., & Chiu, K. C. (2011). Polymerization of aniline under various concentrations of APS and HCl. *Polymer Journal*, 43(8), 667-675.
- Tanoue, R., Kume, I., Yamamoto, Y., Takaguchi, K., Nomiyama, K., Tanabe, S., & Kunisue, T. (2018). Determination of free thyroid hormones in animal serum/plasma using ultrafiltration in combination with ultra-fast liquid chromatography-tandem mass spectrometry. *Journal of Chromatography: A*, 1539, 30-40.
- The Times of India. (2023). Sun Pharma, Lupin recall drugs in US on manufacturing woes. http://timesofindia.indiatimes.com/articleshow/106069616.cms?utm_source=contentofinterest&utm_medium=text&utm_campaign=cppst. (Accessed on 20/02/2024).
- Thienpont, L., Van Uytfanghe K., Beastall G., Faix J. D., Ieiri T., Miller W.G., Nelson J. C., Ronin C., Ross H. A., Thijssen J. H., & Toussaint B. (2010). Report of the IFCC working group for standardization of thyroid function tests; part 3: total thyroxine and total triiodothyronine. *Clinical Chemistry*, 56, 921-929.
- Thorsteinsdóttir, U. A., & Thorsteinsdóttir, M. (2021). Design of experiments for development and optimization of a liquid chromatography coupled to tandem mass spectrometry bioanalytical assay. *Journal of Mass Spectrometry*, 56(9), e4727.
- Unnikrishnan, A. G., Kalra, S., Sahay, R. K., Bantwal, G., John, M., & Tewari, N. (2013). Prevalence of hypothyroidism in adults: an epidemiological study in eight cities of India. *Indian Journal of Endocrinology and Metabolism*, 17(4), 647-652.

- Valentino, M., Imbriano, A., Tricase, A., Della Pelle, F., Compagnone, D., Macchia, E., Torsi, L., Bollella, P., & Ditaranto, N. (2023). Electropolymerized molecularly imprinted polypyrrole film for dimethoate sensing: investigation on template removal after the imprinting process. *Analytical Methods*, *15*(10), 1250-1253.
- van Wassenaeer, A. G., Stulp, M. R., Valianpour, F., Tamminga, P., Ris Stalpers, C., de Randamie, J. S., van Beusekom, C., & de Vijlder, J. J. (2002). The quantity of thyroid hormone in human milk is too low to influence plasma thyroid hormone levels in the very preterm infant. *Clinical Endocrinology*, *56*(5), 621-627.
- Wadhwa, S., John, A. T., Mathur, A., Khanuja, M., Bhattacharya, G., Roy, S. S., & Ray, S. C. (2020). Engineering of luminescent graphene quantum dot-gold (GQD-Au) hybrid nanoparticles for functional applications. *MethodsX*, *7*, 100963.
- Wani T. A., & Zargar S., Majid S., Darwish I. A. (2016). Analytical application of flow immunosensor in detection of thyroxine and triiodothyronine in serum. *Assay and Drug Development Technologies*, *14*(9), 535-542.
- Werhun, A., & Hamilton, W. (2013). Are we overusing thyroid function tests? *British Journal of General Practice*, *63*(613), 404.
- Wilson, L., Franke, C., Ross, N., Sunday, C., Makelane, H., Bilibana, M., Waryo, T., Mapolie, S., Baker, P., & Iwuoha, E. (2015). Electrochemical immunosensor based on the interactions between polypyrrole and cobalt (II) salicylaldimine dendrimer. *International Journal of Electrochemical Science*, *10*, 3207-3222.
- Wu, Z. (2022). Effect of radioimmunoassay on accuracy of thyroid hormone detection. *Contrast Media Molecular Imaging*, *2022*, 9206079.
- Yerawar, C., Deokar, P. G., & Noone, B. (2019). Reversible hair loss due to levothyroxine overdose. *Indian Journal of Endocrinology and Metabolism*, *23*(6), 652-653.

- Yukihiro, T., & Shuichi, M., (2022). Colloidal stability of polypyrrole-ITO conducting inks. *Japanese Journal of Applied Physics*, 61, SE1003.
- Yussuf, A., Al-Saleh, M., Al-Enezi, S., & Abraham, G. (2018). Synthesis and characterization of conductive polypyrrole: the influence of the oxidants and monomer on the electrical, thermal, and morphological properties. *International Journal of Polymer Science*, 2018, 4191747.
- Zhu, H., Wang, Y., Yuan, Y., & Zeng, H. (2011). Development and characterization of molecularly imprinted polymer microspheres for the selective detection of kaempferol in traditional Chinese medicines. *Analytical Methods*, 3(2), 348-355.
- Zhu, P., & Zhao, Y. (2019). Cyclic voltammetry measurements of electroactive surface area of porous nickel: peak current and peak charge methods and diffusion layer effect. *Materials Chemistry and Physics*, 233, 60-67.


List of Publications


1. Singh, D., Roy, S., Mathur, A., & Mahindroo, N. (2024). Ultrasensitive point-of-care device for detection of levothyroxine using molecularly imprinted polyaniline. *Journal of Applied Electrochemistry*, 54(1), 1-15. (Impact factor - 2.4)
2. Singh, D., Bharti, A. & Mathur, A., (2023). Thyroxine biosensors: A Review on Progress and Challenges. *Bioanalysis*, 15, 20. (Impact factor - 2)
3. Singh, D., Shrivastava, A., Raj, R., Mishra, A., Mathur, A., & Mahindroo, N. Development of a molecularly imprinted poly-pyrrole biosensor for rapid and accurate estimation of liothyronine: towards point-of-care quality Assessment (*under communication*).
4. Singh, D., Mathur, A., Arora, S., Roy, S., & Mahindroo, N., (2022). Journey of organ on a chip technology and its role in future healthcare scenario, *Applied Surface Sciences Advances*, 9 100246. (Impact factor - 7.5)
5. Nandi, S.K., Singh, D., Upadhyay, J., Gupta, N., Dhiman, N., Mittal, S.K., & Mahindroo, N., (2021). Identification of tear-based protein and non-protein biomarkers: Its application in diagnosis of human diseases using biosensors. *International Journal of Biological Macromolecules*, 15, 838-846. (Impact factor - 7.7)

Other related publications

6. Singh, D., Bansal, A., Jain, A., Tyagi, L. K., Mondal, S., & Patel, R.K. (2021) GC-MS based lemon grass metabolite analysis involved in the synthesis of silver nanoparticles and evaluation of photo-catalytic degradation of methylene blue. *Biometals*, 34, 1121-1139. (Impact factor - 4.1)
7. Singh, D., Joshi, K., Samuel, A., Patra, J., & Mahindroo, N. (2020). Alcohol-based hand sanitisers as first line of defence against SARS-CoV-2: a review of biology, chemistry and formulations. *Epidemiology and Infections*, 29, 148:e229. (Impact factor - 4.2)
8. Jain, S., Lamba, B. Y., Kumar, S., & Singh, D. (2020). Strategy for repurposing of disposed PPE kits by production of biofuel: Pressing priority amidst COVID-19 pandemic, *Biofuels*, 13, 545-549. (Impact Factor-2.1)
9. Singh, D., & Pahwa, S., (2020) A review on physico-chemical parameters of liposomal doxorubicin. *International Journal of Applied Pharmaceutics*, 1-5. (Cite score - 1.4)
10. Patra, J., Singh, D., Jain, S., Mahindroo, N., (2021) Chapter 13 - Application of Docking for Lead Optimization, Editor(s): Mohane S. Coumar, *Molecular Docking for Computer-Aided Drug Design*, Academic Press, 271-294. (Book chapter : Scopus Indexed Book, Elsevier)

Annexure J: Ethical Approval

 **UPES**
UNIVERSITY OF TOMORROW

 **Great Place To Work**
Certified
FEB 2023 - FEB 2024
INDIA

Registration No: EC/NEW/INST/2022/2820

To, **Mr. Deepanmol Singh**
Assistant Professor
School of Health Sciences & Technology
UPES, Dehradun
Uttarakhand (UK)

Project No: UPES/IEC/DEC/2023/13
Dated: 25/01/2024

Dear Mr. Deepanmol Singh,
The institutional Ethics Committee in its meeting held on 18th Dec 2023 has reviewed and discussed your application submitted to IEC office at UPES, Project No: UPES/IEC/DEC/2024/13 to conduct the research proposal entitled *“Design and Development of Point of Care Device using Nano-Transducers for Monitoring and Analysis of Thyroid Hormones”*.

Following documents were reviewed:

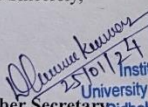
- *Check List*
- *Executive Summary*
- *Experimental Protocol*
- *Inclusion & Exclusion Criteria*
- *Consent Form*

IEC Decision: Approved in its present form

Validity of the ethics approval is till the proposed date of completion (PDC) of the project.

Kindly quote the above reference code in all further communication regarding the above subjects. **Mandatory for researcher to report any adverse events and any change in protocol or information sheet to ethics committee.**

Yours Sincerely,

 **UPES**
UNIVERSITY OF TOMORROW
Institutional Ethics Committee
University of Petroleum & Energy Studies
Bidholi, Via-Premnagar, Dehradun
Member Secretary
Institutional Ethics Committee
UPES, Dehradun

Energy Acres: Bidholi Via Prem Nagar, Dehradun - 248 007 (Uttarakhand), India, T: +91 135 2770137, 2776053/54/91, 2776201, M: 9997799474, F: +91 135 2776090/95
Knowledge Acres: Kandoli Via Prem Nagar, Dehradun - 248 007 (Uttarakhand), India, M: +91 8171979021/2/3, 7060111775

ADVANCED ENGINEERING | COMPUTER SCIENCE | DESIGN | BUSINESS | LAW | HEALTH SCIENCES AND TECHNOLOGY | MODERN MEDIA | LIBERAL STUDIES



PLAGIARISM CERTIFICATE

Date: 15/07/2024

1. I, Dr. Ashish Mathur (Internal Guide), certify that the Thesis titled "Design and Development of a Point of Care device using Nano-transducers for Monitoring and Analysis of Thyroid Hormones" submitted by Scholar Mr. Deepanmol Singh having SAP ID 500080036 has been run through a Plagiarism Check Software (Turnitin) and the Plagiarism Percentage is reported to be 9%.

2. Plagiarism Report generated by the Plagiarism Software is attached.

A handwritten signature in blue ink that reads "Ashish Mathur".

Signature of the Supervisor

A handwritten signature in blue ink that reads "Deepanmol Singh".

Signature of the Scholar

Design and Development of a Point of Care device using Nano-transducers for Monitoring and Analysis of Thyroid Hormones

ORIGINALITY REPORT

9%	7%	6%	3%
SIMILARITY INDEX	INTERNET SOURCES	PUBLICATIONS	STUDENT PAPERS

PRIMARY SOURCES

1	jdgstage.thyroidmanager.org Internet Source	1%
2	www.ncbi.nlm.nih.gov Internet Source	1%
3	www.researchsquare.com Internet Source	1%
4	Yi Ning, Jue Hu, Fangguo Lu. "Aptamers used for biosensors and targeted therapy", Biomedicine & Pharmacotherapy, 2020 Publication	1%
5	Submitted to University of Glamorgan Student Paper	1%
6	Submitted to University Of Tasmania Student Paper	1%
7	Submitted to University of Nottingham Student Paper	<1%